جامعة الأمير محمد بن فهد
PRINCE MOHAMMAD BIN FAHD UNIVERSITY

College of Engineering
Department of Mechanical Engineering
Spring 2016/2017

Senior Design Project Report

Design of Experiments for Studying the Effect of Nano-Additives Lubricant on Vibration Signals of Defective Rolling Element Bearings

Prepared by

	Student Name	Student ID
1	Ahmed Aldakheel	201303886
2	Mohammed Alhawaj	201303710
3	Mohammed Alshubaily	201101678
4	Rami Al Gassab	201301568
5	Sultan Hamdi	201300790

Advisor: Dr. Nader Sawalhi
Co-Advisors: Dr. Faramarz Djavanroodi, Dr. Adrian Cazan

ABSTRACT

Rotating machine components can operate at high speeds and under high load conditions. This operation offers resistance (i.e. friction) to their movement. It causes a lot of wear and tear of surfaces of moving parts. Therefore, the lubricants introduced between two moving or sliding mutual contact surfaces is needed to reduce the friction and temperature between them. In automobiles, almost 15% of the total energy loss comes from the friction generated between the sliding parts. Additives in lubricants come into effect under such conditions. In this report, we are investigating the effect of nano-particles additives to an oil based lubricant on vibrational signals. This required us to modify a previously built test rig by designing: a hydraulic loading system, a new bearing housing and oil tank, a new pulley system configuration, and a modified shaft. We conducted our experimentation by installing a number of faulty and healthy bearings operating at different speeds, loads, and concentrations of nano-particles in the oil based lubricant. We acquired and analyzed data using signal processing tools (LabVIEW and Matlab). Our main objectives from this study is to understand the efficiency of nano-lubricants and what could be the best concentration of nano-particles to add to the oil based lubricant.

Acknowledgments

Our project could not have been successfully completed without the insight, assistance, and input of a number of individuals. To begin with, we would like to show our appreciation and gratitude to the university administration who provided us with a grant to work on our project. This grant provided us with adequate funding that helped us purchase and design different components of the project. Undoubtedly, our senior project would not have reached the level of quality and professionalism that it is at without Dr. Nader Sawalhi (our project advisor and course instructor) guidance and assistance. Dr. Nader showed excellent communication and leadership skills with us. He was always able to respond to our concerns and questions whenever we had any, whether it was during his office hours or on electronic communication platforms. Dr. Nader helped us construct a plan that will ease our work and allow us to progress in our senior project without major hiccups. In addition, Dr. Nader Sawalhi held with us weekly meetings where he explained different aspects of the project that we did not have a grip of and helped us solve problems, thus expanding our knowledge base and clearing questions about topics in the senior project. Moreover, we would like to thank Dr. Faramarz Djavanroodi and Dr. Adrian Cazan (our co-advisors) for their fruitful contribution and helpful insights in our project. They were incredibly helpful in multiple occasions where they provided us with solutions to problems and information about how to select/design different components of the project. We would also like to thank Dr. Nizar Tayem (Electrical Engineering Chairman) for his contribution in this project. Last but not least, we acknowledge Mr. Antonio Ifurong (lab technician/engineer) for his useful input and support regarding the electrical components and circuitry of our project.

Table of Contents

List of Figures

List of Tables

CHAPTER 1
Introduction

1.1 Project Definition

1.2 Aims and Objectives of The Project

1.3 Applications

1.4 History

1.5 Efficiency and Feasibility

This chapter presents an overview of the project design. It explains the background of selecting the project and states the aims and objectives of the project.

1.1 Project Definition

Our project consists of two main parts. Firstly, add modifications to a previously built test rig such as: a hydraulic loading system, bearing housing, oil tank, selection of new bearings, and suspend the nano-particles in the lubricant using ultrasonic. Secondly, conduct experiments to test healthy bearings and defected bearings when lubricated with a nano-additive oil based lubricant. We are going to vary different characteristics of the nano-lubricant such as concentration and particle size to reach a number of conclusions (i.e. vibration signal, friction, wear, and thermal properties).

1.2 Aims and Objectives of The Project

The four main objectives of this project are:

1. Test the vibration signature of rolling element bearings lubricated with different concentrations of nano-additives oil based lubricant, operating under different loads, and at various speeds.
2. Provide a thorough experimental investigation into the effect of different lubricants and nanoparticle additives on the characteristics of the vibration signal and the effect of detecting the presence of the defect and the amount of masking provided.
3. Simulate the effect of nanomaterial additives on the vibration signature. This aims at provided a much needed initial and sound model into the attachments of the nanomaterial particles to the defective area and will form a base for further research into this area.
4. Enrich the body of research with new much needed knowledge into this new twenty first century science.

1.3 Applications

Rotary machines are the core of all industries. Companies focus on implementing preventive and predictive maintenance to predict failure, reduce downtime, and reduce turnaround maintenance time. Our research will attract the interest of the industrial section in the kingdom. Particularly, the interest of large companies like Saudi ARAMCO and SABIC, where quality and predictability is a priority. The vibration analysis test rig we built can be utilised to study how adding nano-particles at different concentrations and sizes affect the vibration signal amplitude, noise, and tribology properties. In addition, the test rig is intended to be modular in design, therefore, additional improvements can be added in the future to conduct experiments on other topics/field of interests.

1.4 History

Nowadays, the industry demands quieter shafts and shaft components. Many researches and studies have been conducted to eliminate vibration and noise from rotary machines. Yet, the trend to minimize noise and vibration by designing the noise out of systems is what drives researchers today. The method used to determine the noise level of ball bearings was consisted of spinning the bearing by hand and holding it to ear. Obviously, this method falls short on today's standards. This test is known for its limitation and inaccuracy for it has been learned that lubrication determined the noise by damping it.

For as long as there been machines, there has been lubricants. In recent years, lubrication is on the pathway to “modernisation” and improving it's efficiency and characteristics. Many concepts and ideas have been generated to catapult lubrication to a whole new level. Recently, studies proposed that using nano-material additive to lubricants can have noticeable impacts on friction, wear, and vibration (explained more in chapter 2).

1.5 Efficiency and Feasibility

Nano-materials penetrates into pores, cracks, and faults this allows less surface build up and allows impregnated self-lubricating parts. Spherical shape nano-particles performs a rolling action on the surface which reduces friction significantly more than the sliding conventional layered compound. Furthermore, due to the stability of the nano-materials, operating life is extended significantly and does not gum up the surface due to high physical stability.

CHAPTER 2

Literature Review

In this section of the report we examine, investigate, analyze, and research previous studies, experiments, published information, and research on the different parts of our project.

2.1 Project Background

Engineers have always been striving to enhance the engineering field which will definitely have a domino effect on numerous fields. With the advancement of science and technology, a lot of the industrial and automotive fields, just to name a couple, have been improving exponentially. Lubrication is not an exception of this noticeable change. In the last decade, research has been showing interest in the effect nano-particles additives have on vibration, noise, and tribology properties when suspended in oil and grease based lubricants. We decided to carry out this topic because there is limited scientific research available in this area. Furthermore, there are a number of challenges in this project, including: implementation of a loading system, numerical analysis of the problem in hand, utilisation of signal processing tools, and eliminating impurities and disturbances from the experiment environment.

2.1.1 Anti-Friction Type Bearing

Bearing is an essential component of all rotary machines. A bearing is defined by the following functions: minimize friction between contacting surfaces, restrict motion of rotating components inside the stationary component, and support load imposed on shaft. There are a many types of bearings used in the industrial field, however we are focusing on one type called Anti-friction bearings.

Anti-Friction Bearings use rolling contact rather than sliding contact. This is because rolling components have low coefficient of friction relative to sliding components. All anti-friction bearing have the following main four components (shown in figure 2.1): inner race/ring, outer race/ring, groove and rolling elements, and a cage that separates and holds the rolling elements. The races/rings are machined to extremely fine tolerances from an alloy steel which has been case hardened so it's hard on the outside and tough in the inside.

Figure 2.1 - Anti-friction rolling element bearing

In our test rig we selected to use self-aligning bearings (shown in figure 2.2) to perform the experiments on. Self-aligning bearing is a type of anti-friction ball bearing that has a special ability to contain (if there is any) misalignment of the shaft. This is due to the outer ring design which has a single spherical raceway with its center of curvature coincident with the bearing axis. While the he inner ring has two raceways to contain the ball's' movements. Collectively, this allows the axis of the inner ring, balls and cage to deflect around the bearing center to automatically correct misalignment caused by housing and shaft machining or installation error [1]. In addition, this bearing is easy to disassemble and assemble back again without any issues.

Figure 2.2 - Self Aligning bearing

2.1.2 Types of Bearing Lubricants

Lubricants are considered to be the blood of rotary machines. A lubricant must be able to: maintain a stable viscosity over a broad range of temperatures, have a good film strength that can support loads, have a stable structure that provides for a long service life, non-corrosive and compatible with adjacent components, and provide a barrier against contamination and moisture. In this part of the report we are going to give a brief background on oil and grease the two types of lubricants that we will use in our experimental setup.

Oil is used to reduce the friction between the surfaces that are in contact with each other, which ultimately reduces the heat generated. Oil is usually found in liquid form when in room temperature, however it becomes solid when it is exposed to extreme cold temperature for a long period of time. Oil lubricant is used at high operational speeds, high temperatures, when excessive heat has to be removed from the bearing, and if there are adjacent components (shaft for example) lubricated with oil. There are many advantages of oil lubrication. Bearings lubricated with oil will exhibit less start up and running torque and have higher speed capability [2]. One disadvantage of oil is that through the life service of bearing oils are subject to losses due to evaporation unlike grease which has properties to stay effective longer [3].

Anti-friction bearings can be lubricated with either mineral or synthetic oil. Mineral oils are extracted from natural crude oil. Mineral oils are the most common and the most favoured type for lubricating rolling bearings because of the low cost of extracting the oils from crude oil. Synthetic oil is manufactured artificially. Synthetic oils are considered for bearing oil in extraordinary cases, i.e. at extreme (low or high) operating temperatures.

In addition to oil, grease can be used to lubricate bearings. American Society for Testing and Materials (ASTM) defines grease as a solid to semifluid product of dispersion of a thickening agent in liquid lubricant [4]. The main components of grease are: oil, a thickener, and additives. The base oil's task is to reduce the friction between moving surfaces. The thickener will convert the fluid to semifluid structure. Additives improve the properties of the present desired, inhibit undesirable properties, and impart new properties. Compared to oil, grease is more able to keep its shape and does not follow the shape of the container. Grease is easy to control; it stays where it is placed, can be used to keep out moisture and dirt, and can withstand heavy shock loads also. In case of long operating life with little maintenance we use grease. Bearings in some applications use oil, but grease is the lubricant of choice for 90% of bearings [5]. When greasing the bearings, the grease should be distributed evenly in the free space between the rolling elements and bearing rings.The bearings must be rotated until all the internal surfaces are covered by grease.

2.1.3 Hydraulic Loading System

In the early 1900's at the beginning of the industrial revolution, the scientific community were astonished that the science has invented a machine that has the ability to lift incredibly heavy objects that was impossible at the time. Since then, lots of advanced research have been done that provided different designs and improvements in the hydraulic loading systems field. Hydraulic loading system is a machinery system that produces work and lifts different weights using a liquid fluid. One advantage of hydraulic loading systems is its harmless to the environment according to some statistics of global market scale of hydraulic products. They operate in a clean and safe environment. Hydraulic loading systems function mainly using Pascal's principle while some uses more complex laws. In addition, some systems operate manually while others use actuator depending on the lifted weight and size. the following section provides some background of Pascal's law. Then, a section that presents the basic parts used on most of the hydraulic loading systems. Lastly, the methodology section demonstrates the different types we looked at during our market search providing each one advantages and disadvantages. Finally, the selected types design, component, operation, and maintenance will be provided.

Hydraulic loading systems are one of the most common application that uses the Pascal's principle. Fairman defines Pascal's principle as "when there is an increase in pressure at any point in a confined fluid, there is an equal increase at every other point in the container". This means that the pressure is equal at both end of any piston. So, the force over area is equal to the force over area at the other end at any closed system. Pascal's law main purpose is to translate small force into larger scaler force at a closed system using a hydraulic fluid. The figure 2.3 explains our method of calculating the force at each end of the piston.

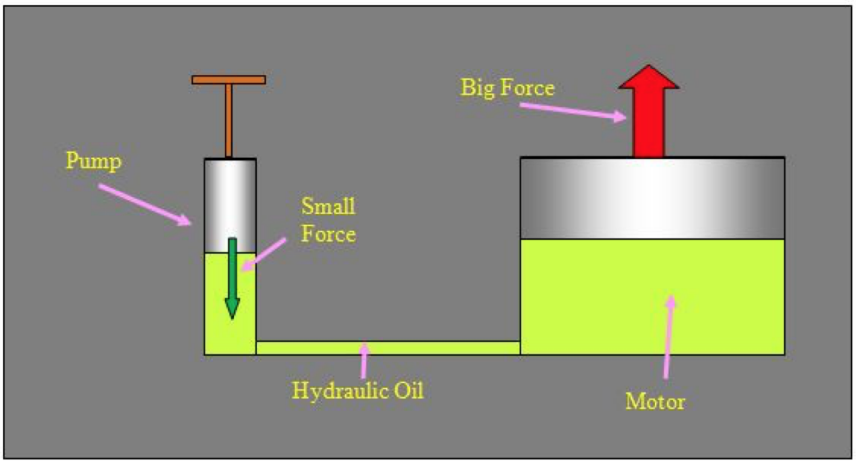

Figure 2.3 – Pascal's law

Equations 2.1 and 2.2 show the main formulae that are used in the Pascal's principle

$$P_1 = P_2 \qquad \text{(Eq. 2.1)}$$

$$F_1A_1 = F_2A_2 \qquad \text{(Eq. 2.2)}$$

Even though hydraulic systems come with different designs, types, and shapes, they all are connected with basic components. These basic components are essential to the function and principle of the hydraulic system. In other words, no hydraulic system can operate without those components. The hydraulic basic components are categorized into three main sections depending

on the function of each component. Firstly, energy converters such are hydraulic pumps, motors, and cylinders. Secondly, energy controllers that are usually called control valves. The last section of the basic components are accessories in which are usually the reservoirs, filters, accumulators, and sensors. The following is brief explanation of each component [6].

The hydraulic pump main function is to supply or move the hydraulic fluid to other components of the hydraulic system. It is one of the most essential components of any hydraulic system because it is responsible for generating the energy inside the system. They could be operated by motor or manually. They come in different shapes and sizes depending on the design of the system. One of the most common types of the hydraulic pumps are axial pumps, radial pumps, gear pumps, and vane pumps.

The second crucial component of any hydraulic system is control valve. Control valves (shown in figure 2.4) are usually found in a variety of locations in the hydraulic system. Their main responsibility is to control the pressure and the fluid flow inside the system. They also provide protection to other components such as the pump. Pressure relieve pump is a famous example of the control valves.

Figure 2.4 - Control Valve

The next important component of hydraulic loading system is an actuator. Actuator (shown in figure 2.5) main propose is operating different components of the system such as the pump. It also provides some control to the required pressure. They are usually electrical machines.

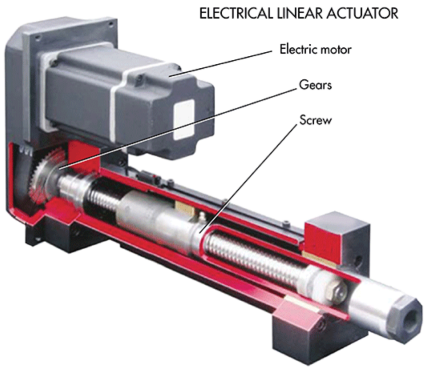

Figure 2.5 - Actuator

Accumulator (shown in figure 2.6) is a common component of any hydraulic system. Its main mission is to store the energy provided from the hydraulic pump. It also absorbs and reduces the pulsation, shocks, and noise. However, one of the drawbacks to the design of accumulators is that it requires to position vertically so the oil goes down.

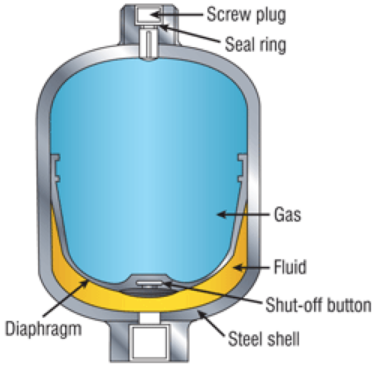

Figure 2.6 - Accumulator

Hydraulic fluid is another major component of a hydraulic loading system. The hydraulic fluid is the medium that carries the transferred power in the hydraulic loading system. Besides carrying the power thought different location of the system, the fluid main objectives are to lubricate, stabilize the shear stress, and to control the corrosion. The most common fluid types are based on mineral oil or water.

Moving on, hydraulic loading systems must contain a filter. Filters are mechanical devices that remove or hold the contaminants inside the system. They are located at several locations, usually between the pump and the cylinder. One issue that comes with filters, they must not be blocked because it will make the pump fail due to cavitation. Thus, filters should always be properly maintained in a regular basis.

Tubes, pipes, and hoses are the pathway of the hydraulic fluid inside the system. They carry the hydraulic fluid from one part to another. They have to withstand the pressure of the system. This reason makes tubes, pipes, and hoses come with different materials and sizes.

Finally, hydraulic systems must have seals. Seals main job is to connect different parts of the system together with any fluid leak. Their importance to the system that they hold they system pressure in order to have the highest possible efficiency.

2.2 Previous Work

2.2.1 Nanoparticles Additives to Oil Based Lubricant

Recently there has been a trend to use nanoparticles as an additive to oil and grease based lubricants. Nano-lubricants are showing promises in tribological properties (reducing wear and friction). Recent revolutionary research in this area is rich however done by limited researchers. It investigates the effect of nano-particle additives on the acquired vibration signal's amplitude, friction, wear, and some specific signal processing tools. Studies [7 and 8] promotes the use of nano-material based lubricants.

Studies show that different characteristics of the nanomaterials have different effects on friction, wear, and vibration. For example, stiffness and damping can be affected by lubricant film [8]. In addition, studies show that mechanical tribology (friction, wear, and vibration) depend on size, concentration, and shape of the nano-material [7 and 8]. Moreover, studies shows that different degrees of viscosity have a noticeable effect of contamination on the wear and vibration levels [9 and 10]. Furthermore, a study addresses the effect of adding nano-materials to lubricants on thermal properties of a gear box [11].

In reference [12], Apandi et. al, investigated vibration characteristics on ball bearing operated with hexagonal boron nitride (hBN) nanoparticle mixed with diesel engine oil. Results concluded that vibration amplitude was reduced by 13.5% for new bearing, 45.5% for outer defect bearing, and 2.6% for inner defect bearing. Their research has also shown that 0.2% vol. concentration of nano-particles is the best concentration in reducing vibration for all type of different bearings compared to other concentrations they implemented.

In reference [13], Prakash et. al, investigated vibration suppression characteristics of ball bearing supplied with nano-lubricant copper oxide (CuO). Their experiment was conducted with 0.2%, 0.5%, and 1%wt.. Results of the 0.2%wt. concluded that vibration amplitude of a new bearing was reduced by 29%, ball defect showed a 34% reduction, the outer defect a showed reduction of 41%. Their results also concluded that reason for the high reduction ratio was the formation of full film lubrication regime and increase of viscosity of lubricant. Furthermore, their results showed the 0.2%wt. concentration of nano-particle seems to produce more reduction in vibration compared to other concentrations.

2.2.2 Test Rig Configurations

To analyze the vibration signatures emitting from defective bearings, we had to design and assemble a test rig that will allow us to do that with high efficiency, outstanding performance, and excellent results. We looked at previously built test rigs and configurations that will help us in the design process of our own. There are a number of variants of test rigs that allow the researchers to test bearings with different operating conditions (speed, loads, and defect sizes).

We started our design by looking at advanced test rigs. A NASA research center in Ohio, called Glenn Research Center, developed a Hybrid Bearing Prognostic Test Rig (shown in figure 2.7) that evaluates the results of sensors when predicting failures of rolling element bearings for space applications [14]. This test rig analysis the failure progression (from initiation to total failure) of conventional and hybrid bearings. In addition, the test rig also tests different operating conditions including: the effects of different lubricants on bearing life, load, oil temperature, vibration, and oil debris. Figure 2.8 shows how the test bearing is placed, lubricated, and loaded.

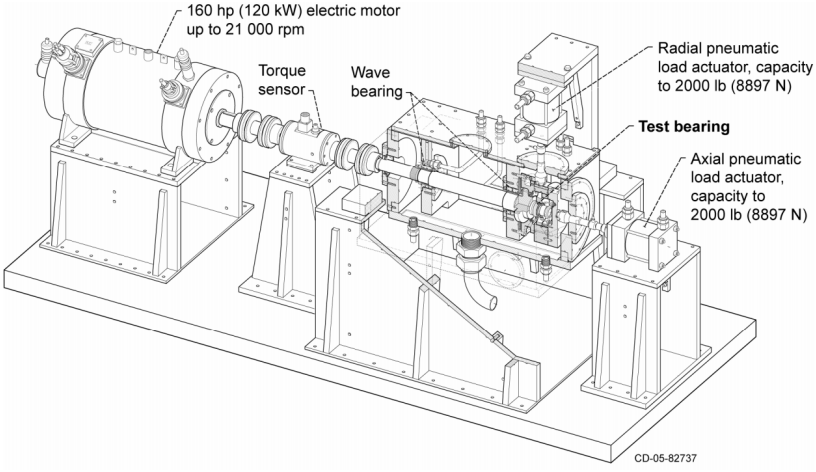

Figure 2.7 - Hybrid Bearing Prognostic Test Rig (Source: [14])

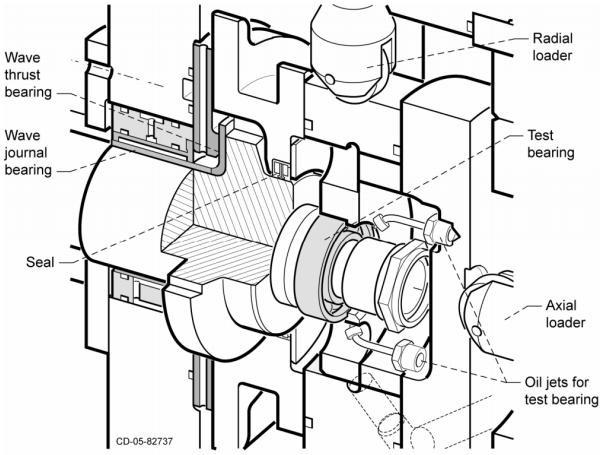

Figure 2.8 - Placement of the test bearing (Source: [14])

Further in our design process we researched other test rigs that can provide us with more ideas on how to implement different parts of our design. A test rig developed by Flack et al. (shown in figure 2.9), characterizes the static and dynamic properties of hydrodynamic journal bearings under different loads and speeds. The test facility is intended to measure the following parameters: "steady and dynamic bearing load, eccentricity/attitude angle, dynamic orbit size/phase, shaft speed, continuous oil film thickness and pressure, oil supply pressure, oil flow rate, shaft surface temperature, oil feed groove temperature, bearing outer shell temperature, housing surface temperature, ambient air temperature, oil discharge temperature, and oil reservoir temperature" [15].

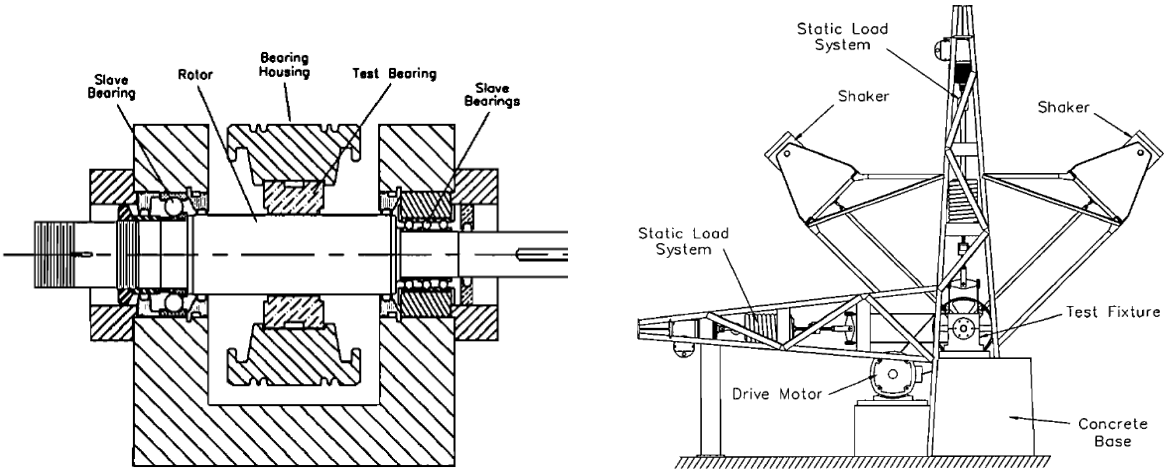

Figure 2.9 - Cross-section view (left) and Test rig view with loading systems (right) (Source: [15])

In Reference [16], Al-Ghamd et. al, conducted experiments to analyze bearing's defect identification and size estimation using accousting emissions (AE) and vibration analysis. They employed a test rig (shown in figure 2.10) with capability of testing under an operational speed range of 10 to 40,000 rpm and under a maximum load capacity of 16 kN (applied using a hydraulic ram). They selected to test on Cooper split-type roller bearings (shown in figure 2.11) because it allowed them to introduce faults to the races.

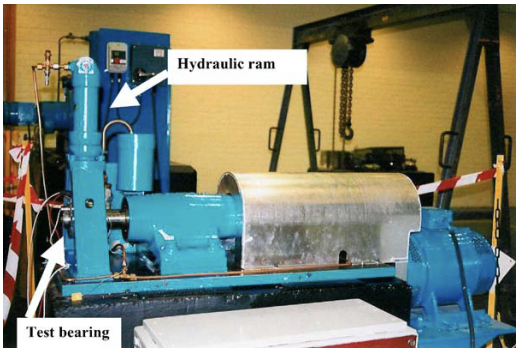

Figure 2.10 - Test Rig Setup (Source: [16])

To measure the acoustic emissions and vibration signals, two sensors were attached to the bearing's housing (shown in figure 2.11). A piezoelectric acoustic emission sensor that was able to operate with a frequency range of 100 to 1000 kHz. In addition, a resonant type accelerometer to measure vibration with a frequency response between 10 and 8000 Hz.

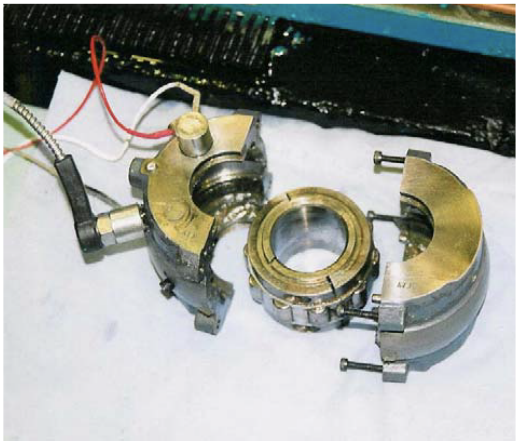

Figure 2.11 - Cooper split-type roller bearing with housing and sensors (Source: [16])

In reference [17], Choudhury et. al, also used acoustic emission to detect bearing faults and and measure vibration. They analyzed the simulated defects using the test rig shown in figure 2.12. They applied a load to the bearing housing using an aluminim lever with a load range of 0.245 kN to 1.225 kN. They selected 5 different sizes of SKF cylindrical roller bearings of NJ series with normal clearance. The sizes were NJ 202, 204, 205, 206, and 207. They selected these bearings because the inner races can be easily dismantled from the bearing and defects can be easily introduced. They carried out measurements using an AET AC 175L transducer with an operational resonant frequency of 175 kHz.

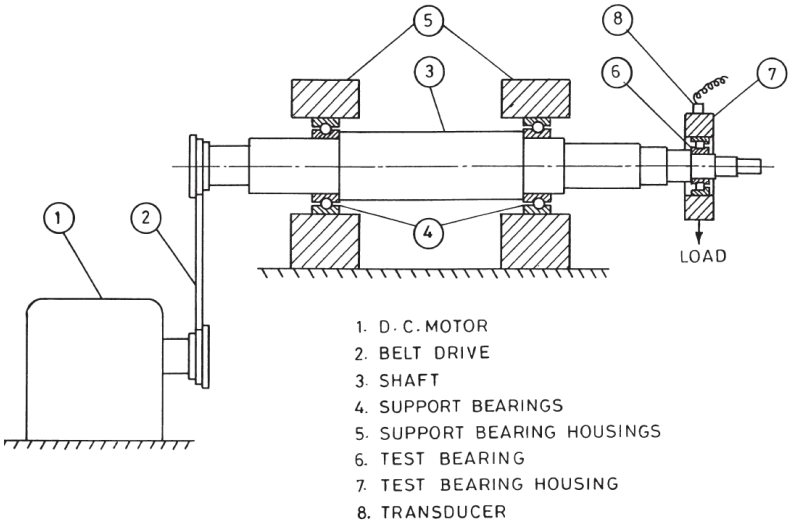

Figure 2.12 - Choudhury's Experimental setup (Source: [17])

2.2.3 Bearing Loading

Loading system have been through a number of designs. Previous students who built the test rig have designed a loading system as shown in figure 2.13. This loading system was designed to hang a static load at the end of a shaft. The load can be manually changed with increasing or decreasing the weight. The Crack Detection Rig shown in figure 2.13 is a device Cleveland State University employs at their facility. This device has the ability to perform a wide range of fault detection. The crack detection rig is built to study the fault effect of bearing, shafts, and disks.

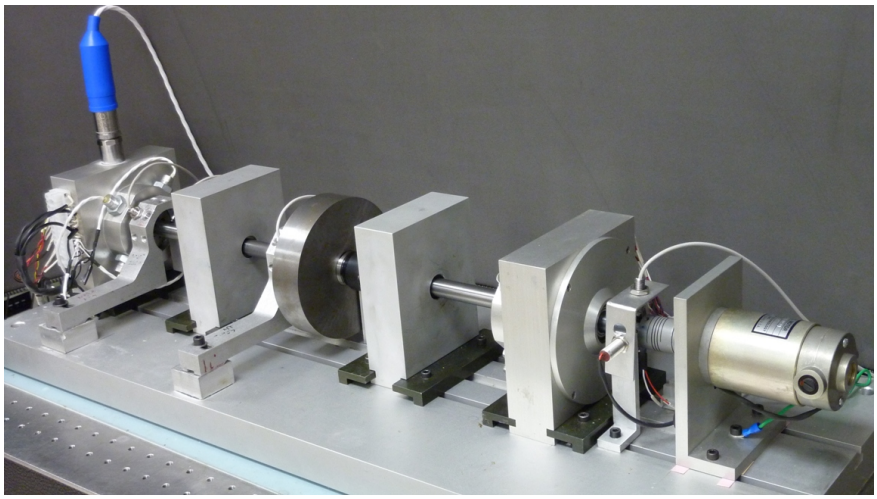

Figure 2.13 - Crack Detection Rig

As shown in figure 2.14 a design of loading system was made to test bearing using hydraulic system. The hydraulic punch applies a force from the bottom to the test part. This device as the article indicate [18] focused on crank shaft slider bearings of large engines.

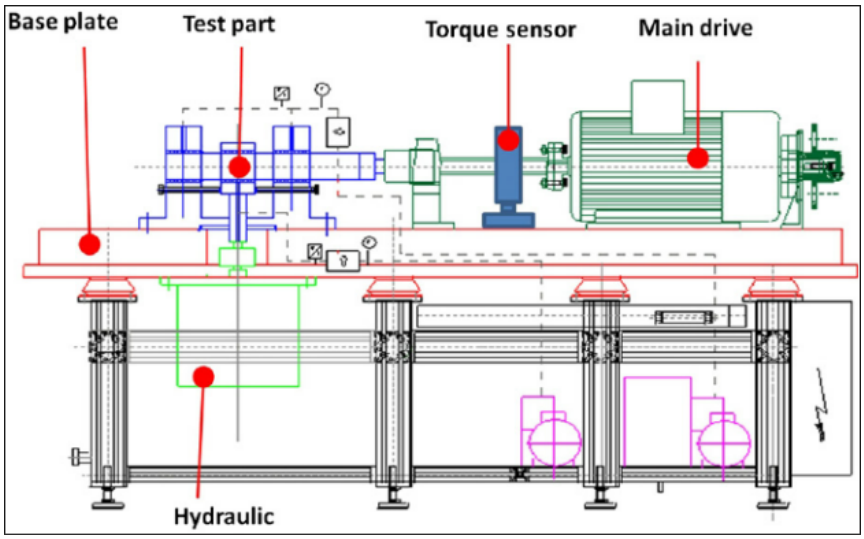

Figure 2.14 - Test rig to test crankshaft slider bearings (Source: [18])

THISBE is the name of the test rig that SKF has developed to test for high-speed bearings by simulating dynamic load conditions [19]. The test rig shown in figure 2.15 is also able to test for static loading vertical and axial using hydraulic press.

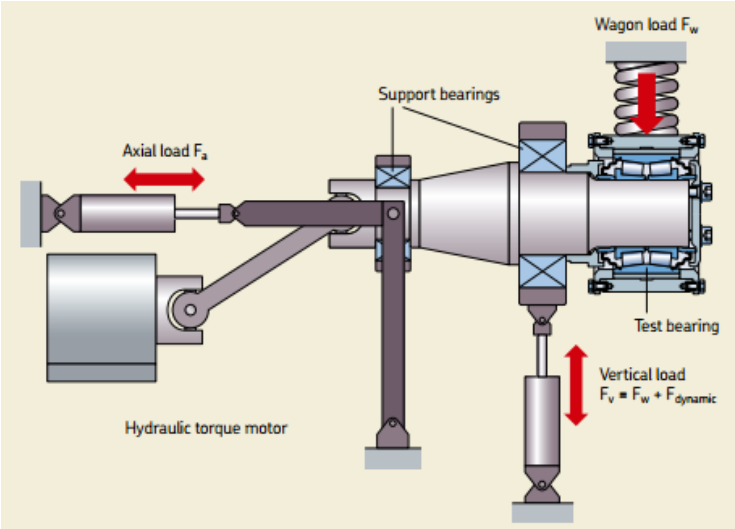

Figure 2.15 - THISBE (test rig for high-speed bearings) (Source: [19])

2.2.4 Bearing Lubrication

Previous work has been conducted to study the effect of lubricant viscosity on the vibration of roller bearings by Serrato et. al [9]. The experiment was performed on NU205 bearings (shown in figure 2.16). The bearings were lubricated with mineral oil, however, without using nano-additives. Different lubricant's grade of viscosity was tested, including: ISO 10 (V1), ISO 32 (V2) and ISO 68 (V3). The vibration was resolved through the preparing and investigation of bearing vibration information, gotten from each of the oil conditions, amid 2 h of trial for temperature adjustment and under a few bearing shaft speeds. The connected spiral load was 10% of the bearing ostensible load. Through root mean square (RMS) investigation of the vibration signals, it was conceivable to recognize particular recurrence groups regulated by the adjustment in oil consistency, which was identified with change in oil film thickness [9].

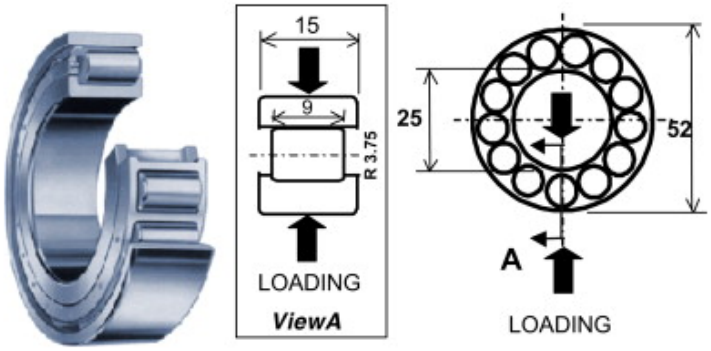

Figure 2.16 - Geometry of NU205 rolling bearing used in the tests

Figure 2.17 shows the equipmental setup they employed to perform the tests.

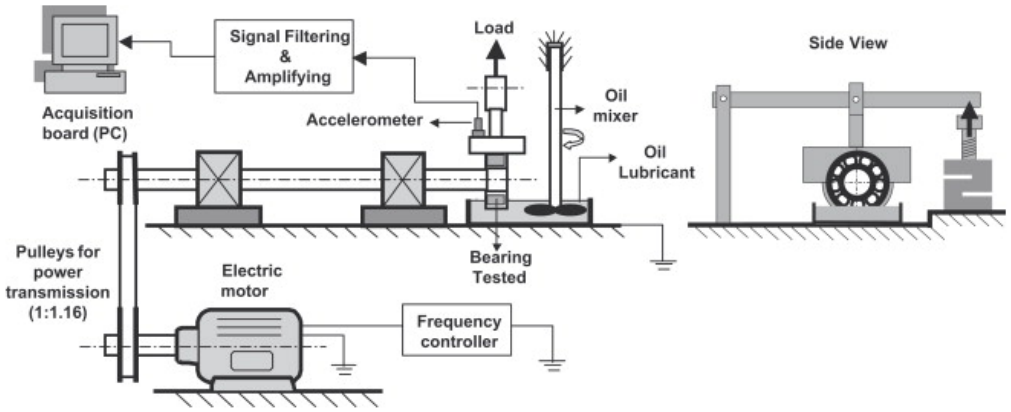

Figure 2.17 - Test rig (source: [9])

Figure 2.18 shows oil temperature for the tested viscosities. A gradual increase in temperature can be observed during the first hour of test and a trend of stabilization in the second hour. According to technical publications of rolling bearings manufacturers [20,21], both increase and stabilization of temperature occur with any type of rolling bearing, and the stabilization is due to equilibrium between production and dissipation of heat in the system.

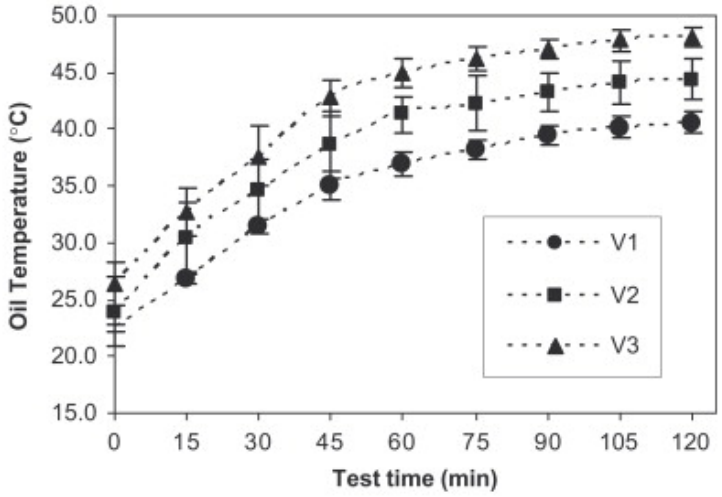

Figure 2.18 - Oil temperature as a function of time. V1: ISO 10; V2: ISO 32; V3: ISO 68.

The result shows that the behavior of the oil film thickness in each viscosity is different. The values of the minimum theoretical oil film thickness are shown in figure 2.19, for all the tested viscosities. The values correspond to the minimum film thickness between the inner race and the roller, which represents the most critical tribological contact in the rolling bearing. Dowson equation [22] was used for film thickness calculation.

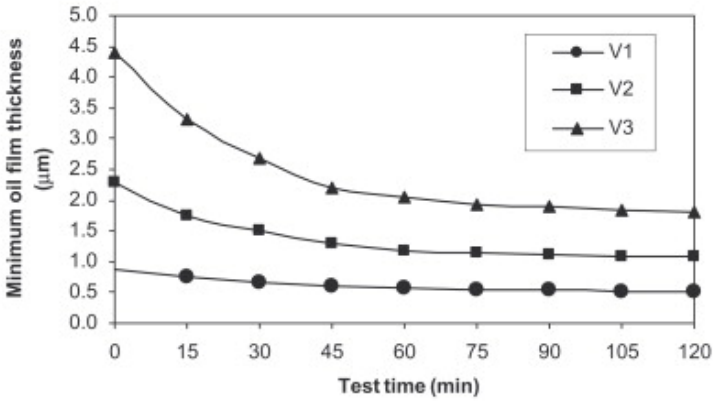

Figure 2.19 - Minimum theoretical oil film thickness

Comparative studies from Mohammed Modu Aji had been studied between bio lubricant from jatropha and neem oil and mineral lubricant [23]. The integral steps required are the methodology, and characterization. The methodology to be used in carrying out the process are: sourcing raw materials, raw material preparation, oil extraction, and modification. The characteristics are: viscosity, viscosity index, refractive index, sulphated ash, acid value, pour point, density, color, Flash point. The instruments and equipment to be used in carrying out the process are: deep freezer, analytical balance capable of determining weights to three decimal places, soxhlet extractor, conical flasks, graduated cylinders, 100 and 500 ml beakers, round bottom flasks, stirrer, refractometer, viscometer, retort stand and clamps, thermometer, furnace, crucible, temperature controlled water bath, pipettes, burette, and test tubes. The properties of the bio-lubricant which are pertinent to lubricity are the viscosities at 40 and 100°C, viscosity index, flash point and the pour point (°C). Table 2.1 shows these parameters.

Table 2.1 - Characteristics of Neem Oil, Jatropha Oil Bio-Lubricant and Engen Super 20w/50

S/NO	PROPERTIES	NEEM OIL BIO LUBE	JATROPHA BIO LUBE	ENGEN SUPER
1	VISCOSITY @ 40°C	190	230	175
2	VISCOSITY @ 100°C	70	140	19.4
3	VISCOSITY INDEX	397	539	127
4	REFRACTIVE INDEX	1.4672	1.4689	1.4815
5	SULPHATED ASH	0.018	0.038	1.000
6	ACID VALUE/TOTAL BASE	1.6	3.9	10.5
7	POUR POINT	1.3	0.2	-30
8	DENSITY	138.8	154.3	90
9	COLOUR	Light brown	black	Light brown
10	FLASH POINT	262	274	234

As a result, neem oil bio lubricant was discovered to have a viscosity of 190 cp at 400C and 70 cp at 1000C, while jatropha oil bio lubricant was having a viscosity of 230 cp at 400C and 140 cp at 1000C. The viscosities of the bio-lubricants were found to be slightly higher than those of the mineral lubricant but could meet the requirement of the ISO VG 46 since its viscosities are within the standard ISO VG 46 range [24]. The viscosity index obtained for Jatropha biolubricant was 539.57, neem oil bio lubricant was 397.62 and it is comparable to other plant based bio lubricant.

2.2.5 Vibration Analysis

Vibration analysis has gained wide acceptance among researchers and engineers to utilize it as a major tool to monitor the health of rotary machines. Unlike other nondestructive testing methods, vibration analysis can provide a definite diagnosis to the source and location of any emerging fault. The vibration spectrum analysis is a popular technique among others such as time domain and time frequency domain for tracking machinery operating conditions. In recent years, intensive research [25, 26, and 27] has been done for rolling element bearings defect diagnosis to ensure performance and extend the bearing life.

In reference [28], Sutrisno et. al, experiments were conducted on 17 ball bearings to test and estimate the Remaining Useful Life (RUL). Their testing was based on three main conditions:

Condition 1: seven ball bearings operated at 1800 rpm with 4 kN radial load.
Condition 2: seven ball bearings operated at 1650 rpm with 4.2 kN radial load.
Condition 3: three bearings operated at 1500 rpm with 5 kN radial load.

Following the above conditions, Sutrisno et. al collected data samples at 10 second intervals at a 25.6 kHz sampling rate and 0.1 second duration by mounting two accelerometers on the bearing housing to measure vibration in the vertical and horizontal directions. Sutrisno et. al were able to develop three methodologies that used both frequency and time domains which included: root mean square, peak, crest factor, and kurtosis of the vibration signals. The three methodologies were: “Moving Average Spectral Kurtosis and Bayesian Monte Carlo”, “Soft Computing Model with Support Vector Regressor”, and “Vibration Frequency Signature Anomaly Detection and Survival Time Ratio”. They concluded that method three was the most accurate overall among the three methods.

In reference [29], Janjarasjitt et. al, introduce a modified form of a Correlation Integral Algorithm, which they call Partial Correlation Integral. The algorithm they developed is able to analyze vibration data obtained while a life test of a rolling element bearing is running. Janjarasjitt et. al, combined their algorithm with a surrogate data testing technique, which introduces a huge advantage over other techniques. This combination does not require any information about the type of bearing, operating conditions such as speed and load, or fault type. Their experimental setup is shown in figure 2.20.

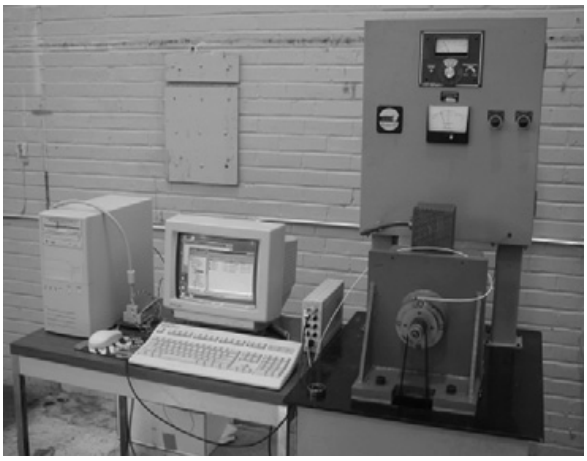

Figure 2.20 - Bearing condition diagnosis and prognosis experimental setup

In Janjarasjitt's study, two 6204 2RS1 SKF bearings were mounted on the shaft of the test system, which were introduced to an axial load of 154.22 kg. Vibration data were received from two PCP 353C65 sensors, one was stud mounted and the other was magnetically mounted (as shown in figure 2.21).

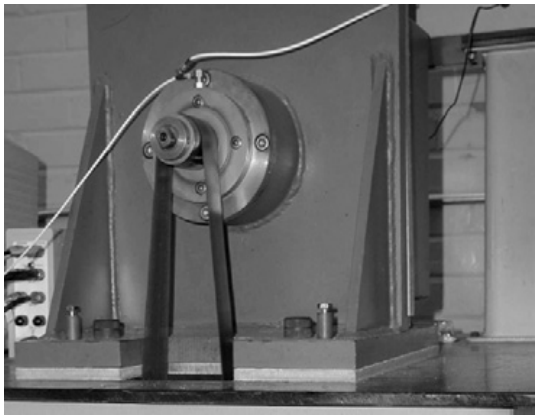

Figure 2.21 - Sensors mounted on bearing housing

Time domain analysis technique is one of the most used techniques to analyze vibration signal waveform for it's simplicity and ease of use. Time domain analysis is the process in which statistical features are computed from the vibration data. The statistical methods that are used in this work is Root Mean Square (RMS) and Kurtosis (Kt). The time domain graph contains many layers of signals (shown in figure 2.22). We used Fast Fourier Transformation (FFT) to filter noise and other deterministic components.

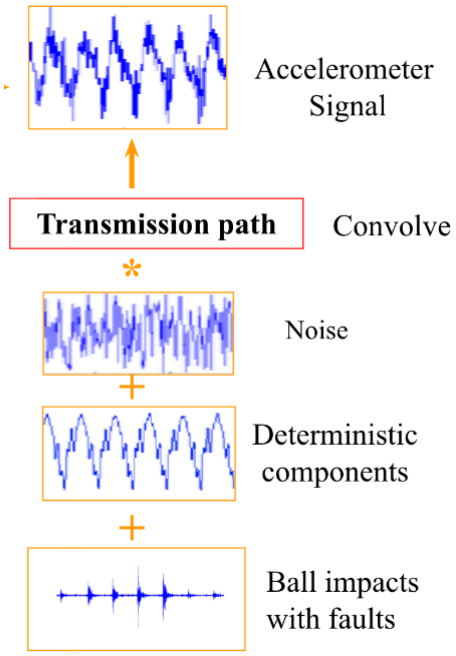

Figure 2.22 - Accelerometer signal layers

CHAPTER 3

System Design

In this section of the report, we are presenting how we approached designing of the new and modified test rig including the constraints we faced, the methodology of our design, the calculations, selection of components, and subsystems of our test rig.

3.1 Design Constraints

While designing our new test rig, we faced constraints and different limitations that we had to work on so that our test rig will be economically efficient, modular, easy to manufacture and repair, safe to use, meet operational standards of the bearings, allow experimentation without errors, and grant effortless future improvements and modifications. The following are clearly stated constraints that will allow future design implementation to be consistent with our design and follow the same criteria.

3.1.1 Testing

To analyze the vibration signature of the rolling element bearings we are utilising piezoelectric-type sensors and signal processing tools. We have attached a low-cost accelerometer (Industrial ICP® Model 603C01) to the bearing housing to receive the vibration signals emitting from the bearing. The accelerometer data sheet can be found in figure 3.1. In addition, we attached a thermocouple to analyze the temperature readings during the operation. Next, we will utilise NI's LabVIEW to present and export vibration signal data. Finally, we are also utilising MATLAB to produce graphs that will show the vibration signal.

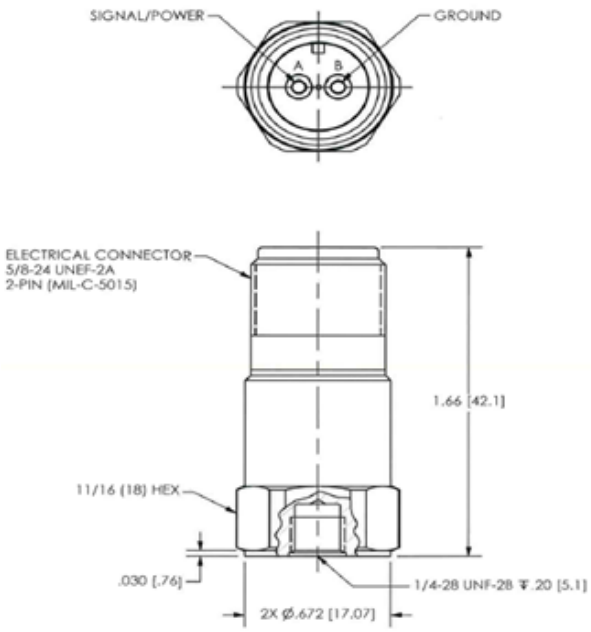

- **Sensitivity:** (±10%) 100 mV/g (10.2 mV/(m/s²))
- **Frequency Range:** (±3dB) 30 to 600000 cpm (0.5 to 10000 Hz)
- **Measurement Range:** ±50 g (±490 m/s²)
- **Weight:** 1.8 oz (51 gm)
- **Electrical Connector:** 2-Pin MIL-C-5015

Figure 3.1 - Industrial ICP® Accelerometer Model 603C01 data sheet

3.1.2 Bearing size

Our selection of the bearing mainly depended on the shaft diameter and ability of introducing simulated defects (explained further in section 3.4.1). The test bearings must be stable (do not jerk under high load/speed) and fit the shaft without any wiggle room. Since the outer diameter of our shaft is 30 mm, we matched the inner diameter of the bearing to that of the outer diameter of the shaft. Detailed bearing dimensions can be found in section 3.4.1 of this report. Moreover, we needed the bearings to have the ability to be dismantled for introducing simulated defects.

3.1.3 Speed Range

Following the standards published by SKF, the bearings must operate under a maximum speed of 8000 rpm with grease lubricant and 11000 rpm with oil lubricant. Therefore, we designed our pulley system to operate under three different speed ranges: 1700 rpm, 3400 rpm, and 6800 rpm.

3.1.4 Loading

Following the standards published by SKF, it is crucial that the bearings operate under maximum dynamic & static load of our bearing. The basic dynamic load rating of the bearing is 22.5 kN, and the maximum static loading is 8.75 kN. Our experiment is going to operate under 4.5 kN.

3.1.5 Physical

Our test rig table is 800 mm in length, 300 mm in width, and 30 mm in thick. As shown in figure 3.3 below, we will place our motor, shaft, bearing, bearing housing, plummer block bearing, pulleys, sensor, and other equipment on this table. The old test rig is shown in figure 3.2.

Figure 3.2 - Old test rig

We selected some materials and fabricated others. Oil tank, casing, and the table are the fabricated materials, while hydraulic pump, hydraulic jack, and pressure gauge are the selected materials.

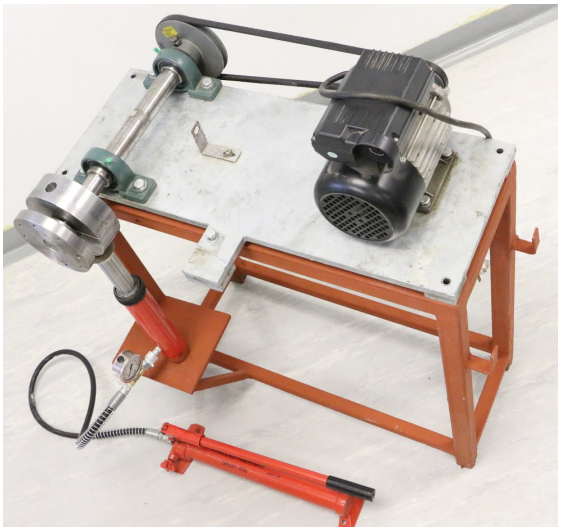

Figure 3.3 - New and modified test rig

3.2 Design Methodology

While designing a new modified test rig, we went through many iterations of designs and prototypes to reach the highest quality possible, simplify manufacturability and assembly, and use an automated loading system for more accurate results.

3.2.1 Bearing Housing and Oil Tank

When designing the housing and oil tank we kept in mind a few needs: protection, durability, dimensions, movement of the bearing, holding/keeping the bearing in place, sustainability, manufacturability, ease of maintenance and assembly, cost, and the environment. We decided to design and build a bearing housing to improve safety while conducting the experiment, function as a holder for the bearing, and an attachment location for the sensor. In addition, the housing will host the loading system which will be directly attached to the housing joining the hydraulic jack's piston to the bearing. Furthermore, we designed the oil tank for two main purposes: to enable continuous lubrication of the bearing and mixing of the nano-additives to the lubricant.

To attach the housing and tank we went through numerous stages and designs to try and perfect the design. In each prototype, we tried to enhance the quality, manufacturability, and ease of assembly while solving issues that appeared at every stage.

The first design (shown in figure 3.4) is a circular housing, a rectangular oil tank, and a hydraulic piston all welded together.

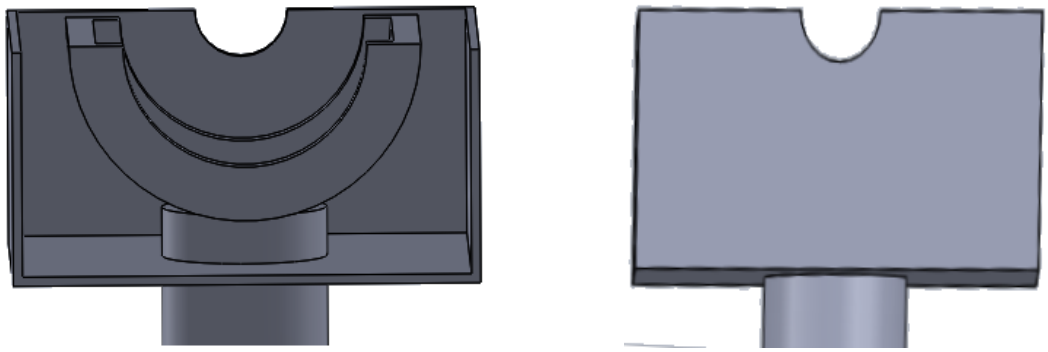

Figure 3.4 - CAD drawing of the first design of bearing housing and oil tank

This design needed many improvements as the oil tank's volume was exceeding our needs by holding more oil than we required leading to more nano-particles additives used. Moreover, the rectangular design of the tank causes the lubricant and nano-particles to latch and form residue in the corners.

Taking a second approach to the design we focused on solving the issue of the oil and nano-particles sticking and forming residue in the corners. Moreover, the second design needed to contain less volume to decrease the amount of oil and nano-particles used which will decrease the overall cost. The second design (shown in figure 3.5) was a circular bearing housing and tank, thus bettering the lubricant flow.

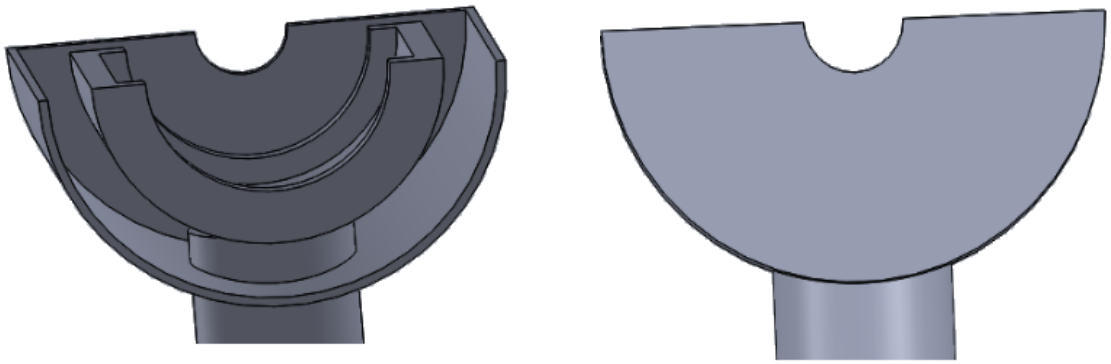

Figure 3.5 - CAD drawing of the second design of bearing housing and oil tank

After completing this design, we discovered that the volume is still above our requirements. Thus, a pump will be needed to circulate the oil, leading to external vibrations causing disturbances in the experiment results.

In order to reduce the amount of oil, a third design (shown in figure 3.6) has been made. The third design improves two more issues: less lubricant volume and removing the need of a pump. This design enables self-circulation as the bearing balls allow a smooth flow of the lubricant.

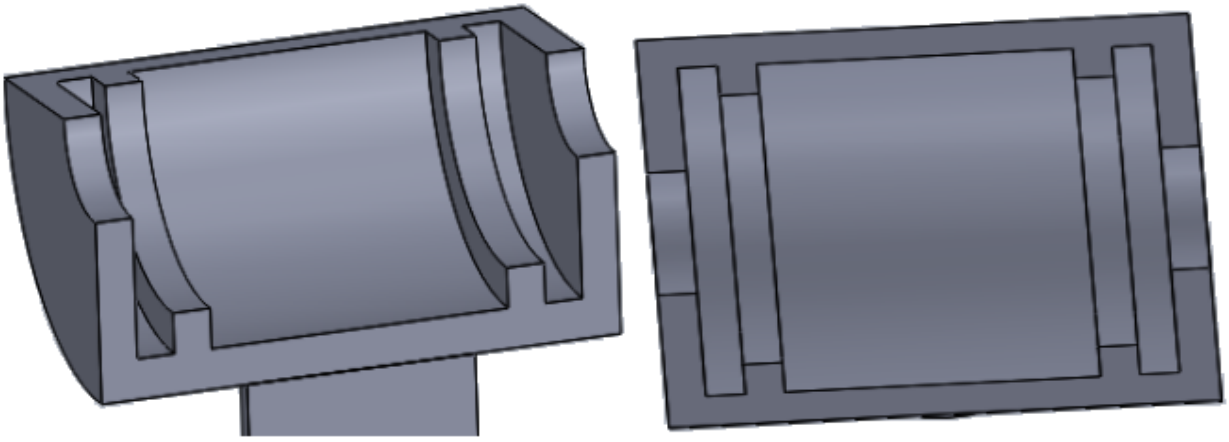

Figure 3.6 - CAD drawing of the third design of bearing housing and oil tank

This design shows the best housing between the three current designs. However, a new issue surfaced. This design, provides obstacles when we try to drain and replace the oil, this is because, the housing is welded to the piston. Therefore a fourth and final design is needed to finalise the design of the bearing housing and by adding some modifications. The final design allows easy drainage and replacement of the oil, easy cleaning of the oil, and eliminates the residual stress that is caused by the weldment of the hydraulic jack's piston to the oil tank. The final design can be found in section 3.5.1 of this report.

3.2.2 Hydraulic Loading System

To apply load to the bearings in our experiment setup we looked at numerous ways to do so. We looked at static hanging loading, dynamic loading (i.e. a disk with unbalanced forces), a hydraulic ram, levers, and hydraulic jack. We finally landed on the decision after careful consideration to use a static hydraulic loading system. In this section of the report we discuss our approach on choosing the type of static hydraulic loading system that we will employ to apply load to the bearings.

We started to look at types of hydraulic presses to load the bearings. Hydraulic press (shown in figure 3.7) is a device used widely today in industry for different purposes such as forging, coining, metal forming, punching, and blanking. This tool has the ability to generate a high compressive force by applying pressure to fluid. In simple words, hydraulic press uses a small piston to lift a large piston applying Pascal's' principle.

Figure 3.7 – A typical hydraulic press

We considered employing a hydraulic press because it has a simple, complete design. Hydraulic presses that are sold in the Saudi market come with pre-existing pressure gages that will help us read the amount of force we are applying to the bearings. However, we needed to select a better hydraulic loading system because hydraulic presses are heavy and exceeds our budget. Thus, we had to look at other alternatives.

We then looked at hydraulic jacks/screw jacks (shown in figure 3.8). Hydraulic jack is a hydraulic loading system machine that lifts high weights using a small force. The most famous use for the jack is lift the cars to replace flat tires. We considered using a hydraulic jack because of its cheap price and its abundance in the market. Unfortunately, hydraulic jacks with pre-existing pressure gages is not available in the Saudi market. Therefore, fabrication is needed to attach a pressure gage to the jack. As previously explained, the pressure gage is required in order to know the force we are applying to the bearing. We had to search for a workshop that could fabricate our pressure gauge to the jack, we found that it is impossible to do so because it would affect the jack efficiency. Consequently, we had to look for another design of hydraulic system.

Figure 3.8 – Hydraulic Jack

We finally decided to utilise a hydraulic body-frame repair kit (shown in figure 3.9) as our hydraulic loading system. Hydraulic body-frame repair kit is an excellent choice because it has many uses in the industrial field. Its simple and modular design is what made this system special. The reasons why we selected this system are presented in section 3.4.4 of the report.

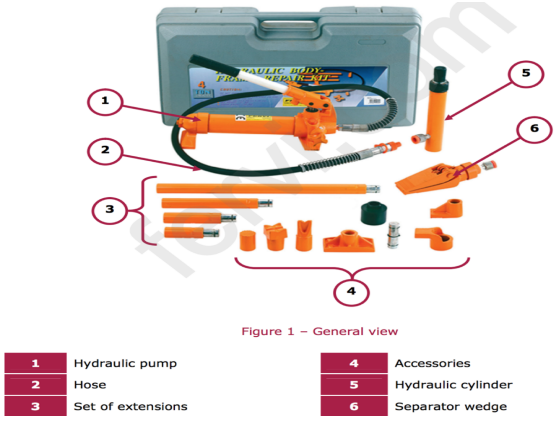

Figure 3.9 – Hydraulic Body-frame Repair Kit

3.2.3 Pulleys and Belts

Pulleys and belts are meant to transmit the motor force to the shaft. There are a number of pulleys and belts as shown in figure 3.10. In our test rig design we consider to use one of two options either with round belt or V-belt (shown in figure 3.11). According to Precision Industrial Components, round belts are used for low-load and low-torque applications [30]. In our experiment we are looking for a belt that can operate under high torque. Therefore we decided to choose V-belts because it meets our requirements regarding efficiency, horsepower range, low vibration between driver and driven pulleys, and oil and heat resistance [31].

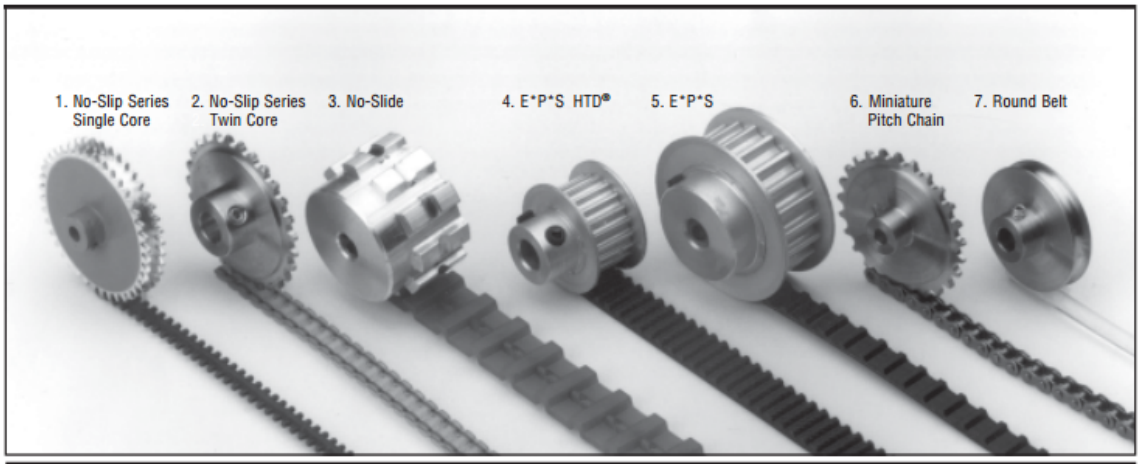

Figure 3.10 - Types of pulleys and belt (Source [30])

The main V-belt components are:

1) **Belt body** made of a special rubber compound which provides, due to its excellent mechanical characteristics, high transmission efficiency and assures a minimum rubber wear off;
2) **Tensile member** consisting in high-strength low-stretch cords, which grant length stability over the belt life time;
3) **Fabric jacket or cover** made of fabric, protecting the tensile member and permitting the use of back side idler.

Figure 3.11 - V-belt components (Source [31])

3.3 Calculations and Design Verification

In this section we made a comparison between previous students work calculation with the new updated modified changes calculation.

3.3.1 Previous Pulley Calculations

Previous students have done the calculation as shown below. In order to make sure we have done our calculation to compare with the previous work. The differences between our work and previous work is that they use two pulleys on the shaft. One pulley with 150 mm outside diameter and the other is 300 mm outside diameter. While our calculation will have 15 cm on the shaft and 75 mm on the motor. Than we flip the pulleys to 150 mm on the motor and 75 mm on the shaft.

Table 3.1 - Pulley Available data

Available Data	
Motor Pulley Diameter	75 mm
Shaft Pulley Diameter	150 mm
Coefficient friction of motor pulley	$\mu = 0.25$
Coefficient friction of shaft pulley	$\mu = 0.20$
Shaft to shaft Center Distance	512.5 mm
Motor speed	3400 rpm
Power transmission	1.5 Kw
Density belt	1000 kg/ m^3
Belt thickness	11 mm
Allowable stress for the belt	2 MPa

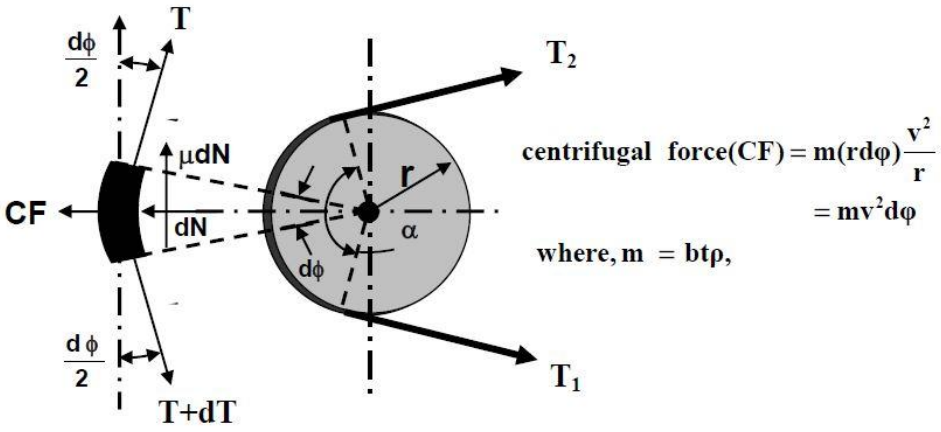

Figure 3.12 - Forces created by a belt

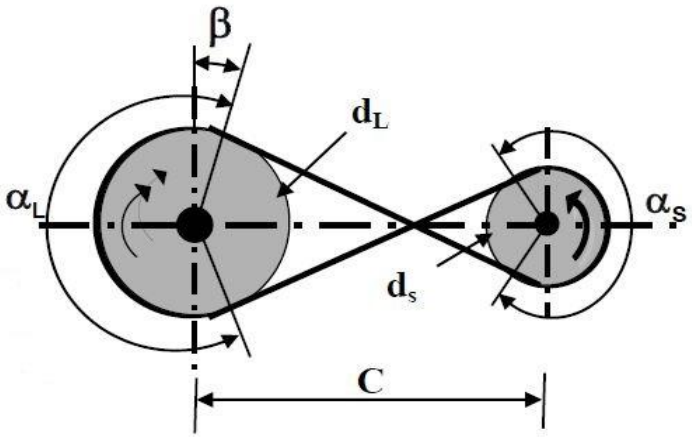

Figure 3.13 - Angles Forces created by a belt; cross loop belt

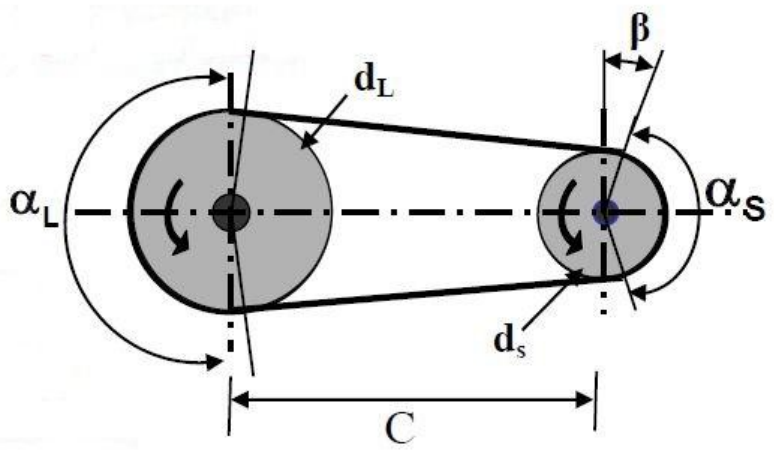

Figure 3.14 - Angles Forces created by a belt; open loop belt

$$\beta = sin^{-1}\left(\frac{d_L - d_s}{2C}\right) = sin^{-1}\left(\frac{15-7.5}{2*51.25}\right) = 4.196^{\circ} \quad \text{(Eq. 3.1)}$$

$$\alpha_L = 180 + 2\beta = 188.4^{\circ} = 3.288\ Rad \quad \text{(Eq. 3.2)}$$

$$\alpha s = 180 - 2\beta = 171.4° = 2.99\ \text{Rad.} \quad \text{(Eq. 3.3)}$$

$$L\ (\text{open}) = \frac{\pi}{2}(d_L - d_S) + 2C + \frac{1}{4C(d_L - d_S)^2} = 1.381\ m = 1381\ mm \quad \text{(Eq. 3.4)}$$

$$\text{Velocity} = \frac{\pi \times d_S \times rpm}{60 \times C} = 26.05\ m/s \quad \text{(Eq. 3.5)}$$

$$\text{Mass of belt} = bt\rho = \frac{b}{10^3} \times \frac{11}{10^3} = 0.011b\ kg/m^2 \quad \text{(Eq. 3.6)}$$

$$m \times v^2 = 7.464b\ N \quad \text{(Eq. 3.7)}$$

Now, (Eq. 3.8)

$$\mu_S \times \alpha_S = 0.20 \times 2.99 = 0.7475$$

$\mu_L \times \alpha_L = 0.25 \times 3.288 = 0.6576$ (Eq. 3.9)

So, our design will be governed by the large pulley (shaft pulley)

$$\frac{T_1 - 7.464b}{T_2 - 7.464b} = e^{0.6576} = 1.93$$ (Eq. 3.10)

Power equation

$$P = (T_1 - T_2) \times v \implies \frac{P}{v} = (T_1 - T_2) = 57.58\ N$$ (Eq. 3.11)

Stress = $\frac{F}{A}$

$$2\ MPa = \frac{F}{5 \times 10^{-6}} \implies F = 10\ N$$ (Eq. 3.12)

Again: (Eq. 3.13)

$$T_1 = 2 \times b \times 10\ N \implies T_1 = 10b$$

(Eq. 3.13) into (Eq. 3.10) (Eq. 3.14)

$$\frac{10b - 7.464b}{T_2 - 7.464b} = 1.93$$

Again (Eq. 3.13) into (Eq. 3.11) : (Eq. 3.15)

10b – T2 = 57.58

Now, (Eq. 3.15) into (Eq 3.14) (Eq. 3.16)

$$\frac{10b - 7.464b}{10b - 57.58 - 7.464b} = 1.93$$

b = 47.119 mm (Breadth of the belt)

from (Eq. 3.13)

$T_1 = 10 \times 0.047119 = 0.47119\ N$

$T_2 = 0.47119b - 57.58 = 57.109\ N$

Thus;
The torque on the shaft is:
Torque $T = F \times D = 56.638 \times 0.15 = 8.5\ N.m$ (Eq. 3.17)

And the moment is: (Eq. 3.18)
$M = 28.32 \times 0.04 = 1.133\ N.m$

$$C\ (\text{shaft radius}) = \left[\left(\frac{2}{\pi \times allowable\ stress}\right) \times \sqrt{M^2 + T^2}\ \right]^{\frac{1}{3}} \quad \text{(Eq. 3.19)}$$

$$C\ (\text{shaft radius}) = \left[\left(\frac{2}{\pi \times 80\ MPa}\right) \times \sqrt{1.133^2 + 8.5^2}\ \right]^{\frac{1}{3}} = 4.09 \times 10^{-3}\ m$$

So the diameter = 8.173 mm

Using Safety Factor = 3 >>>> this means that the shaft diameter will be:

8.173 * 3 = 24.519 mm.

3.3.2 New Modified Pulley Calculations

According to Precision Industrial Components [19] we can calculate the length of the belt for open and close loop using equation below.

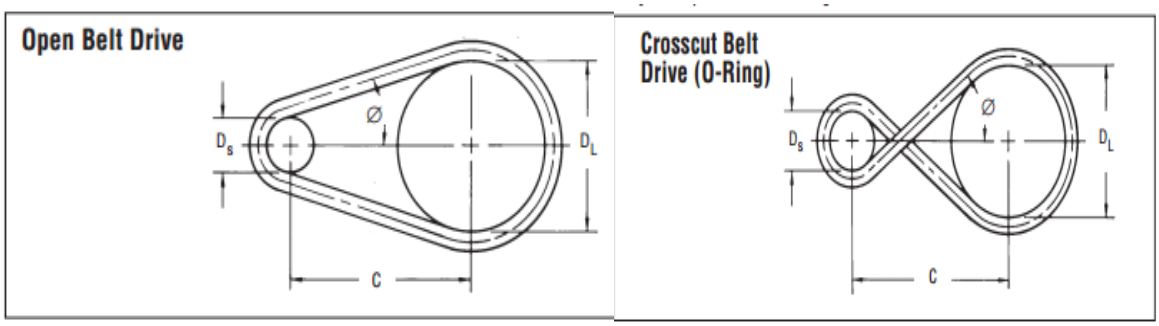

Figure 3.15 - Open belt and Crosscut belt (Source [19])

For pulleys ratio of 1:2 and 2:1 the length of the belt is:

$$\theta = sin^{-1}\left(\frac{d_L - d_s}{2C}\right) = sin^{-1}\left(\frac{15-7.5}{2*51.25}\right) = 4.196^{\circ} \quad \text{(Eq. 3.20)}$$

$$L = \frac{\pi}{2}(D_L + D_S) + \frac{\pi\theta}{180}(D_L - D_S) + 2C\ cos\theta \quad \text{(Eq. 3.21)}$$

$$= \frac{\pi}{2}(15 + 7.5) + \frac{\pi * 4.196}{180}(15 - 7.5) + 2 * 51.25 * cos(4.196)$$

Length of the belt = 1381 mm *(Source [19])*

The RPM to Linear Velocity formula is :

v = r × RPM × 0.0010472

Motor:

$$\omega = \frac{RPM \times 2\pi}{60} = \frac{3400 \times 2\pi}{60} = 356.047\ Rad/s \quad \text{(Eq. 3.22)}$$

Torque is:

$$T = \frac{P_{out}}{\omega} = \frac{1500}{356.047} = 4.2129\ N.m \quad \text{(Eq. 3.23)}$$

RPM to Linear Velocity formula is :

v = r × RPM × 0.0010472

For pulleys 75 mm:

$$v = r \times RPM \times 0.0010472 = \frac{75}{10 \times 2} \times 3400 \times 0.0010472 = 13.3518\ m/s \quad \text{(Eq. 3.24)}$$

For pulleys 150 mm:

$$v = r \times RPM \times 0.0010472 = \frac{150}{10 \times 2} \times 3400 \times 0.0010472 = 26.7036\ m/s \quad \text{(Eq. 3.25)}$$

Shaft:

For pulleys 150 mm at ration of 1:2

$$\omega = \frac{RPM \times 2\pi}{60} = \frac{1700 \times 2\pi}{60} = 178.0236 \text{ Rad/s} \quad \text{(Eq. 3.26)}$$

Torque is:

$$T = \frac{P_{out}}{\omega} = \frac{1500}{178.0236} = 8.4258\ N.m \quad \text{(Eq. 3.27)}$$

$$v = r \times RPM \times 0.0010472 = \frac{150}{10 \times 2} \times 1700 \times 0.0010472 = 13.3518\ m/s \quad \text{(Eq. 3.28)}$$

For pulleys 150 mm at ration of 1:1

$$\omega = \frac{RPM \times 2\pi}{60} = \frac{3400 \times 2\pi}{60} = 356.047 \text{ Rad/s} \quad \text{(Eq. 3.29)}$$

Torque is:

$$T = \frac{P_{out}}{\omega} = \frac{1500}{356.047} = 4.2129\ N.m \quad \text{(Eq. 3.30)}$$

$$v = r \times RPM \times 0.0010472 = \frac{150}{10 \times 2} \times 3400 \times 0.0010472 = 26.7036\ m/s \quad \text{(Eq. 3.31)}$$

For pulleys 75 mm at ration of 2:1

$$\omega = \frac{RPM \times 2\pi}{60} = \frac{6800 \times 2\pi}{60} = 712.0943 \text{ Rad/s} \quad \text{(Eq. 3.32)}$$

Torque is:

$$T = \frac{P_{out}}{\omega} = \frac{1500}{712.0943} = 2.1065\ N.m \quad \text{(Eq. 3.33)}$$

$$v = r \times RPM \times 0.0010472 = \frac{75}{10 \times 2} \times 6800 \times 0.0010472 = 26.7036\ m/s \quad \text{(Eq. 3.34)}$$

3.3.3 Shaft Calculations

As a result of the circular section of the shaft, it can be subjected to cyclic or fatigue stress, which is caused by combined bending and torsional load.

The three major fatigue methods used in design and analysis are the stress-life method, the strain-life method, and the linear-elastic fracture mechanical method. The following numerical calculations are based on the stress-life method for its wide range implementation for a wide range of design application, plentiful supporting data, and adequate representation of high cycle application.

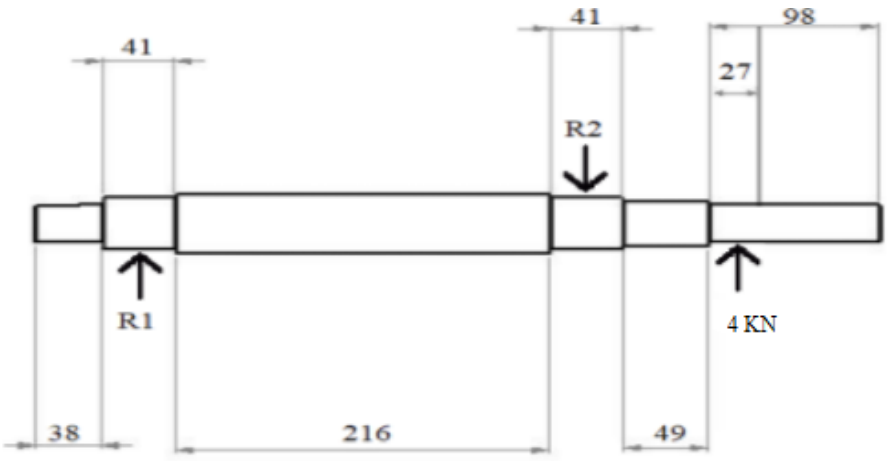

Figure 3.16 - Free Body diagram of the shaft

$$\Sigma F_y = 0$$

$$R_2 - R_1 = 8.75kN$$

$$\Sigma M_{R_1} = 0$$

$$R_1(20.5 + 216 + 20.5) = 8.75(13.5 + 49 + 20.5) \quad \text{(Eq. 3.35)}$$

$R_1 = 2.83kN$ By substituting into

$$R_2 = -11.58N \quad \text{(Eq. 3.36)}$$

The force and moment diagrams (figures 3.17 and 3.18) are shown below.

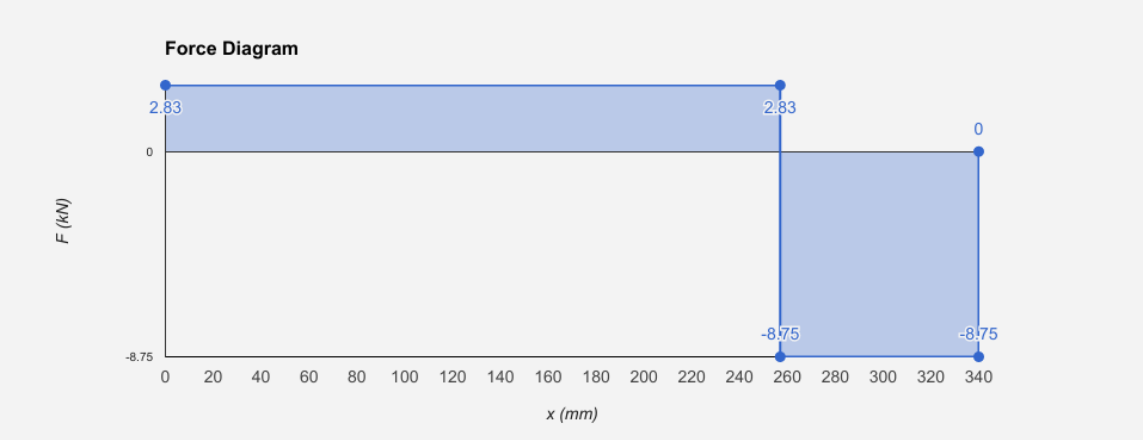

Figure 3.17 - Force diagram of the shaft

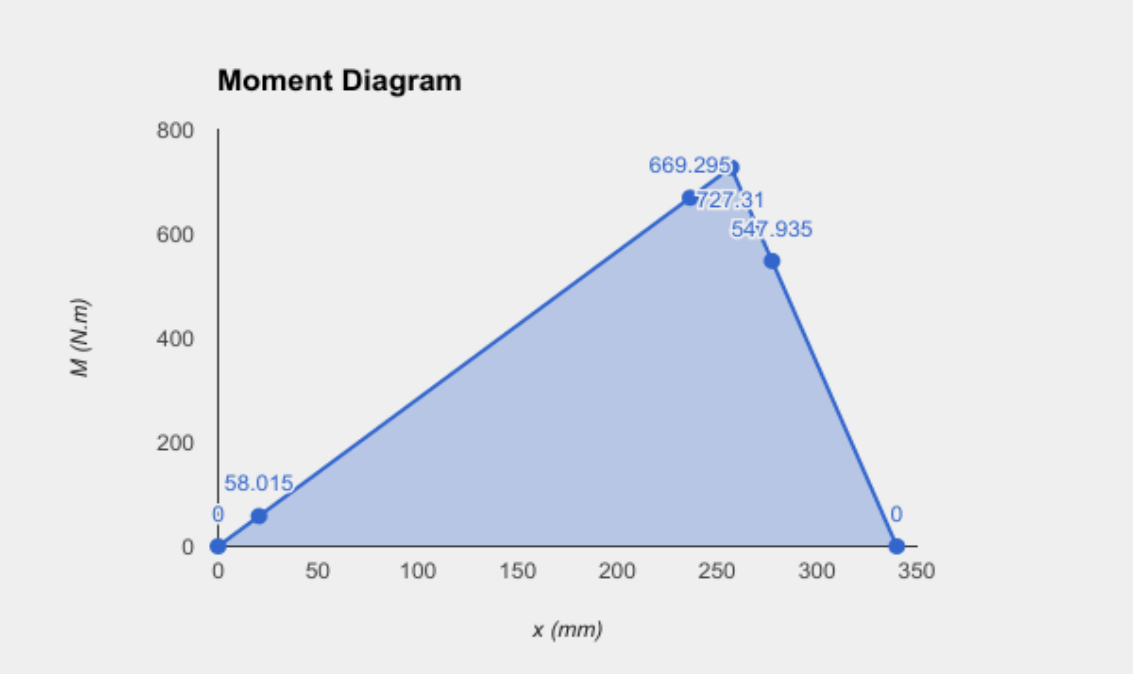

Figure 3.18 - Moment diagram of the shaft

From a free-body diagram analysis (*Figure 3.4*), the bearing reaction forces are found to be 2.83 kN and -11.73 kN. The critical location will be at fillet between the 35 mm and the 30 mm diameters, where the bending moment is large, and the stress concentration is larger than any other section of the saft. The bending moment at this point is M = 669.295 N·m.

$$\sigma_{rev} = \frac{Mc}{I} = \frac{669.295 \times 15}{\frac{\pi}{64} \times 30^4} = 115.1 Mpa \quad \text{(Eq. 3.37)}$$

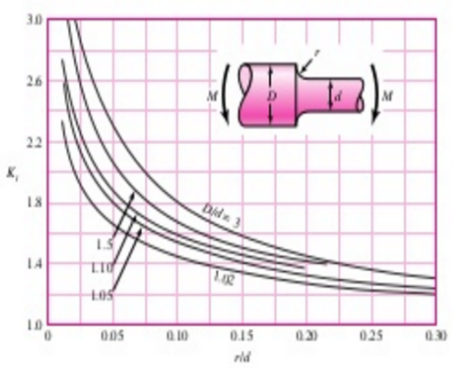

Figure 3.19 - D/d=1.17, r/d=0.1 k_t =1.6

Figure (3.20) estimates Notch sensitivity (q) to 8.1-8.4.

Utilizing equation (3.38); note that equation (3.38) and (3.39) apply to steel and S_{ut} in kpsi.

$$\sqrt{a} = 0.246 - 3.08(10^{-3})S_{ut} + 1.51(10^{-5})S_{ut}{}^2 - 2.67(10^{-8})S_{ut}{}^3 = 0.069 \quad \text{(Eq. 3.38)}$$

$$q = \frac{1}{1+\frac{\sqrt{a}}{\sqrt{r}}} = 0.83 \quad \text{(Eq. 3.39)}$$

$$K_f = 1 + q(K_t - 1) = 1.498 \quad \text{(Eq. 3.40)}$$

$$S_e{}' = 0.5 S_{ut} = 317.5\ MPa \quad \text{(Eq. 3.41)}$$

$$k_a = a S_{ut}{}^b = 4.51(635)^{-0.265} = 0.8155 \quad \text{(Eq. 3.42)}$$

$$k_b = 1.24(30)^{-0.107} = 0.86 \quad \text{(Eq. 3.43)}$$

$$k_c = 1 \quad \text{(Eq. 3.44)}$$

$$S_e = k_a k_b k_c S_e{}' = 222.7\ MPa \quad \text{(Eq. 3.45)}$$

$n_f = \frac{S_e}{K_f \sigma_{rev}} = 1.29$ this indicates infinite life.

The deflection of the test rig's shaft must be limited in order to provide integrity and stability of the rig as well as producing sound data. Furthermore, the experiment requires the members of the test rig not to vibrate or deflect severely in order to safely support the intended loading.

One of the commonly used methods of determining deflection is the elastic curve method. This method allows for determining the deflection and slope at specific points on a shaft or beam. Moreover, this method involves the use of integration, discontinuity functions, and the method of superposition.

$$EI\frac{d^2v}{dx^2} = M(x) \qquad \text{(Eq. 3.46)}$$

$$EI\frac{d^2v}{dx^2} = \frac{F(83)}{257}x - \frac{F(340)}{257}(x-257) \qquad \text{(Eq. 3.47)}$$

$$EI\frac{dv}{dx} = \frac{F(83)}{514}x^2 - \frac{F(340)}{514}(x-257)^2 + C_1 \qquad \text{(Eq. 3.48)}$$

$$EIv = \frac{F(83)}{1542}x^3 - \frac{F(340)}{1542}(x-257)^3 + C_1x + C_2 \qquad \text{(Eq. 3.49)}$$

The constants C_1 and C_2 of the integration are determined by evaluating the functions for shear, moment, slope, or displacement at particular point on the shaft on which the valve of the function is known.

Boundary Conditions:

@ x = 0, v = 0

From (2)

$C_2 = 0$

@ x=257, v=0

From (2)

$C_1 = (3555.2)F$

Therefore, $v = \frac{1}{EI}(\frac{F(83)}{1542}x^3 - \frac{F(340)}{1642}(x-257)^3 + 3555.2Fx)$ (Eq. 3.50)

Equation 3.19 is very powerful because it enables us to predict magnitudes and directions of deflection at any point within the shaft. It must be noted that the equation is based on the assumption that EI (the product of modulus of elasticity of the shaft and moment of inertia on nonpolar axis) is constant throughout the shaft.

$EI = 210Gpa \times 42411.5\ mm^4 = \ kN.mm^2$

V = 1.58 x10^{-3} m, *deflection of shaft* @$x = 0$ (v) $= 1.58\ mm$

Fatigue analysis of the 18 mm diameter section of the shaft

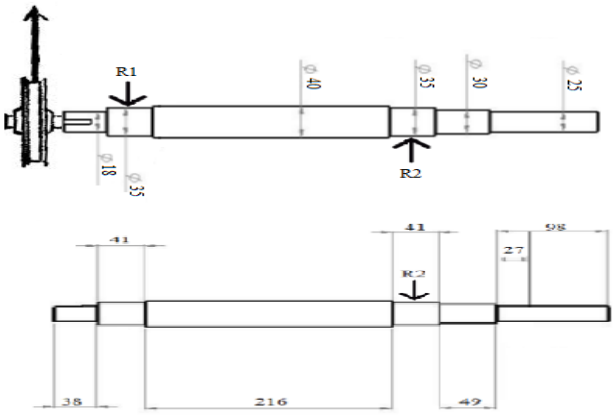

Figure 3.20 - Free Body Diagram of the x-y plane

$\Sigma F_y = 0$

$R_1 - R_2 = 57.6\ N$ (Eq. 3.51)

$\Sigma M_{R_1} = 0$

$R_1(20.5 + 216 + 20.5) = 57.6(38 + 41 + 216 + 20.5)$

$R_1 = -70.7\ N$ By substituting into equation 1

$R_2 = 13.1\ N$ (Eq. 3.52)

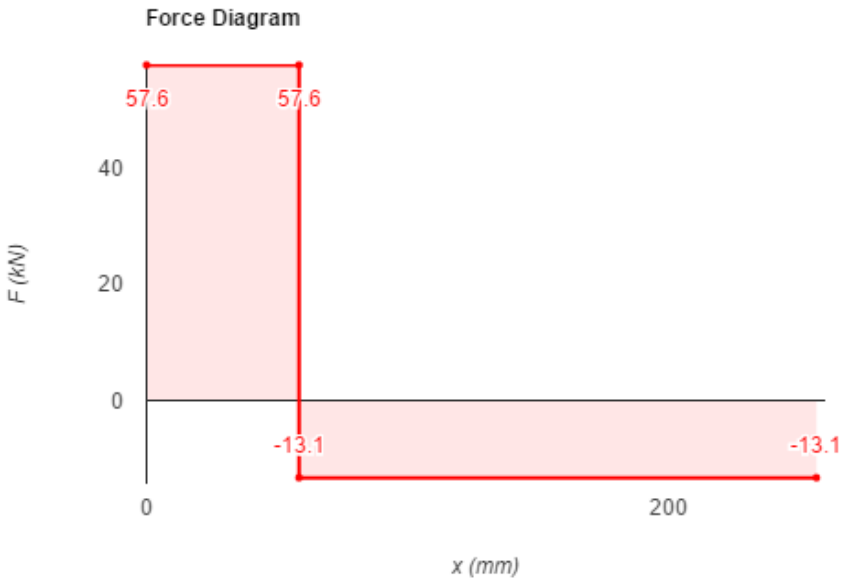

Figure 3.21 - Force diagram

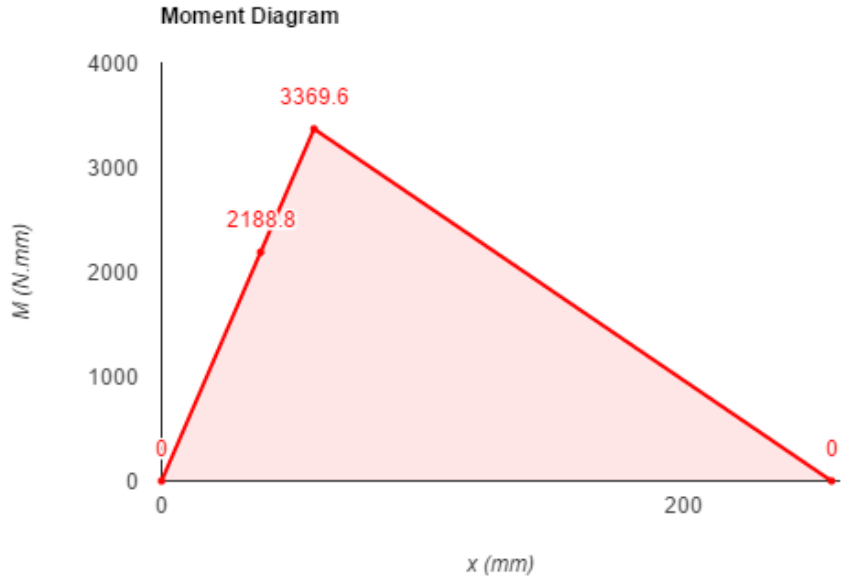

Figure 3.22 - Moment diagram

$$\sigma_{rev} = \frac{Mc}{I} = \frac{2.1888 \times 9}{\frac{\pi}{64} \times 18^4} = 3.823\ KPa \qquad \text{(Eq. 3.53)}$$

The reversible stress at this section is very small, therefore, fatigue is very unlikely. The calculations below illustrate this fact.

Figure (A-15-9) D/d=1.94, r/d=0.167 k_t=1.6

Figure 6-21 estimates Notch sensitivity (q) to 8.1-8.4.

Utilizing Eq. 3.38; note that Eq. 3.38 and Eq. 3.39 apply to steel and S_{ut} in kpsi.

$$\sqrt{a} = 0.246 - 3.08(10^{-3})S_{ut} + 1.51(10^{-5})S_{ut}{}^2 - 2.67(10^{-8})S_{ut}{}^3 = 0.06956 \quad \text{(Eq. 3.54)}$$

$$q = \frac{1}{1+\frac{\sqrt{a}}{\sqrt{r}}} = 0.83 \quad \text{(Eq. 3.55)}$$

$$K_f = 1 + q(K_t - 1) = 1.498 \quad \text{(Eq. 3.56)}$$

$$S_e{}' = 0.5S_{ut} = 317.5\ MPa \quad \text{(Eq. 3.57)}$$

$$k_a = aS_{ut}{}^b = 4.51(635)^{-0.265} = 0.8155 \quad \text{(Eq. 3.58)}$$

$$k_b = 1.24(30)^{-0.107} = 0.86 \quad \text{(Eq. 3.59)}$$

$$k_c = 1 \quad \text{(Eq. 3.60)}$$

$$S_e = k_a k_b k_c S_e{}' = 222.7\ MPa \quad \text{(Eq. 3.61)}$$

$n_f = \frac{S_e}{K_f \sigma_{rev}} = 38887$ this indicates infinite life.

This section is calculation for static failure analysis. The Maximum Shear Stress theory states that failure occurs when the maximum shear stress from a combination of principal stresses equals or exceeds the value obtained for the shear stress at yielding in the uniaxial tensile test.

$$\sigma = \frac{32M}{\pi d^3} = 436.3MPa \quad \text{(Eq. 3.62)}$$

$$\tau_{xz} = \frac{16T}{\pi d^3} = 2.75MPa \quad \text{(Eq. 3.63)}$$

$$\tau_{max} = \sqrt{(\frac{\sigma}{2})^2 + \tau^2_{xz}} = 218.2MPa \quad \text{(Eq. 3.64)}$$

$n = \frac{S_y}{2\tau_{max}} = 2.1$

3.4 Design Selection

3.4.1 Selection of the Bearings

To select the appropriate bearings that we can use in the experiments, we had to select the bearings based on their ability to allow us to introduce simulated defects, be able to withstand shaft deflection, match the shaft diameter, and have adequate static load rating. Therefore, we selected Self Aligning 2306 bearings (shown in figure 3.23) to perform our experiments on.

Figure 3.23 - Self Aligning 2306 bearings

Figure 3.24 is the detailed dimensions of the bearing and its calculations data.

Dimensions

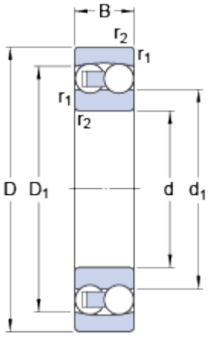

Abutment dimensions

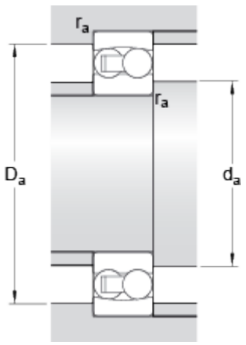

d		30	mm
D		72	mm
B		27	mm
d_1	≈	41.9	mm
D_1	≈	59.8	mm
$r_{1,2}$	min.	1.1	mm
d_a	min.	37	mm
D_a	max.	65	mm
r_a	max.	1.1	mm

Calculation data

Basic dynamic load rating	C	31.2	kN
Basic static load rating	C_0	8.8	kN
Fatigue load limit	P_u	0.45	kN
Reference speed		18000	r/min
Limiting speed		13000	r/min
Permissible angular misalignment	α	3	°
Calculation factor	k_r	0.05	
Calculation factor	e	0.44	
Calculation factor	Y_0	1.4	
Calculation factor	Y_1	1.4	
Calculation factor	Y_2	2.2	

Mass

Mass bearing	0.5	kg

Figure 3.24 - Self aligning 2306 bearing data sheet

3.4.2 Selection of the Oil-based Lubricant

Our selection process of an oil-based lubricant was primarily based on viscosity. We kept in mind multiple characteristics that must considered when choosing a lubricant. Firstly, we looked at the viscosity-temperature relationship, characterized by the viscosity index (VI). For rolling bearings, oils with a VI of at least 95 are recommended. Next, we looked at the fact that we need an oil with a viscosity ratio (shown in figure 3.25) greater than one ($\mathbf{k > 1}$), this is because we need an oil that will form an adequate thick oil film in the contact area between the rolling elements and raceways. Finally, we calculated the rated viscosity ($\mathbf{\nu_1}$) using the graph in figure 3.23, by connecting the bearing mean diameter ($\boldsymbol{d_m = 0.5(D+d)}$, ***mm***), and the rotational speed of the bearing (***n, r/min)***.

$d_m = 51mm$, Rotational speed = 1700, 3400, 6800 rpm.

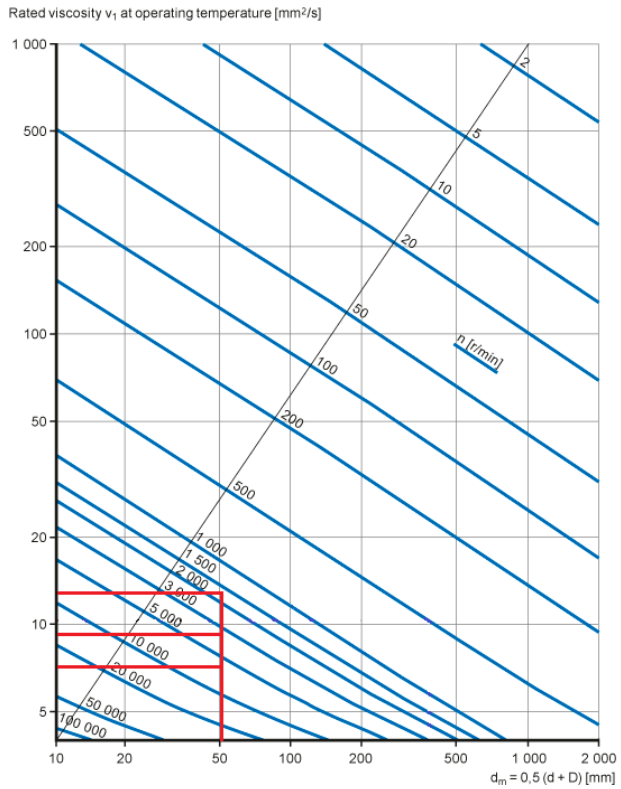

Figure 3.25 - Graph to calculate rated viscosity

We finally landed on a decision to use Shell's Helix HX5 15W-40 as the oil-based lubricant. This is because, it meets our requirements (shown in table 3.2). In addition, due to the high viscosity ratio between the lubricant and the bearing, we expect for a hydrodynamic film lubrication to exist and no fatigue will occurs.

Table 3.2 - Shell Helix HX5 15W-40 Oil properties

Properties			Method	Shell Helix HX5
Viscosity Grade				15W-40
Kinematic Viscosity	@40°C	cSt	IP 71	105.4
Kinematic Viscosity	@100°C	cSt	IP 71	13.9
Viscosity Index			IP 226	132
Density	@15°C	kg/l	IP 365	0.885
Flash Point (PMCC)		°C	IP 34	220
Pour Point		°C	IP 15	-30

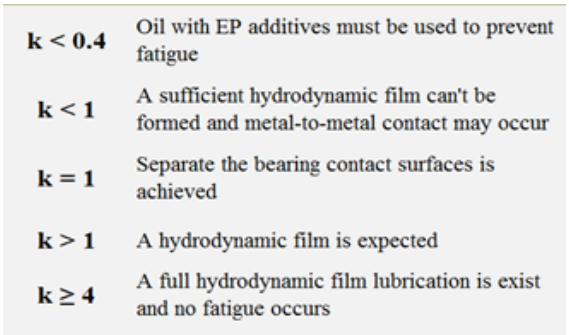

Figure 3.26 - Lubrication Condition

Table 3.3 - 15W-40 oil viscosity properties at different operation speed

Rotational Speed (r/min)	**1700**	**3400**	**6800**
Viscosity (v) @ 40°C (mm^2/s)	105.1	105.1	105.1
Required viscosity @ 40°C (mm^2/s)	12.7	9.15	6.72
Viscosity Ratio (k)	8.25	11.5	15.6

3.4.3 Selection of the Nano-particles

Choosing the nano-particles, we kept in mind that we need a type of nano-particles that will not scratch the surface of the bearing or cause external tribological damage to the bearings, have small sized spherical shaped nano-particles, and be budget-friendly to the limited funding we are working with. Therefore, we chose 30nm and 70nm spherical Copper nano-particles (shown in figure 3.27). The copper nano-particles are softer than mild iron (the alloy that is the bearing made from), thus, the bearing will not be scratched or damaged.

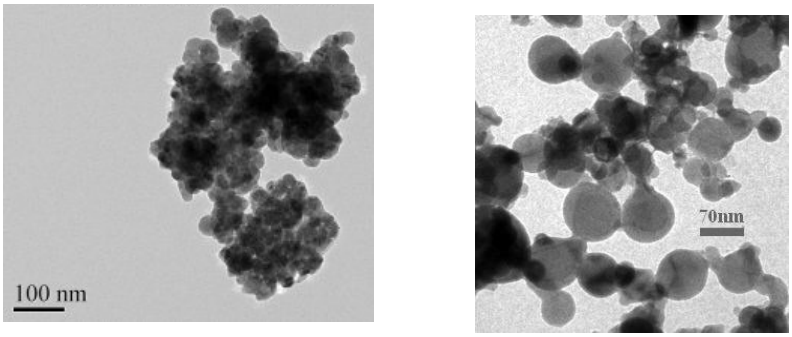

Figure 3.27 - Copper (a) 30nm and (b) 70nm nano-particles

Copper (Cu) Nanoparticles **(partially passivated)**
Copper (Cu) Nanoparticles Estimated Shell Thickness: 0.5 - 1.00nm - Cu2O
Copper (Cu) Nanoparticles Purity: 99% (metal basis)
Copper (Cu) Nanoparticles APS: 30 nm
Copper (Cu) Nanoparticles SSA: 35 m^2/g
Copper (Cu) Nanoparticles Color: black brown
Copper (Cu) Nanoparticles Bulk Density: 0.15 - 0.35 g/cm^3
Copper (Cu) Nanoparticles True Density: 8.94 g/cm^3
Copper (Cu) Nanoparticles Making Method: Made by electrochemical method

Copper (Cu) Nanoparticles Certificate of Analysis					
Cu	Fe	Sn	Mn	Ni	[Cu2O]
99%-metal Basis	205ppm	238ppm	50ppm	300ppm	5.2wt%-for safe shipping only, no major effect

Copper (Cu) Nanopowder
Copper (Cu) Nanopowder Purity: 99.9% (metal basis)
Copper (Cu) Nanopowder Color: Saddle brown
Copper (Cu) Nanopowder APS: 70 nm
Copper (Cu) Nanopowder SSA: 6-8 m^2/g
Copper (Cu) Nanopowder Morphology: spherical
Copper (Cu) Nanopowder Bulk Density: 0.21 g/cm^3
Copper (Cu) Nanopowder True Density: 8.9 g/cm^3
***Flammable, UN 3089**

Copper (Cu) Nanoparticles Certificate of Analysis-%								
Cu	As	Sb	Pb	Sn	Fe	Ni	Bi	O
**≥99.9	≤0.002	≤0.002	≤0.001	≤0.001	≤0.006	≤0.0042	≤0.001	1.76

Figure 3.28 - Copper 30nm and 70nm nano-particles data sheets

3.4.4 Design of the Hydraulic Loading System

After careful considerations that were explained in section 3.2.2, we selected the Hydraulic Body Repair Frame Kit due to numerous reasons. Firstly, it provided us with the load range we required. Secondly, the system allowed us to easily attach our pressure gage using a T-joint. In addition, its inexpensive price and abundance in the market did help in the decision making. Lastly, the system is easily operated. Therefore, we purchased this system and assembled it with our test rig. The specifications of the model we selected are shown in table 3.4. The parts are shown in figure 3.29 and table 3.5.

Table 3.4 - Hydraulic Body Repair Frame Kit Specifications

Description	**Measurements**
Volume	740mm * 400mm * 180mm
Net weight	26 Kg
Gross weight	30 Kg
Capacity	4 ton to 10 ton
Max lifting height	137mm
Lifting range	135mm

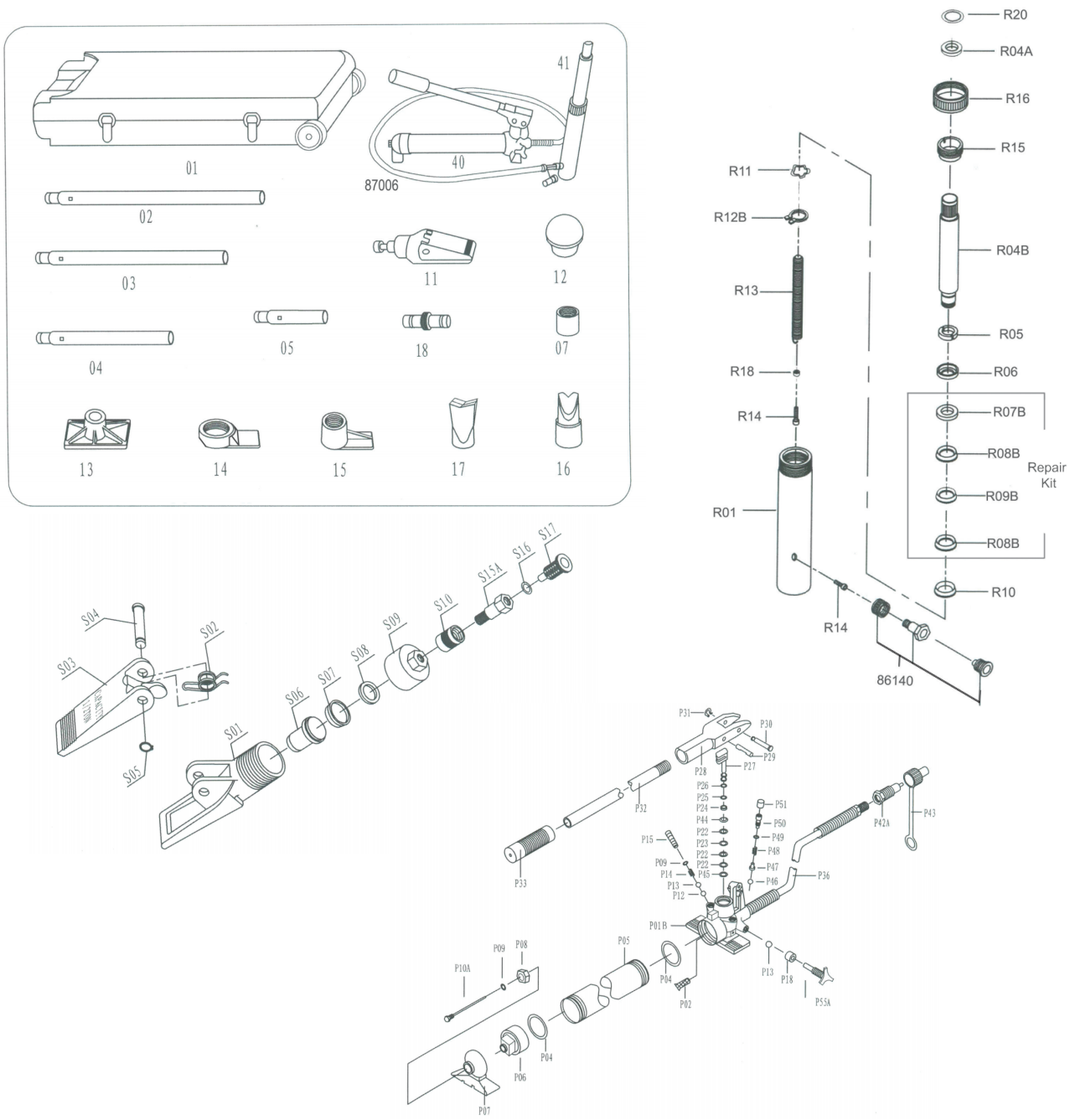

Figure 3.29 - Hydraulic Body Repair Frame Kit Parts

Table 3.5 - Parts Names

Part No.	Description
811-01	Blow Mold Case
811-A02	24" Extension Tube
811-A03	21" Extension Tube
811-A04	10" Extension Tube
811-A05	5" Extension Tube
811-07	Serrated Saddle
811-11	Spreader Ram
811-12	3 1/4" Rubber Head
811-13	Flat Base
811-14	Spreader Ram Toe
811-15	Spreader Plunger Toe
811-16	Wedge Head
811-17	90° V-Base
811-18	Lock on Connector
811-40	10 Ton Hydraulic Unit
811-41	10 Ton, 6" Stroke Ram
87006	6 ft. Hose With Half Coulping
811-R12B	Snap-Ring "C"
811-R13	Spring
811-R15	Ring
811-R16	Protecting Cap
811-R14	Screw
811-R18	Bushing
811-R20	Ring "C"
86140	1/4" hydraulic coupler
811-R01	Cylinder
811-R04B	Ram
811-R04A	Bearing
811-R05	Bearing
811-R06	Bushing
811-R07B	Cap Ferrule(C2600p)
811-R08B	V Seal (Uletan)
811-R09B	V Seal (SS400)
811-R10	Spreader
811-R11	Washer

Part No.	Description
11-S01	Lower Duck Bill
11-S02	Spring
11-S03	Upper Duck Bill
11-S04	Pivoting Pin
11-S05	Cir Clips
11-S06	Piston
11-S07	Cup Seal
11-S08	Washer
11-S09	End Cap
11-S10	Coupling Ring
11-S15A	Couping Bolt
11-S16	Bolt O-Ring
11-S17	Dust Cap
11-P01B	Pump Housing
11-P02	Filter
11-P04	Seal
11-P05	Pump Reservoir
11-P06	Reservoir End Cap
11-P07	Pump Foot
11-P08	Nut-Housing
11-P09	O-Ring
11-P10A	Dip Stick(Oil Level CK)
11-P12	Ball Valve
11-P13	Ball Valve
11-P14	Spring
11-P15	Overload Stem
11-P18	Spacer
11-P22	Seals (Complete Set)
11-P23	Seal
11-P24	Lower Spanner Nut
11-P25	Seal
11-P26	Upper Spanner Nut
11-P27	Plunger
11-P28	Pump Pivot Brm Arm
11-P29	Pivot Arm Pin
11-P30	Pivot Arm Pin
11-P31	Cir Clip
11-P32	Pump Handle Assy
11-P33	Grip
11-P36	Hose
11-P42A	Coupling
11-P43	Dust Cap
11-P44	Back-up Ring
11-P45	Back-up Ring
11-P46	Steel Ball
11-P47	Spring Plunger
11-P48	Spring
11-P49	O-Ring
11-P50	Screw (Safety Valve)
11-P51	Plastic Cap
11-P55A	Release Valve Stem

3.5 Product Subsystems and Components

In this section of the report we present and explain briefly the different parts/components that we assembled together to build our final test rig (shown in figure 3.30). In addition to the pictures shown in this section, detailed 2D Solidworks drawings can be found in Appendix #.

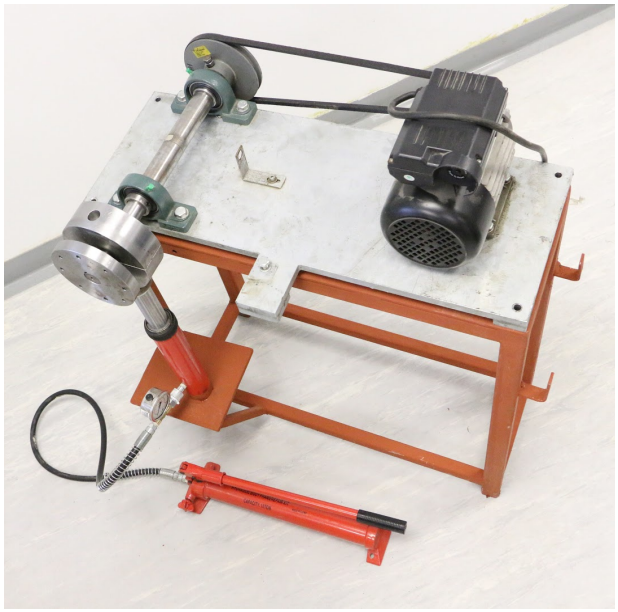

Figure 3.30 - The complete assembly

3.5.1 Bearing Housing and Oil Tank

The first component of our test rig is a combination of a bearing housing and oil tank (shown in figure 3.31). After completing the design prototypes in section 3.2.1, we reached a final design which will allow an easy way to replace the oil and make the bearing housing and oil tank portable. This design allows the piston to fit inside a hollow pipe, allowing us to remove the housing whenever we need to.

Figure 3.31 - Bearing housing (left), oil tank (right)

3.5.2 Shaft

The shaft (shown in figure 3.30) is 50 cm long, and a major thickness of 4 cm. It is made of medium carbon steel. We added fillets (shown in figure 3.33) with different dimensions for stress relieving.

Figure 3.32 - Shaft

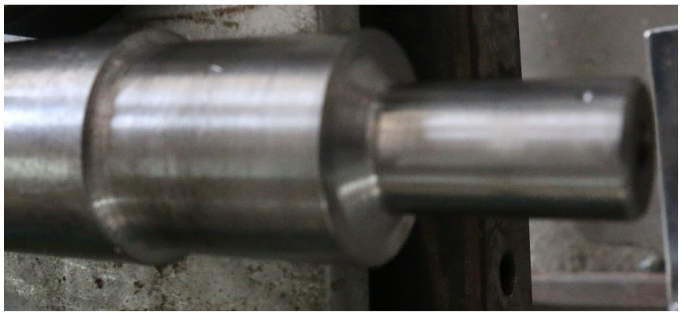

Figure 3.33 - Shaft fillets

3.5.3 Motor

The motor (shown in figure 3.34) is a single phase (60Hz). Its power is 2 HP. The Manufacturer is E.M.Z. The voltage is 220 V and the current is 10.3 A.

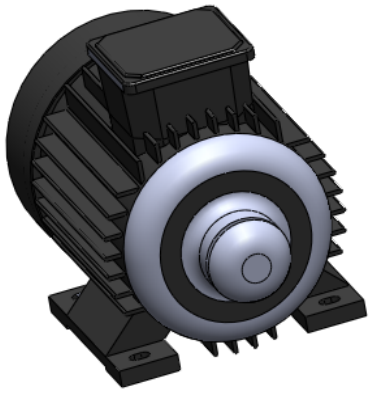

Figure 3.34 - CAD drawing of Electric Motor E.M.Z

3.5.4 Pulleys and Belt

We employed three pulleys (shown in figure 3.35): 2 bigger ones (150mm outer diameter), and one smaller one (75mm outer diameter). By changing the pulleys it allows use to conduct our experiment with three different speeds. In addition, the belt that connects the driver and driven pulley is … in length.

Figure 3.35 - Pulleys with belt (left), the three pulleys without belt (right)

3.5.5 Plummer/Pillow Block Bearings

We added two pillow block bearings (shown in figure 3.36) to the shaft for support. The plummer block outer diameter is 72mm it holds a UC207 ball bearing that fits and holds the shaft.

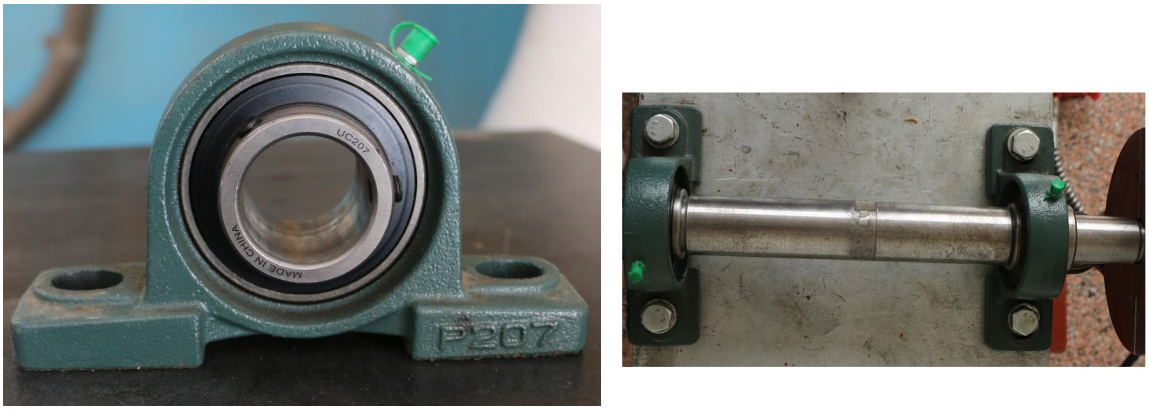

Figure 3.36 - Pillow block bearing (left), Pillow bearing assembled with the shaft (right)

3.5.6 Protection Cage

Safety is the number one priority for us. The protection cage (shown in figure 3.37) purpose is to increase the safety of the researchers/students during conducting the experiment. The cage will be placed on top of the test rig. It is lightweight to be removed easily and made from a strong material to protect in case of belt break or other unfortunate accident.

Figure 3.37 - Safety cage (left), Safety cage placed on test rig (right)

3.5.7 Unbalanced Dynamic Load Disk

The previously built test rig was aimed to be tested on static load only. Dynamic load is a good modification to test for nano-particle additives performance and efficiency. The design of a cylindrical disk load gave us the ability to test with a pre-specified dynamic load. We designed the disk to have eight total holes, with four holes has larger diameter the the remaining four. The holes chosen to be four to make the cylindrical shape uniform. Different loads will be attached to the holes which will give us different dynamic load. The disk is shown below in figure 3.38.

Figure 3.38 - Unbalanced Dynamic Load

3.5.8 Hydraulic Loading System and Pressure Gage

This combination allows us to apply an automated load that we can monitor and control to obtain better, more efficient data.

Figure 3.39 - Hydraulic Loading System and Pressure Gage

3.5.9 Ultrasonic Sensor and Electrical Circuit

To suspend the nanoparticles in the oil based lubricated we required three ultrasonic sensors mounted in multiple locations on the oil tank (shown in figure 3.38). Hence, an electrical circuit (shown in figure 3.41) was also needed that controls the ultrasonic frequency, current, and resistance.

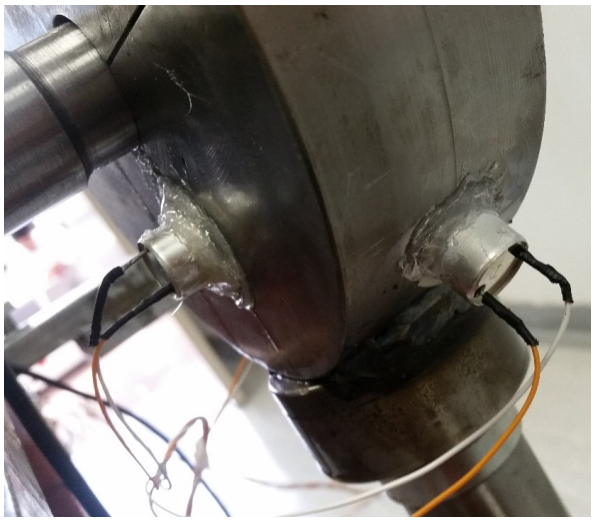

Figure 3.40 - Ultrasonic sensors mounted on oil tank

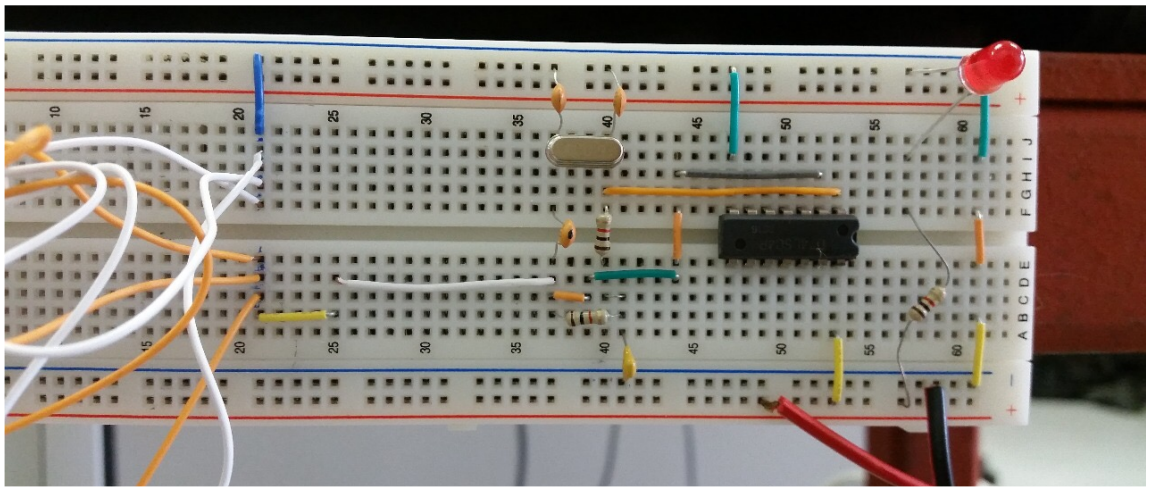

Figure 3.41 - Electrical circuit that controls ultrasonic sensors

3.6 Implementation

Building this test rig, we intended it to be modular, have effortless repairability, easily manufactured, and high durability. We contracted with workshops that assisted us in fabricating some components. Using our manufacturing and design skills, we carefully selected the machining process of each component (i.e. lathe machine, milling, and drilling). However, we were limited by market availability of some machining process alternatives. In contrast, we do not need to fabricate all components. Some components (i.e. pulleys, bearings, and hydraulic loading system) were selected and adjusted according to our design dimensions (explained further in section 3.4). Our selection processes were based on calculations, published standards, and catalogs. In our design concept generation process, we developed many alternatives to most of the components. We went through many designs and prototypes to reach a design that is adequate for our needs. The alternatives and design process is explained in detail in section 3.2. After gathering and completing the construction of all the components, we assembled them together using bolts and welding. After the assembly phase was completed, we commissioned the test rig twice. Once without load, and once with applied load. However, after running the test rig again, we faced a problem with vibrations coming from the steel pulleys we installed. Thus, we had to replace the old steel pulleys with newer aluminium ones. After a few more test runs, an obstacle surfaced. The motor that was available when we received the old test rig was only able to handle two of the three loads we intended to run the experiment under. Therefore, due to the limited time we have, we were forced to operate with the two lower loads.

CHAPTER 4

System Testing and Analysis

4.1 Data Acquisition

4.1.1 Test rig with sensors

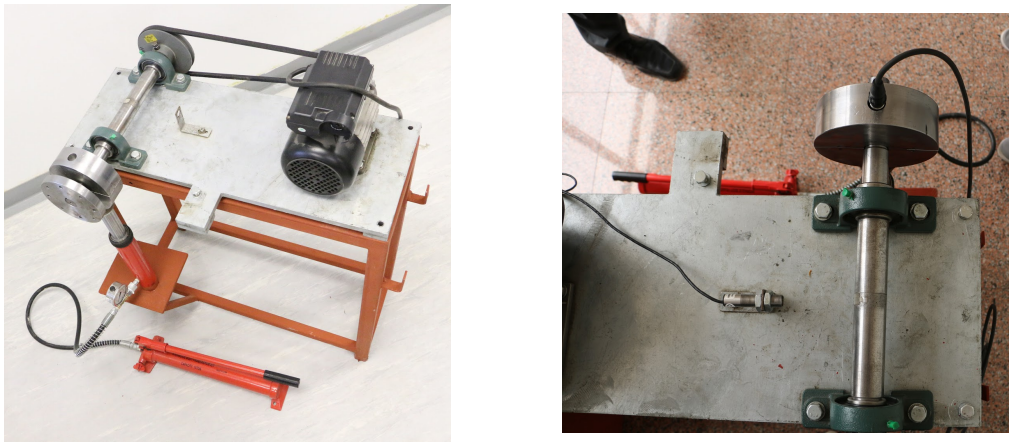

(a) (b)

Figure 4.1 - (a) Vibration Bearing Test Rig (b) Accelerometers and Tachometer

The test rig used to generate the data for this project is shown in Figure 4.1. It consists of a bearing housing connected with a hydraulic jack that applies a static hydraulic load. The test rig is driven by a constant speed motor through a belt-pulley system to give an operating speed of around 1750 r/min. The test rig was fitted with an accelerometer (as shown in Figure 4.1b) and a tachometer to get a speed reference. Data were acquired at a sampling rate of 60,000 samples/s (Hz). In total, two main fault sizes were introduced to the inner and outer races of the bearing in the testing as shown in Figure 4.1. The seeded notches were created using an electrical discharge machining (EDM). The sizes of the notches are 1 mm and 2 mm.

4.1.2 Details of the bearing `

The frequencies that rolling element bearings generate as balls or rollers pass over the raceways are called the fundamental fault frequencies. These frequencies are functions of the bearing's geometry, specifically, pitch diameter and ball or roller diameter and the relative speed between the raceways.

BPFI → Ball Pass Frequency Inner (Inner race)

BPFO → Ball Pass Frequency Outer (Outer race)

FTF → Fundamental Train Frequency (Container)

BSF → Ball Spin Frequency

Ball Diameter = 11.7 mm

Pitch Diameter = 51 mm

Table 4.1- Bearing Frequency

Bearing Frequencies	Formulas	Magnitude
BPFO	$\frac{nf_r}{2}\{1 - \frac{d}{D}cos\Phi\}$	121.2 Hz
BPFI	$\frac{nf_r}{2}\{1 + \frac{d}{D}cos\Phi\}$	193.4 Hz
FTF	$\frac{f_r}{2}\{1 - \frac{d}{D}cos\Phi\}$	11.018Hz
BSF	$\frac{D}{2d}f_r\{1 - (\frac{d}{D}cos\Phi)^2\}$	59.03Hz (2xBSF) 118.06 Hz

4.3 Analysis and Discussion of Acquired Data

4.3.1 Time Domain Analysis

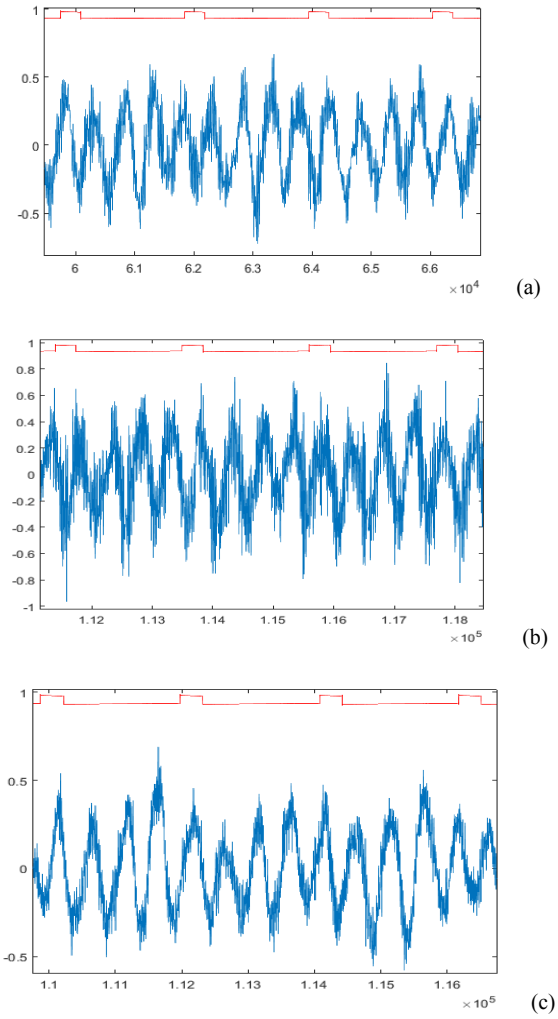

Figure 4.2 - Time domain signal for healthy bearing loaded with 40 bar (a) 0% nano (b) 0.5% 30 nm (c) 0.5% 70 nm

Figure 4.2 shown above is the time domain signal of a healthy bearing loaded with 40 bar. It compares effect of different sizes of nano additives added at the same concentration to the oil based lubricant in the healthy bearing. Figure 4.2(a) presents the time domain signal of 0% nano-particles. Figure 4.2(b) presents the time domain signal of 0.5% of 30 nm nano-particles. Figure 4.2(c) presents the time domain signal of 0.5% 70nm nano-particles. 70 nm nano-particles additives demonstrates a lower noise content compared with 30 nm additive and with 0% nano-particles.

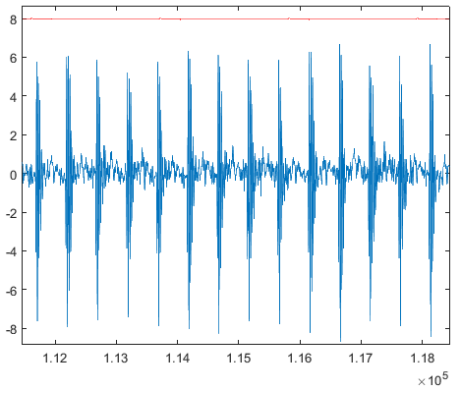

(a)

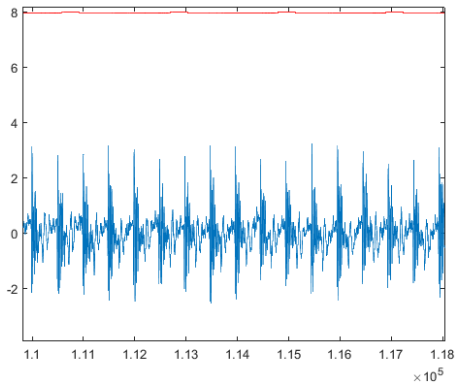

(b)

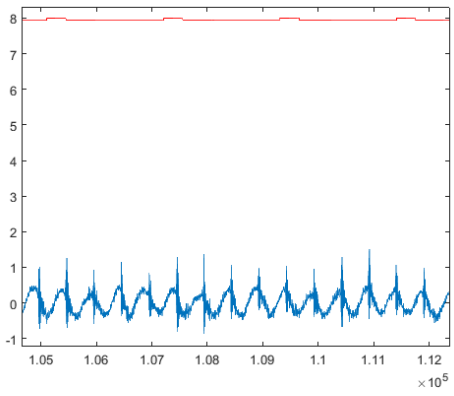

Figure 4.3 - Time domain signal for 1mm outer race defected bearing loaded with 40 bar (a) 0% nano (b) 0.5% 30 nm (c) 0.5% 70 nm

Figure 4.3 illustrates the time domain signal of a 1mm outer race defected bearing at a constant 40 bars load. Figure 4.3(a) presents the time domain signal of 0% nanoparticles. Figure 4.3(b) presents the time domain signal of 0.5% of 30 nm nanoparticles. Figure 4.cc(c) presents the time domain signal of 0.5% 70nm nanoparticles. Figure 4.3(a) indicates that the amplitude value is approximately 6. After adding the 30 nm nanoparticles to the defected bearing, the amplitude value drops to approximately 3. Figure 4.3(c) amplitude value is approximately 1. This results indicates that the process of adding the nanoparticles indeed damped the amplitude of this defected bearing around 6 times. The 70 nm size is more preferable than the 30 nm due to the fact that the decreasing effect of the 70nm is greater than the 30 nm.

The Root Mean Square (RMS) value is used as an indicator of how much energy is embedded in the vibration signal. Therefore, if the value of RMS exceeds recommended levels the bearing may be damaged. Moreover, it is an excellent tool for inspecting and following noise levels throughout the signal. It is represented as:

$$RMS = \sqrt{\frac{1}{N}\sum_{n=0}^{N-1}(x(n) - \mu)^2} \qquad \text{Eq. 4.1}$$

The following figures represent RMS values for a healthy bearing at 1800 rpm and 20-40 bar load with vority of nanoparticles concentration ranging from 0% to 0.5% of 30 nm and 70 nm.

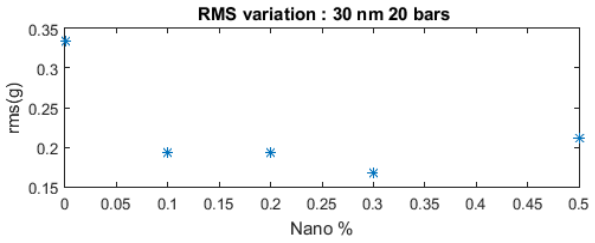

(a)

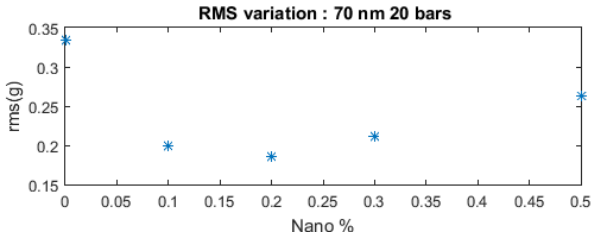

(b)

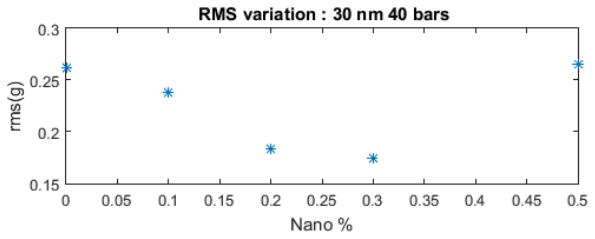

(c)

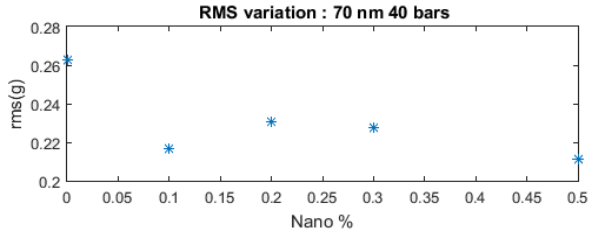

(d)

Figure 4.4 - RMS values for a healthy bearing (a) 30 nm 20 bars (b) 70 nm 20 bars (c) 30 nm 40 bars (d) 70 nm 40 bars

Figure 4.4 illustrates the effect of nanoparticles additives on the energy content of the vibration signal of healthy bearing at two loads. Figure 4.4(a) shows clear evidence that the rms value drops the more nanoparticles we add to the lubricant. However, once the percentage of the nao-particle exceeds 0.3%, the rms value increases which indicates an increase in the intensity of the power content of vibration. As we increase the load to 40 bar we noticed a similar trend as the value of rms decreases with the increase of the percentage of the nanoparticles until we exceed 0.3%. For the 70 nm nanoparticles, it act into a similar pattern to the 20 nm until it reaches 0.2%. We observe an increase in the rms value in the contrary of 30 nm nanoparticles.

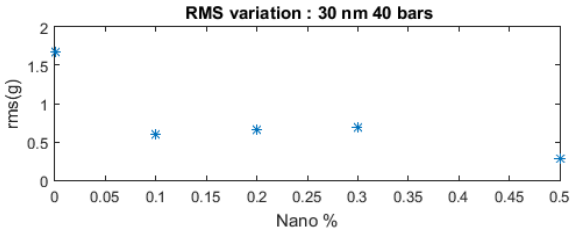

(a)

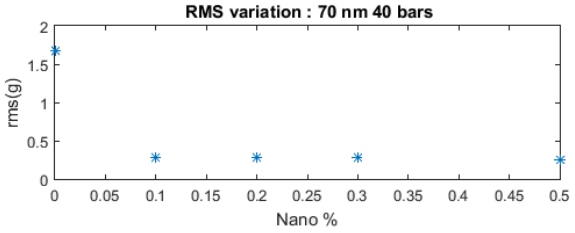

(b)

Figure 4.5 - RMS values for 1 mm outer race defected bearing (a) 30 nm 40 bars (b) 70 nm 40 bar

We notice a similar trend for the 1 mm outer race fault bearing as the value of RMS descends with the increase of nano additive.

4.3.2 Frequency Analysis

FFT Analysis (Fast Fourier Transform) is a powerful tool to diagnose bearing faults, unbalance, and abnormalities. Frequency demodulation envelope is used to calculate a curve that shows the defective bearing signals. If the period between peaks gives one of the bearing's frequencies, the bearing might be damaged.

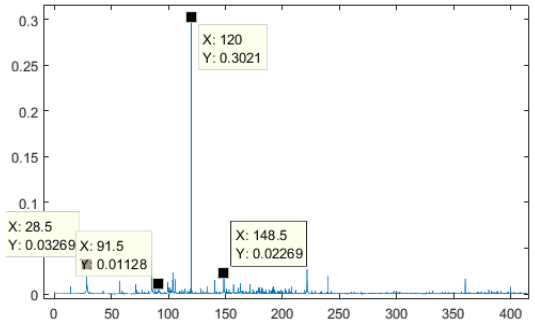

(a)

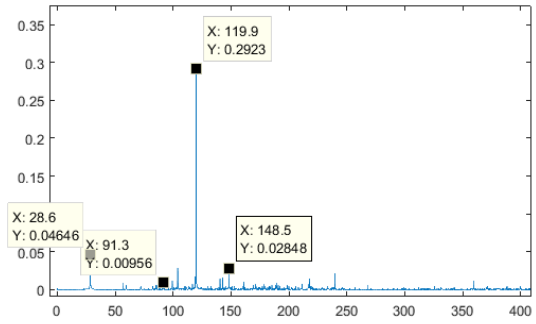

(b)

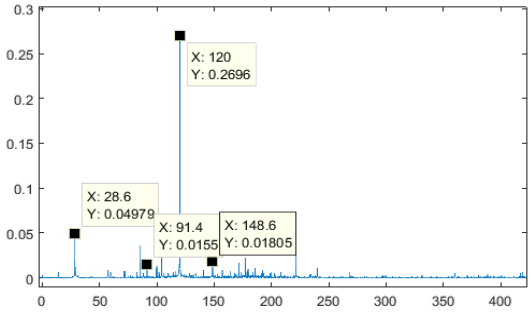

(c)

Figure 4.6 - FFT Analysis for healthy bearing loaded with 40 bar (a) 0% nano (b) 0.5% 30 nm (c) 0.5% 70 nm

Figure 4.6 is the FFT analysis of a healthy bearing that is constantly loaded with 40 bars. Figure 4.6(a) shows the FTT of a healthy bearing before adding nano-particles. Figure 4.6(b) shows the FFT analysis after adding 0.5% of 30 nm to the lubricant. Figure 4.6(c) illustrates the FFT analysis of a healthy bearing after adding 0.5% 70nm size to the lubricant. Looking at figure 4.6 we observe the bearing natural frequencies such as BPFO, BPFI, FTF, and BSF with the absence of high frequencies excitations.

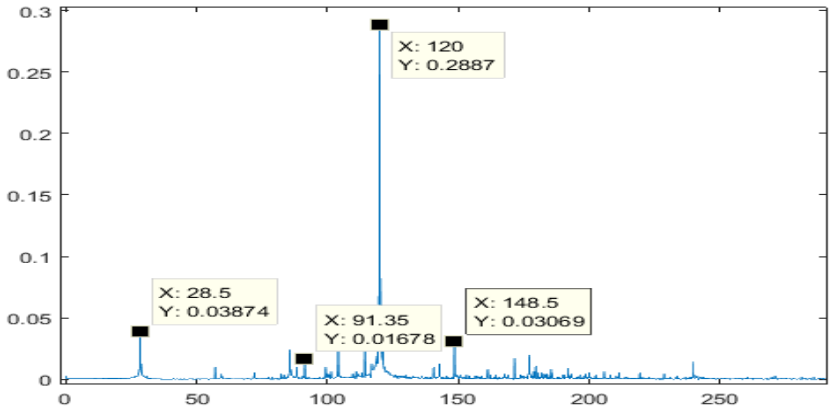

(a)

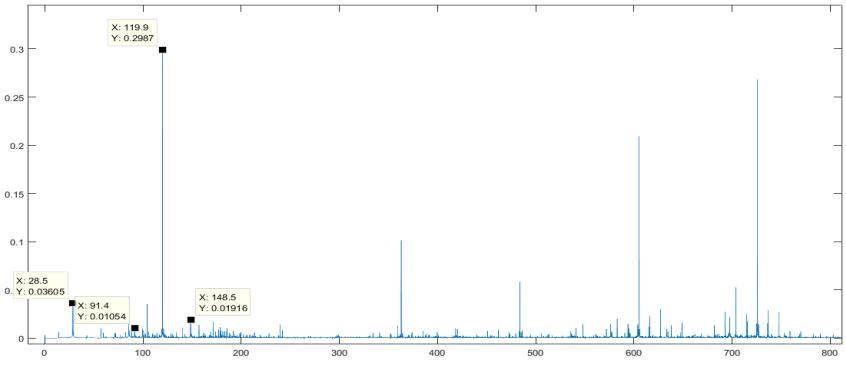

(b)

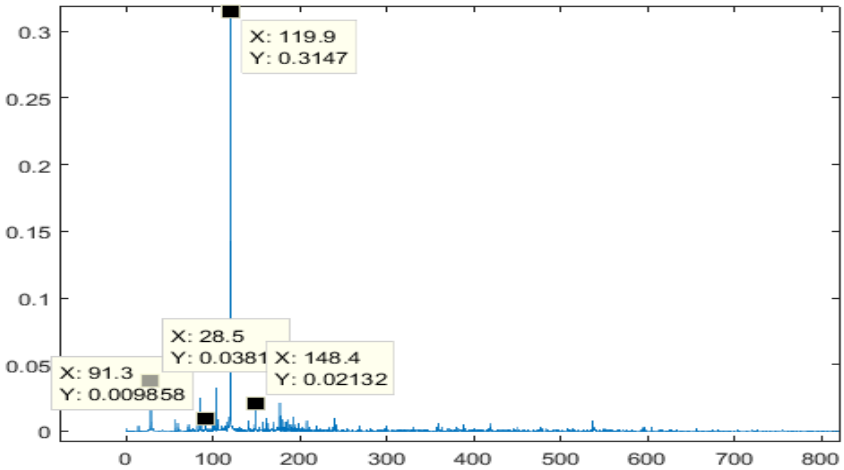

(c)

Figure 4.7 - FFT Analysis for 1mm outer race defected bearing loaded with 40 bar (a) 0% nano (b) 0.5% 30 nm (c) 0.5% 70 nm

Figure 4.7 is the FFT analysis of a 1 mm outer race defected bearing that is constantly loaded with 40 bars. Figure 4.7(a) shows the FTT of a defected bearing before adding nano-particles. Figure 4.7(b) shows the FFT analysis after adding 0.5% of 30 nm to the lubricant. Figure 4.7(c) illustrates the FFT of a healthy bearing after adding 0.5% 70 nm size to the oil. 0.5% 30 nm nanoparticles shows high frequency resonance that is around 355 Hz, which is exactly at the BPFO. This means that a fault on the outer race is detected. The 70 nm additive has a greater healing effect as the BPFO amplitude has vanished from data given in figure 4.7(c).

4.3.3 CPB Analysis

CPB analysis is very helpful tool to analyze the vibration in which we narrow bands in the low frequency region and we widen the bands in the high frequency. We have created a mask from the oil lubricant to compare the results of adding nano-particles spectra for the CPB analysis. We looked at changes above 6 dB, which means that amplitudes have doubled. In the comparisons we see that the high resolution bands above 5 KHz have increased as a result of the nano additives which in general means that the noise level have increased as shown in figure 4.blah.

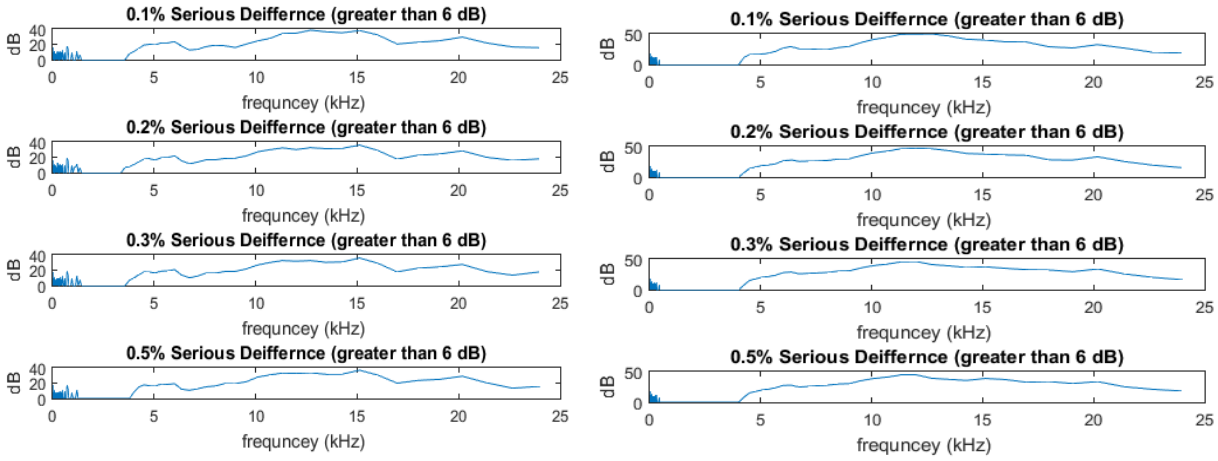

Figure 4.8 - CPB analysis of 1 mm outer race defected bearing

4.3.4 Kurtosis Excitation in different bands (Wavelet kurtogram)

Since the simulated defect generates a shock every time balls or rollers passover it, it generates periodical impulses that gives structural resonances that can be detected and measured by sensors or transducers. These high frequency vibrations are analyzed utilizing a variety of high frequency analysis with high first peak such as Kurtosis, or with shocks' period such as Envelope analysis. Kurtosis is a statistic indicator by which the impulsive character of a signal in time domain can be defined.

$$Kurtosis = \frac{1}{N}\sum_{i=1}^{N}(x_i - \mu)^4$$

x_i = *vibration amplitude in time domain*
μ = *average*
N = *tests number*

It must be noted that signals with Gaussian distribution have a Kurtosis value of 3. While non-Gaussian signals such as impulsive shocks have a Kurtosis value bigger than 3.

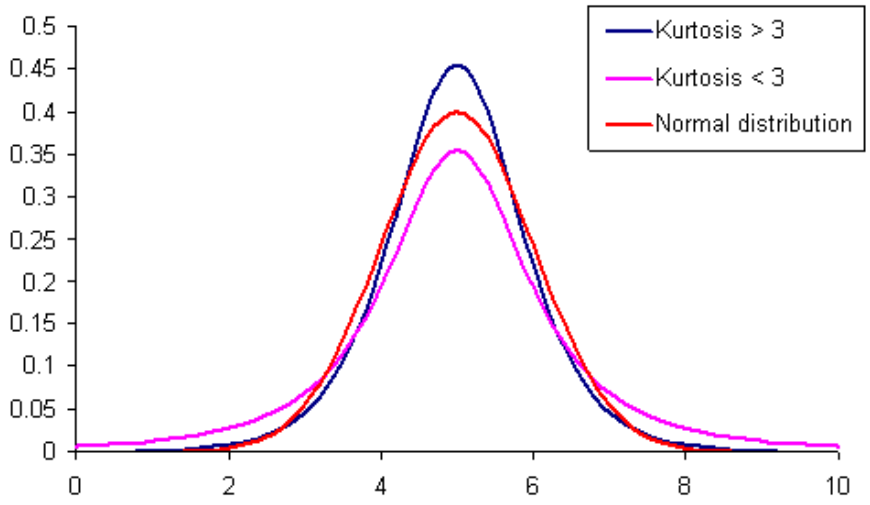

Figure 4.9 - A typical kurtosis waveform

The figure shown below (figure 4.10), illustrates the response of a healthy bearing when operated with 30 nm and 70 nm nano-additive under the load of 40 bar.

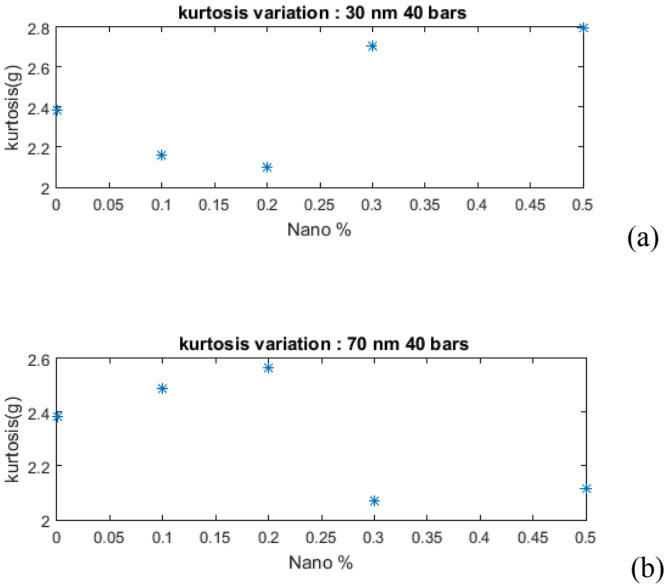

Figure 4.10 - Kurtosis analysis for healthy bearing (a) 30 nm 40 bar (b) 70 nm 40 bar

Figure 4.10 presented a few indications. Firstly, when the bearing is lubricated with 30 nm nano-additives it resulted into lowest kurtosis value of 2.1 at 0.2% nano-additives. When the bearing is lubricated with 70 nm nano-additives it resulted into lowest kurtosis value of 2.1 at 0.3% nano-additives.

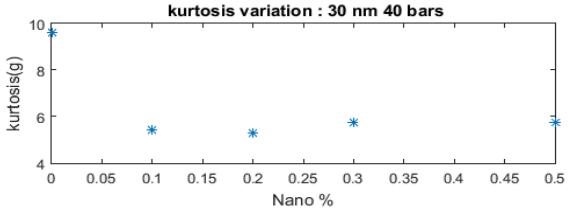

(a)

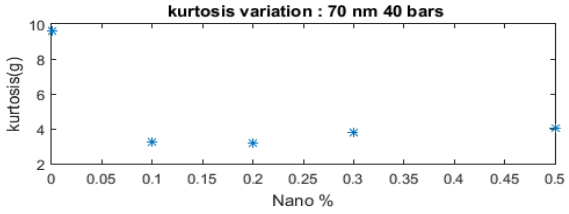

(b)

Figure 4.11 - Kurtosis analysis for 1 mm outer race defected bearing (a) 30 nm 40 bar (b) 70 nm 40 bar

Kurtogram gives us an indication of the bands with high impulsiveness. This introduces an insight to examine high frequencies individually and see what isn't possible with KURTOSIS. Figures 4.12 represent the wavelet kurtogram of a 1 mm outer race defected bearing. We can clearly see the resonance of BPFO which is around 119 Hz. periodic harmonic high frequencies appear on the 70 nm additive.

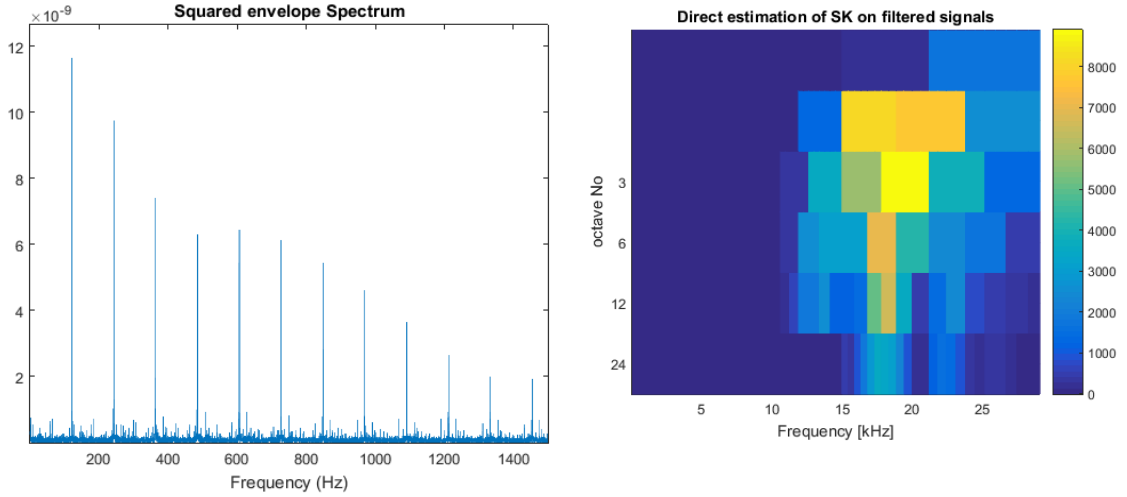

Figure 4.12 - Wavelet Kurtogram of 1 mm outer race defected bearing *0% nano*

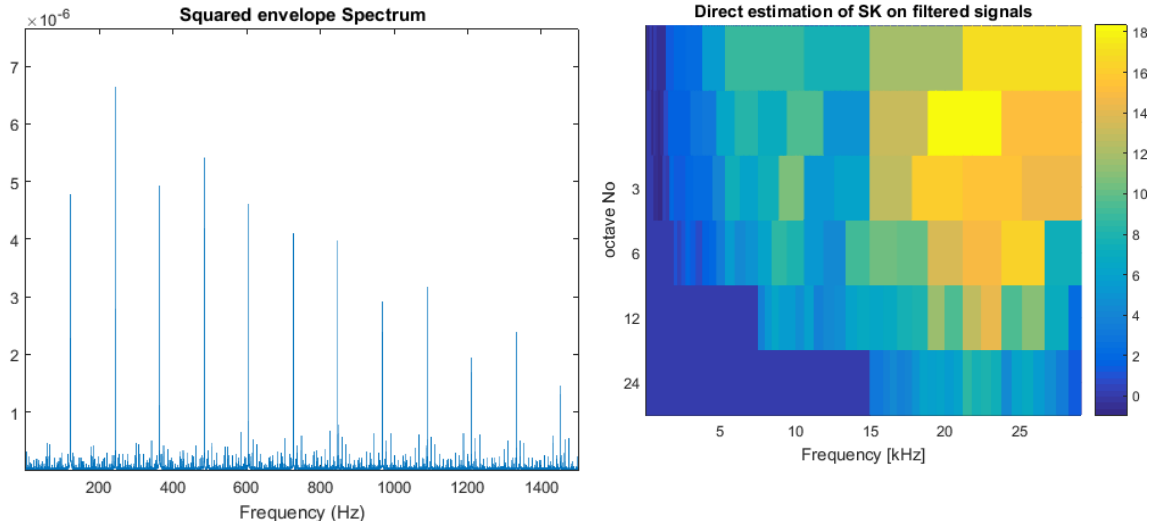

Figure 4.13 - Wavelet Kurtogram of 1 mm outer race defected bearing *0.5% 30nm nano*

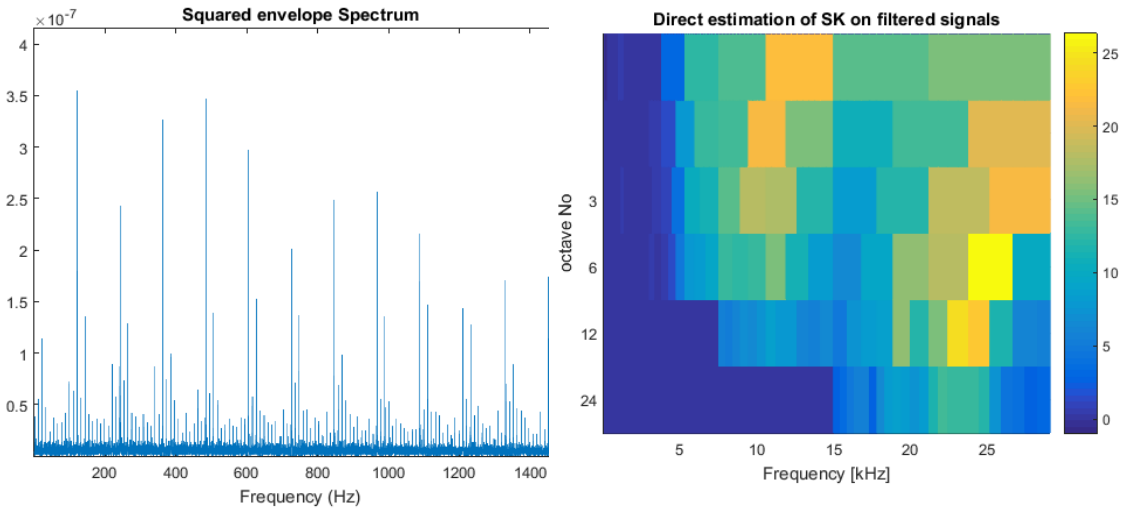

Figure 4.14 - Wavelet Kurtogram of 1 mm outer race defected bearing *0.5% 70 nm nano*

4.3.5 Findings

All the described tests have been made to analyze ball bearing during operation of 1800 rpm under load of 20-40 bar. As the above graphs show, KURTOSIS, RMS, FFT, CPB and Wavelet Kurtogram, are reliable indicators of real time bearing running. Kurtosis indicator decreases as more nano-additive are added; and reaches maximum effectiveness around 0.2% concentration. Our results show that 70nm copper nano-particles are excellent additives. RMS indicates that the energy of the vibration drops despite the existence of faults on either races.

CHAPTER 5

Project Management

5.1 Project Plan

5.2 Contribution of Team Members

5.3 Project Execution Monitoring

5.4 Challenges and Decision Making

5.5 Project Bill of Materials and Budget

5.1 Project Plan

As Mr. Benjamin Franklin once said “Failing to plan is planning to fail". Without a plan we would fail to meet deadlines, fall behind schedule, spend more money than needed due to more money spent on workshops to finish the tasks with less time, and stress out leading to not presenting the best work we could possibly do. In the first week of the semester, we constructed a gantt chart to plan future tasks, have a clear short-term vision of the future, and know vaguely what we are doing. In addition, we nominated as a group a team leader, divided tasks among team members, assigned days to meet as a group, met with advisor and co-advisors to clear things up and decide on days to meet with them, set a clear budget of the project, started working on CAD drawing and bill of materials (presented in figure 5.2 and also in Appendix #), started researching previous work, and finally starting the design process. The gantt chart is shown in figure 5.1.

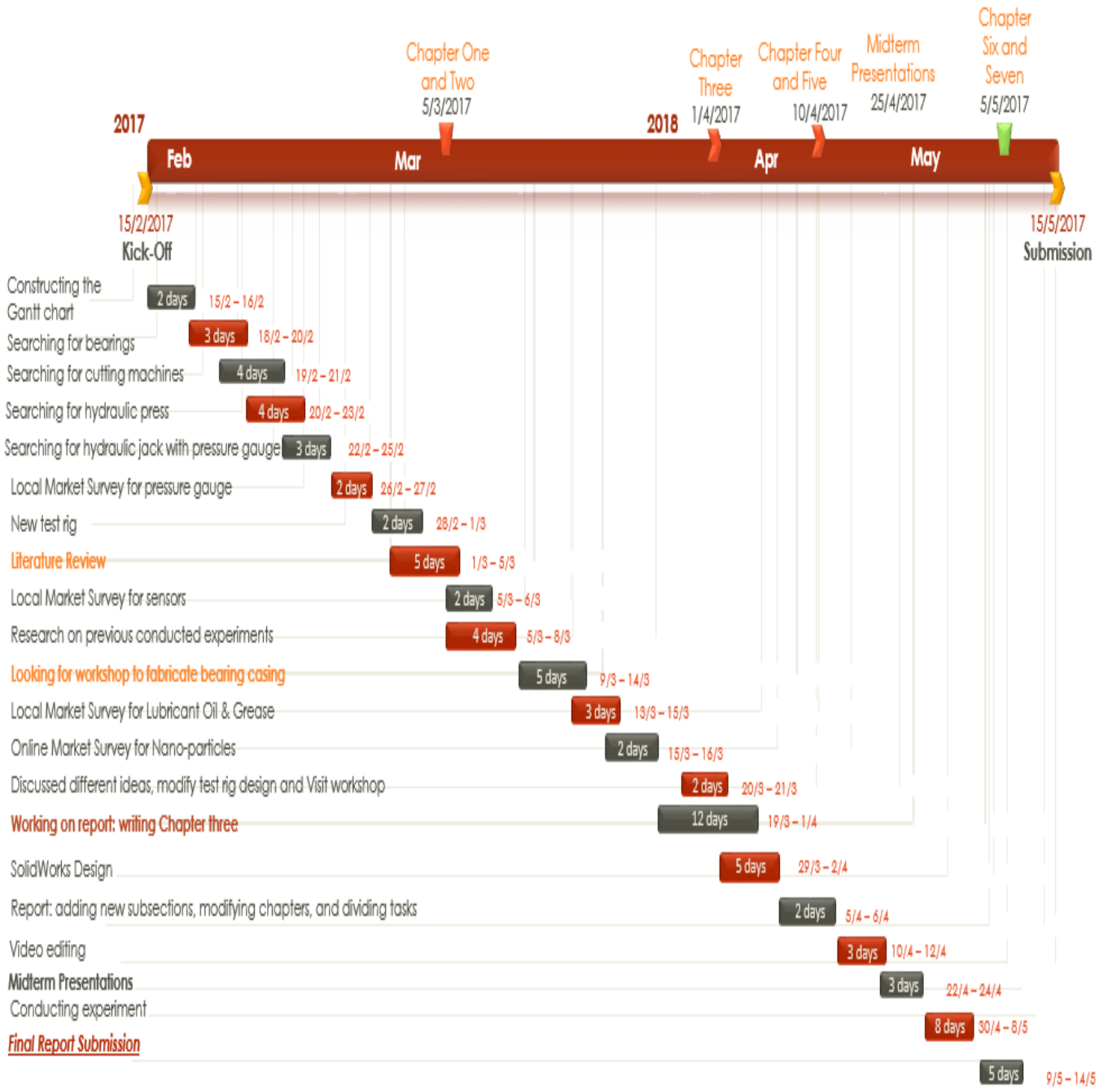

Figure 5.1 - Gantt Chart

.

5.2 Contribution of Team Members

The tasks in our project were divided evenly, depending on skills and time preference. We split our team into two smaller groups to work on different tasks simultaneously and be more productive. For example, a group works on fabrication and purchasing of the project's components, while the other group does research on previous work, market survey of different components of the project, and plan future tasks. Next, the group's trade tasks and work on new tasks or continue working on old/unfinished tasks. This helped us finish our work in a timely manner and avoid procrastination and wasting time. Table 5.1 clearly states the tasks we completed and shows who worked on which tasks.

Table 5.1 - Tasks and who they were assigned to

Tasks	Assigned
Local and online market survey for bearings	Sultan, Shubaily
Local market survey for hydraulic press	Ahmed, Sultan
Local Market Survey for cutting machines	Ahmed, Sultan
Working on the new design for test rig	ALL
Local market survey for hydraulic jack	Ahmed, Sultan, Shubaily
Local market survey for pressure gauge	Ahmed, Sultan
Local market survey for hydraulic press	Ahmed, Sultan
Learning how to fabricate Hydraulic with gauge	Alhawaj, Sultan
Local market survey for current sensor	Sultan
Local market survey for mini pump online	Sultan
Local market survey for workshop to design housing for the new bearing	ALL
Local market survey for electric discharge machine	Shubaily, Sultan, Ahmed
SolidWorks Design	Shubaily, Sultan
Searching for new hydraulic system	Ahmed, Sultan, Shubaily
Constructing the gantt chart and planning next steps of the project	Ahmed, Rami
Group meeting to find alternative design solutions for new test rig	ALL

Local and Online Market Survey for sensors	Shubaily, Rami, Sultan
Online Market Survey for Nanoparticles	Rami, Alhawaj
Research previous conducted experiments	ALL
Literature Review	ALL
Visit workshop ● Documenting machining of new test rig ● Getting updates and follow ups	ALL
Paint	Alhawaj, Sultan
Working on report: writing chapter 2 and 3	ALL
● Bearing vibrations	Ahmed, Rami
● Bearing Loading	Ahmed, Sultan, Alhawaj
● Test Rigs	Rami
● Lubrication Oil & Grease	Shubaily, Alhawaj
● Nano-additives	Rami
● Design selection	Rami
● Shaft Calculations	Alhawaj
● Pulley and its calculations	Sultan
● Design constraints	Shubaily
Video	Rami
Brochure, banner, poster	Rami
Documenting the process of the experiments and fabrication (photos, video, updates)	Rami
Working on report: writing chapter 4,5,6, and 7	ALL
Conducting experiments	Ahmed, Alhawaj, Shubaily, Sultan
Data acquisition	Alhawaj, Sultan

5.3 Project Execution Monitoring

To execute this project in a satisfactory way, we had to construct a road map that contains crucial dates such as meetings, phases of the project, assembling of the project, testing, and data analysation. To do so, in the first week of the semester, we allocated a couple of days of each week that rarely changed to meet with our advisor (Dr. Nader Sawalhi). If we decided to postpone the meeting we will inform each other and inform Dr. Nader Sawalhi at least 24 hours in advance. We made a Whatsapp (messaging phone application) group to send announcements, updates, questions, and time of meetings. In addition, we opened a file sharing cloud service folder/group (Google Drive) where we post all the work that is completed or currently in progress. The meetings with Dr. Nader orbited around questions, extra information on different aspects of the project, modifications to design of the new test rig, and modifications to the report. In addition to the meetings with Dr. Nader, we had meetings with the co-advisors (Dr. Roodi and Dr. Adrian) where we also discussed information on different aspects of the project. Moreover, we met as a group nearly everyday of the week to work on the project simultaneously and share with each other updates and follow ups.

Other than meetings we also planned testing work. Our tests depend directly on the test rig we built, and so we couldn't start the experiments without finishing the test rig first. Therefore, the experiments had to be the final task of the project before finalising of the report. However, that does not mean we focused more on the test rig than the actual experiments. According, to our gantt chart and our plan we had enough time to complete all the tasks.

5.4 Challenges and Decision Making

Conflicts and misunderstanding can occur in any team work. Our group is not an exception or immune to this issue. However, with the leadership, conflict resolution, and critical thinking skills we obtained from experience along our educational career we were able to solve teamwork related issues that could have hindered the progress of our team. In addition to the previous skills, we nominated a team leader that would be beneficial to the team. It is crucial to vote for a team leader for a few reasons including: act as a mediator between team members, delegate tasks, be firm with commands/task assigning, and have the last word on decisions (after discussion and brainstorming with the team members).

In addition to teamworking difficulties, there were several occasions where our budget and schedule were affected slightly. For example, after contracting with a workshop on fabricating several components of the project, they completed only a small part of tasks we delegated to them and informed us that they can not continue working on the fabrication. This forced us to spend more time than intended on looking for another workshop. Furthermore, due to our essential need of introducing highly precise simulated defects, we desired a machine called Electrical Discharge Machine that only one workshop in the Eastern Province possess. Therefore, the workshop monopolized the market and set an outrageous price for each defect they introduce. These bothersome limitations were not able to slow the team's progress significantly. We were able to find an alternative workshop with cheaper prices to fabricate the components we require. In addition, we negotiated with the workshop that introduced the defects for a special discount since we are university students with limited funds.

Due to our project's nature, one of the main tasks was to improve the old test rig and add modifications that would advance the workability of the test rig. We faced challenges in improving several components. Firstly, the old oil tank was rectangular in shape with an open design. It did not allow continuous lubrication of the bearings, was causing oil leaks and overflowing of the oil, and prevented the oil to fully disperse. Secondly, The bearing was not protected by a housing that will allow us to apply load and attach sensors. Thirdly, the previous loading system was basic and did not allow us to know the exact magnitude of the load we were applying. Fourthly, the previous pulleys did not allow testing to be done under multiple speeds. Lastly, the shaft did not have fillets which caused high stresses in different regions of the shaft. With our collective engineering skills acquired from university courses and assistance provided by the advisor and co-advisors, we were able to present huge improvements to the old test rig. Since our test rig has great potential, it can still be improved further in the upcoming semesters by adding additional modifications that will allow more experiments to be conducted on it.

Time available to work on a project this sophisticated was a challenge to us. However, we were able to complete the test rig in time.

5.5 Project Bill of Materials and Budget

We utilised Solidworks to present an illustration of the different parts of the test rig assembly. The bill of materials is shown in figure 5.2. The bill of material will be shown in more detail in appendix #.

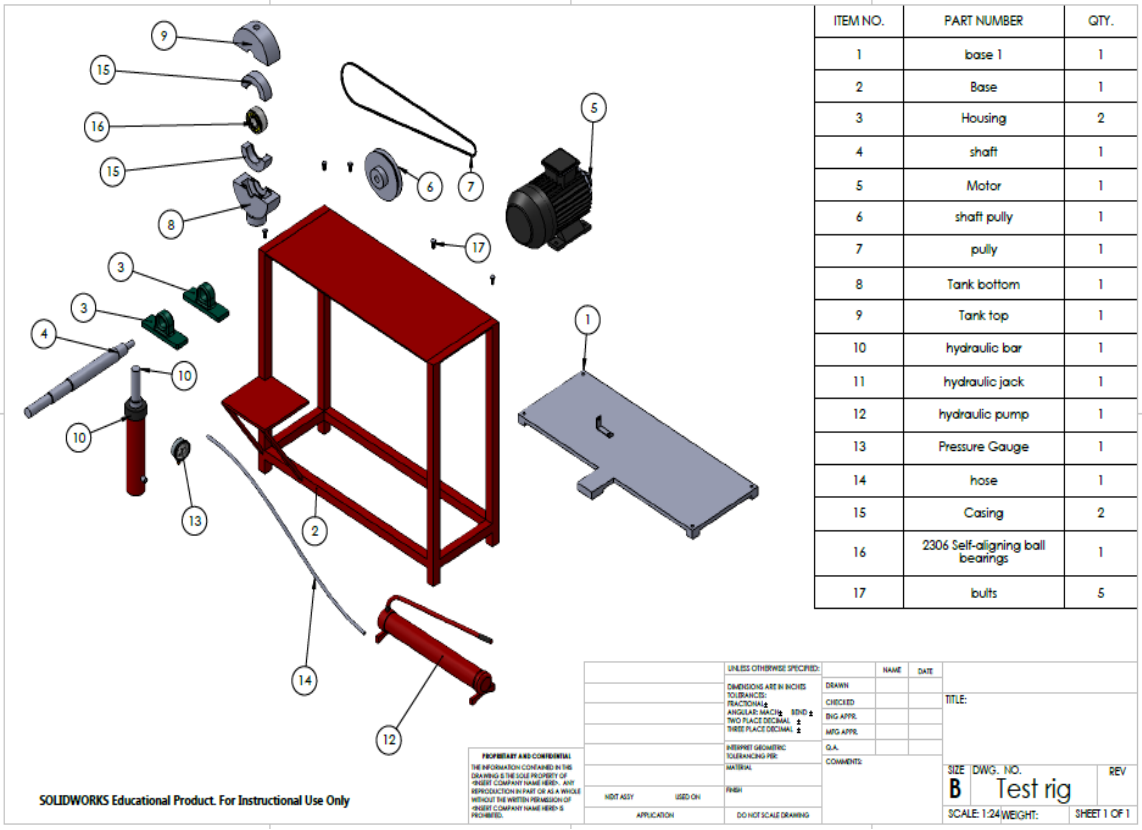

ITEM NO.	PART NUMBER	QTY.
1	base 1	1
2	Base	1
3	Housing	2
4	shaft	1
5	Motor	1
6	shaft pully	1
7	pully	1
8	Tank bottom	1
9	Tank top	1
10	hydraulic bar	1
11	hydraulic jack	1
12	hydraulic pump	1
13	Pressure Gauge	1
14	hose	1
15	Casing	2
16	2306 Self-aligning ball bearings	1
17	bolts	5

Figure 5.2 - The Bill of Materials

Even though we had some hiccups with workshops and introducing faults to the bearings, we did not exceed our initial budget. Our expenses is presented in table 5.2.

Table 5.2 - Expenses of purchases and fabrication

	Items	Cost (SAR)	Quantity	Details
1	Lubricant (Grease+ Oil)	105	3	LJMT 3/1, 15w40
2	Copper Nano Particles	1692	2	30nm, 70nm
3	Bearings	640	11	2306 Koyo
4	Safety Box and Pulley System	455	1	
5	Loading Mechanism/Fabrication			
5.1	Bearings Cases	1400	2	
5.2	T-connection	20	1	
5.3	Pressure Gage	145	1	2000 psi TECSIS
5.4	Hydraulic System	390	1	10 TON
5.5	Pressure Calibration	250	1	UKAS
5.6	Belt	38	2	OPTIBELT-VB
5.7	Bolt	5	6	
6	Paint	35	2	JACK
7	Cable Ties	22	1	VOLT
8	Pump	25	1	
9	Ultrasonic Sensor + Circuit	150	2	
10	Bearing defect fabrication	600	4	
11	Plummer Block Bearing	120	2	
	Total	6092		

CHAPTER 6

Project Analysis

6.1 Life-long Learning

6.1.1 New Knowledge

6.1.2 New Hardware and Software tools

6.1.3 Project and Time Management Skills

6.2 Impact of Engineering Solutions

6.3 Contemporary Issues Addressed

6.1 Life-long Learning

We chose this project due to its sophistication and the numerous opportunities it will provide us. It is considered a higher level research project, which inspired us to pursuit it and expand our knowledge. Our advisor was a great source of information when we needed further clarification of concerns/questions. In addition, we used website such as Google Scholar and Youtube to gain knowledge about different aspects of the project.

6.1.1 New Knowledge

Our project consisted of topics that we did not cover thoroughly in our bachelor degree plan (i.e. vibration and statistical analysis of vibration data), which encouraged us even further to seek it and enable us to gain experience in those fields. We gained experience in those fields by many ways. Firstly, our advisor partnered us with a team from the Electrical Engineering Department that had a similar interest to us. The electrical engineering team helped us clarify different questions and concerns we had regarding the project. Secondly, we self-studied those topics by studying documents our advisor provided that explained in detail different aspects of the topics. Thirdly, by researching previous work and studies, we absorbed information other researchers published that explained those topics even further.

6.1.2 New Hardware and Software tools

In addition, we utilised fairly new hardware to us that presented challenges to us. Firstly, sensors including accelerometer and tachometer were new to us, this is because we did not utilise them in many cases before. Similarly to the new topics we were introduced to we seeked help from documents provided by our advisor, learning from previous work and studies, and help from students in the electrical engineering department. We were successfully able to gain knowledge about sensors (i.e. how they operate). Furthermore, we used data processing tools including LabVIEW and Matlab that we had a brief background on, and so we had the opportunity to experience them. We were able to learn new skills in those tools using assistance provided by our advisor, youtube videos, and help from electrical engineering students who have a huge experience with them due to extensive work with them in projects and class work.

6.1.3 Project and Time Management Skills

Working on projects in teams is always a rich bank of new experiences and skills. Working on this project forced us to face problems and lean towards critical thinking to solve them. In addition, we learned excellent project and time management skills such as gantt chart to properly manage our time and avoid late completion of tasks. Moreover, working on a project like this, teached us that team members must be flexible and compromise every once in awhile to meet in a middle ground with other team members. Furthermore, working on this project helped us more on setting a budget efficiently and follow it as close as possible.

6.2 Impact of Engineering Solutions

This project is expected to attract the interest of industry giants like Saudi ARAMCO and SABIC. This test rig is helpful for predictive and preventive maintenance. It can help companies save a lot of money by decreasing down time. The following are some of the expected benefits of the project presented:

(i) Provide an insight into the role of the nanomaterial lubricant additives and its effects on the noise and vibrations of machines.

(ii) Promote the development of a base fundamental model for vibrations from machines with nanomaterial lubricant additives.

(iii) Advanced signal monitoring techniques will be developed to examine the effects of the nanomaterial additives on the wear.

(iv) Develop a knowledge base in Prince Mohammad Bin Fahd University of nanomaterial lubricants and vibration analysis.

(v) Put Saudi Arabia on the map of the topic of nano-additive lubricant impact on the noise and vibration of machines.

(vi) The test rig we developed and its data acquisition system will provide a solid starting ground for other students to continue working on it as their senior project. In addition, a lot of publications are expected from the project.

6.3 Contemporary Issues Addressed

As explained above, industry giants are always striving to reduce turnaround time. Therefore, they seek predictive and preventive maintenance to avoid wasting expensive time on shutdown. Test rigs like ours, allow these companies to test their rotating equipment bearings periodically to avoid operating with an inefficient defected bearing. In addition, the results we obtained will help companies decide whether or not adding nano-particles to oil based lubricants is a good investment.

CHAPTER 7
Conclusions and Future Recommendations

7.1 Conclusions

7.2 Future Recommendations

7.1 Conclusions

In conclusion, we have experienced an unparalleled expeerience. We selected this project due to its sophistication and the numerous opportunities it will provide us. It is considered a higher level research project, which inspired us to pursuit it even further and expand our knowledge base. We have described tests have been made to analyze ball bearing during operation of 1800 rpm under load of 20 and 40 bar. Our findings show that Kurtosis, RMS, FFT, CPB And Wavelet Kurtogram are reliable indicators of real time bearing running. Kurtosis indicator decreases as more nano-additive are added; and reaches maximum effectiveness around 0.2% concentration. Our results show that 70nm copper nano-particles are excellent additives. RMS indicates that the energy of the vibration drops despite the existence of faults on either races. This project is unique to other projects because it uses pure copper nano particles that was not used before for this application. In addition, we added ultrasonic sensors to suspend the nano-particles in the lubricant in a new never been done before configuration. We have faced in a few different aspects of the project however we were able to overcome them and succeed. For example we faced challenges in implementing an adequate loading system, a functional bearing housing and oil tank, and torque transformation system (motor to shaft). Furthermore, there were topics that we did not cover in our degree courses (i.e. vibration and statistical analysis of vibration data) that presented more challenges to us. However, facing these challenges and overcoming them have strengthened our engineering skills, encouraged us even further to seek it, enable us to gain experience in those fields, and made us think more critically and effectively.

7.2 Future Recommendations

Recommendation 1 Replace the current motor with dc powered motor in order to control speed that provides high loads

Recommendation 2 Replace the pulley belt mechanism with coupling. This will improve in reducing the vibration especially the external belt vibration

Recommendation 3 Replace the hydraulic system with a better loading design such as screw mechanism loading

Recommendation 4 Insert current sensors to measure the correlation between load and current

Recommendation 5 Use a more frictionless surface on a petri dish so no nano-particles stick on its surface to control the percentage accuracy

Recommendation 6 Modify the Support on the tray on which the hydraulic press is seated

Recommendation 7 Conduct the experiment with different types of lubricant such as grease

CHAPTER 8
References

[1] Robinson, T. L. (1932). U.S. Patent No. 1,888,361. Washington, DC: U.S. Patent and Trademark Office.

[2] Hamrock, B. J., & Dowson, D. (1981). Ball bearing lubrication: the elastohydrodynamics of elliptical Contacts.

[3] Signer, H. R. (1982). *U.S. Patent No. 4,334,720*. Washington, DC: U.S. Patent and Trademark Office.

[4] ASTM D 288, Standard Definitions of Terms Relating to Petroleum. Retrieved from http://machinerylubrication.com/Read/1352/grease-basics

[5] Bearing Lubrication: Oil vs. Grease. Retrieved from http://www.bearingtips.com/bearing-lubrication-oil-vs-grease/

[6] BASIC HYDRAULICS AND COMPONENTS. (1995). Retrieved March 15, 2017, from https://yuken-usa.com/pdf/special/Basic_Hydraulic_And_Components_(Pub._ES-100-2)_.pdf

[7] Ricardo S, Marcia M and Linilson P. Effect of lubricant oil viscosity and contamination on the Mechanical signature of roller bearing. Twelfth International Conference on Sound and Vibration 87 (2005). 514-567.

[8] Tyagi, D.K and Jain, A.K., Experimental study of vibration characteristics of roller bearing using mixed nanofluids: A review. International Journal of engineering and development, issue 4, vol. 3 (May, 2014). 855-859.

[9] Serrato-Castillo, R., Maru, M. M., & Padovese, L. R. (2005, July). Effect of lubricant oil viscosity and contamination on the mechanical signature of roller bearings. In *Twelfth international congress on sound and vibration* (pp. 11-14).

[10] Jiao, D., Zheng, S., Wang, Y., Guan, R., & Cao, B. (2011). The tribology properties of alumina/silica composite nanoparticles as lubricant additives. *Applied Surface Science*, *257*(13), 5720-5725.

[11] Koppula, S. B., & Sudheer, N. V. V. S. (2016). A Review on Effect of Adding Additives and Nano Additives on Thermal properties of Gear Box Lubricants. International Journal of Applied Engineering Research, 11(5), 3509-3526.

[12] Apandi, N. S. R., Ismail, R., Abdollah, M. F. B., & Ramlan, R. (2016) VIBRATION CHARACTERISTIC ON BALL BEARING OPERATED WITH HEXAGONAL BORON NITRIDE (HBN) NANOPARTICLE MIXED WITH DIESEL ENGINE OIL.

[13] Prakash, E., Kumar, S., & Muthu Kumar, K. (2013). Experimental studies on vibration characteristics on ball bearing operated with copper oxide nano particle mixed lubricant. International Journal o Engineering and Technology (IJET).

[14] Dempsey, P. J., Certo, J. M., Handschuh, R. F., & Dimofte, F. (2005). Hybrid bearing prognostic test rig.

[15] Flack, R. D., Kostrzewsky, G. J., & Taylor, D. V. (1993). A hydrodynamic journal bearing test rig with dynamic measurement capabilities. *Tribology transactions*, *36*(4), 497-512.

[16] Al-Ghamd, A. M., & Mba, D. (2006). A comparative experimental study on the use of acoustic emission and vibration analysis for bearing defect identification and estimation of defect size. *Mechanical systems and signal processing*, *20*(7), 1537-1571.

[17] Choudhury, A., & Tandon, N. (2000). Application of acoustic emission technique for the detection of defects in rolling element bearings. Tribology international, 33(1), 39-45.

[18] Priestner, C., Allmaier, H., Priebsch, H. H., & Forstner, C. (2012). Refined simulation of friction power loss in crank shaft slider bearings considering wear in the mixed lubrication regime. *Tribology International*, *46*(1), 200-207.

[19] Kuře, G.: Tests, test runs and applications of rolling bearings in railway vehicles. ZEV Glasers Annalen 113 (1989) 6–7, pp. 313–322.

[20] Fag Interamericana AG. Rolling bearing lubrication. Publication no. WL 81 115/4 SE, 1997(b).

[21] Fag Interamericana AG. Rolling bearing faults. Publication no. WL 82 102/2 SE, 1997(a).

[22] Harris TA. Rolling bearings analysis. Mechanics of lubrication in concentrated contacts, USA/Canada: Wiley, 1984. pp. 342–78, 565pp [Chapter 12].

[23] Mohammed Modu Aji, Shettima Abba Kyari and Gideon Zoaka (2015).Comparative Studies Between Bio Lubricants From Jatropha Oil, Neem Oil And Mineral Lubricant (Engen Super 20w/50)

[24] Bilal, S, Mohammed-Dabo I, Nuhu M, Kasim, S, Almustapha I and Yamusa Y. Production of biolubricant from Jatropha curcas seed oil, Department of Chemical Engineering, Ahmadu Bello University, Zaria. Nigeria. Centre for Energy Research and Training, Ahmadu Bello University, Zaria. Nigeria. Accepted 28 August, 2013

[25] J. Chebil, M. Hrairi, N. Abushikhah, Signal analysis of vibration measurements for condition monitoring of bearings, Australian Journal of Basic and Applied Sciences, 5(1) (2011) 70-78.

[26] Z. KÕral, H. Karagülle, Vibration analysis of rolling element bearings with various defects under the action of an unbalanced force, Mechanical Systems and Signal Processing. 20 (2006) 1967-1991.

[27] S.A. Abdusslam, F. Gu, A. Ball, Bearing fault diagnosis based on vibration signals, Proceedings of Computing and Engineering Annual Researchers Conference (2009) 93-98.

[28] Sutrisno, E., Oh, H., Vasan, A. S. S., & Pecht, M. (2012, June). Estimation of remaining useful life of ball bearings using data driven methodologies. In Prognostics and Health Management (PHM), 2012 IEEE Conference on (pp. 1-7). IEEE.

[29] Janjarasjitt, S., Ocak, H., & Loparo, K. A. (2008). Bearing condition diagnosis and prognosis using applied nonlinear dynamical analysis of machine vibration signal. Journal of Sound and Vibration, 317(1), 112-126.

[30] Precision Industrial Components. (2007). Belts and Pulleys. Retrieved April, 2017, from http://pic-designcatalog.com/images/pdfcat/section_5.pdf

[31] MEGADYNE RUBBER. (2009, March). V-BELTS: rubber v-belts . Retrieved April, 2017, from http://www.exvalos.cz/soubory/File/MEGADYNE_V-BELTS%202009.pdf

Appendix A

Healthy Bearing Experimental Procedure

1. Wear protective personal equipment (PPE) such as latex gloves, face masks, and safety goggles
2. Obtain an electronic scale balance, and place a graduated cylinder, press the tare button to zero the balance, and add 30 ml of 15w-40 oil to the graduated cylinder.
3. Measure the equivalent weight of 30 ml of oil
4. Release the hydraulic valve so the half the lower the oil tank moves down
5. Carefully insert the bearing in which the experiment will be conducted on
6. Align the bearing with the inside of the oil tank, make sure the outer race of the bearing is properly seated on top of the oil tank
7. Apply load of 10 bar
8. Pour the oil from the graduated cylinder into the oil tank, the proper way is to pour within both sides to minimize oil leakage through the shaft opening
9. Assemble the upper half of the oil tank with the lower half
10. Apply load until the pressure gage indicates 20 bar
11. On the designated computer unit, press run in the labview menu and wait till the data recording is complete
12. Save the file as a text file and import to matlab
13. Repeat steps 10 to 12 for 40 bar load and 60 bar load
14. Release the pressure load until it indicates 10 bars again
15. Stop the motor
16. Repeat steps 10 to 15 for other speeds. Rearrange pulley system with respective ratio to test on the two other speeds of 3400 rpm and 6800 rpm.

Defective Bearing Experimental Procedure

1. Place petri dish on electronic balance, press the tare button to zero the balance, add 30 nm nanoparticles small amount at a time until it reaches the desired weight amount.
2. Release the hydraulic valve so the half the lower the oil tank moves down
3. Carefully insert the bearing in which the experiment will be conducted on
4. Align the bearing with the inside of the oil tank, make sure the outer race of the bearing is properly seated on top of the oil tank
5. Apply load by the hydraulic until it reaches 10 bar
6. Pour the oil from the graduated cylinder into the oil tank.
7. Add the 30 nm nanoparticles to oil in oil tank
8. Assemble the upper and lower half of the oil tank
9. Start the motor, let the motor run for at least five minutes. Make sure the ultrasonic sensors are operating to suspend the nanoparticles in the oil
10. Apply load until the pressure gage indicates 20 bar
11. On the designated computer unit, press run on the labview menu and wait till the data recording is complete
12. Repeat steps 10 and 11 for 40 bar and 60 bar load
13. Release the pressure load until it indicates 10 bars again
14. Stop the motor
15. Save the files as a text file and import to matlab
16. Disassemble the tank
17. Add more nanoparticles till desired concentration is reached
18. Repeat steps 8 to 15 for new concentration of nanoparticles
19. Clean the bearings and oil tank to remove completely old oil and nano-particles (explained in section 4.1.3)
20. Repeat the above steps for 70 nm nanoparticles

Bearing Cleaning Procedure

1. Soak the bearings in a bucket containing recommended solvent (Gasoline 91 in our case).

Figure 4.1 - Soaking bearings in bucket with solvent

2. After nanoparticles and oil is removed, move the bearing into another clean bucket of solvent.
3. Dry the bearings using compressed air. Make sure compressed air contains no moisture.

Figure 4.2 - Drying the bearings with compressed air

4. After cleaning, inspect the bearing thoroughly for leftover dirt and damage.
5. Lubricate the races of the bearing.
6. Rub the bearings with a clean dry paper towel or cloth rag and label it.

Hardware and Software Requirements

To conduct the tests properly we need specific hardware equipment that will allow us to have accurate results. In addition, we need software programs that will allow us to acquire and present data.

Name	Specifications	Quantity	Image
Electronic Scale balance		1	
Graduated cylinder	100 ml	1	
Beaaker	100 ml	1	
Glass dripper bottle		1	
Nano-particles	30 nm and 70 nm	100g/each size	

Spatula		1	
Petri Dish		1	
Zip-ties		20	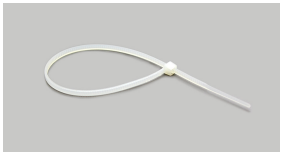
PC-Based Platform for Test and Measurement	NI PXIe-1062Q	1	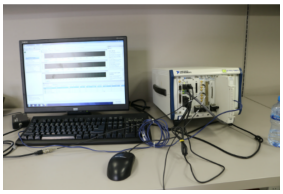

The software requirements are:

1. Computer
2. Operating System: Windows 7
3. Signal processing tool and Data acquiring software: LabVIEW and Matlab
4. Microsoft Excel

Appendix B

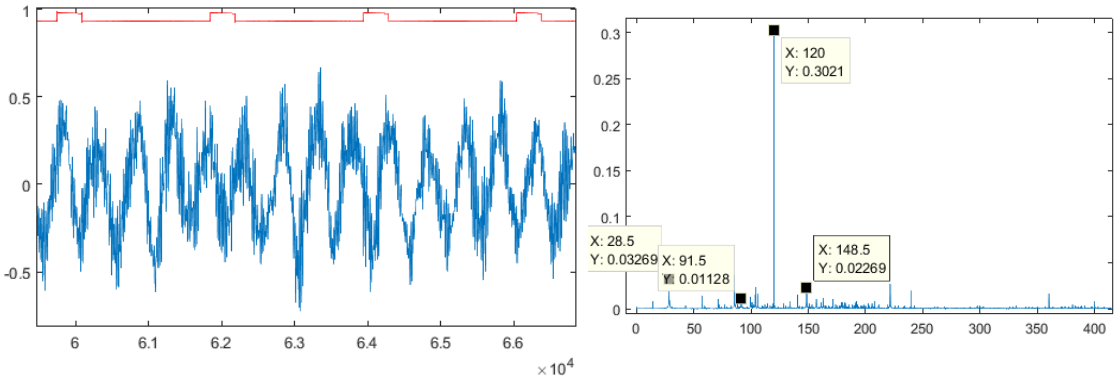

Figure B1 - Time domain and FFT signal for healthy bearing loaded with 40 bar 0% 30 nano

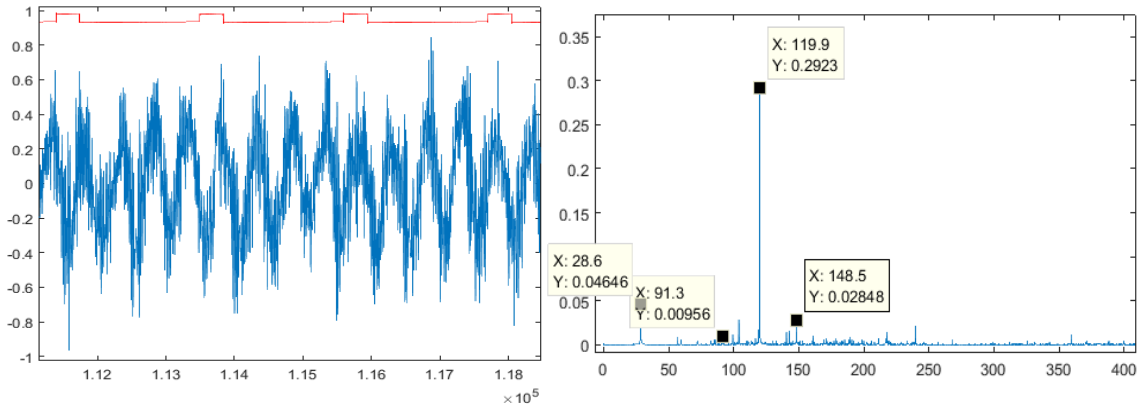

Figure B2 - Time domain and FFT signal for healthy bearing loaded with 40 bar 0.5% 30 nano

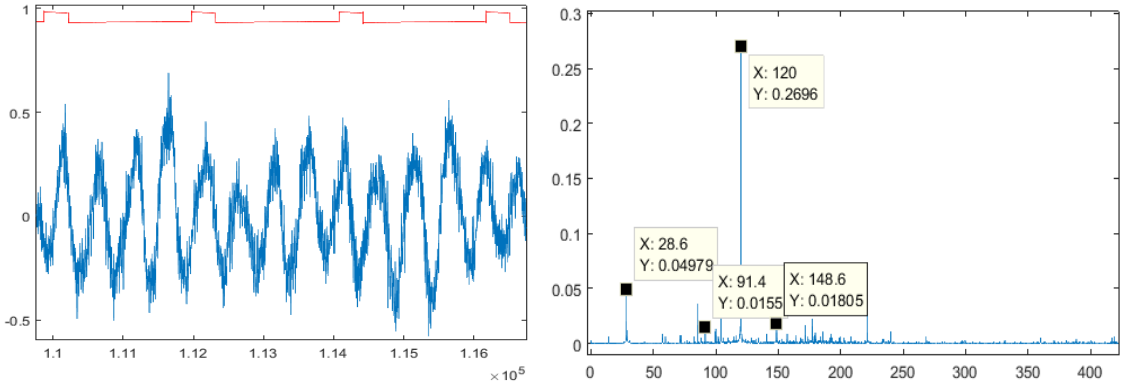

Figure B3 - Time domain and FFT signal for healthy bearing loaded with 40 bar 0.5% 70 nano

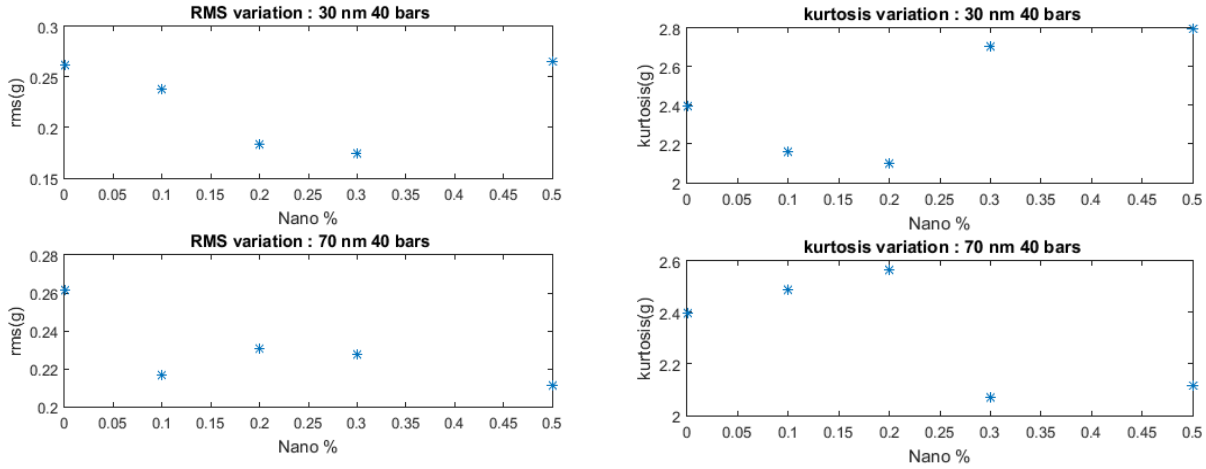

Figure B4 - RMS and Kurtosis values for a healthy bearing

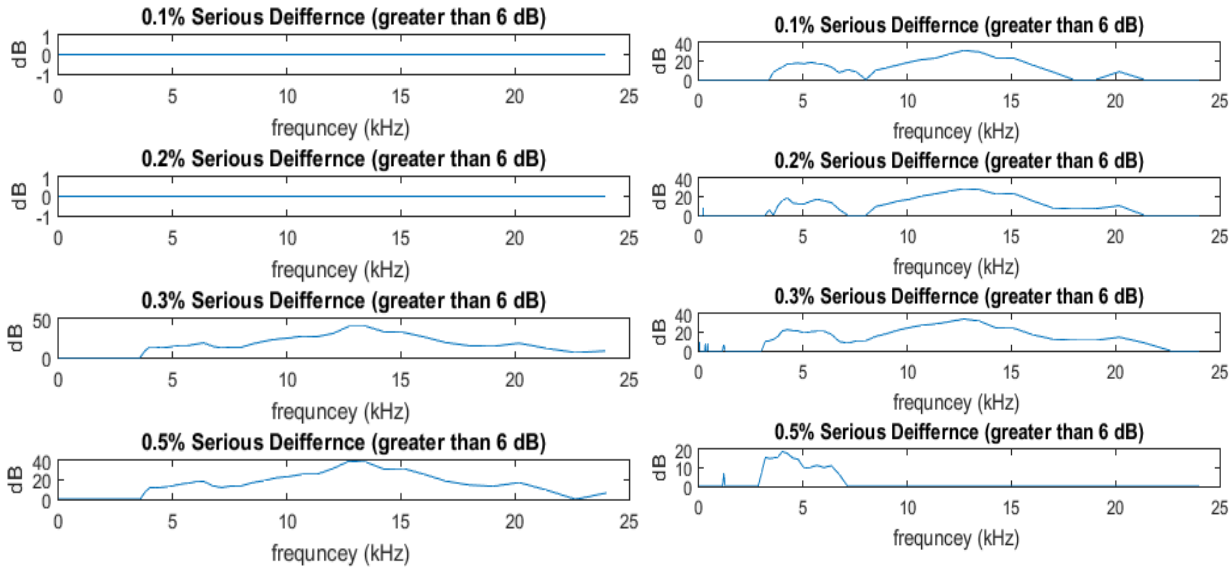

Figure B5 - 1/12 CPB Analysis for a healthy bearing on the left 30 nm on the right 70 nm at 40 bars

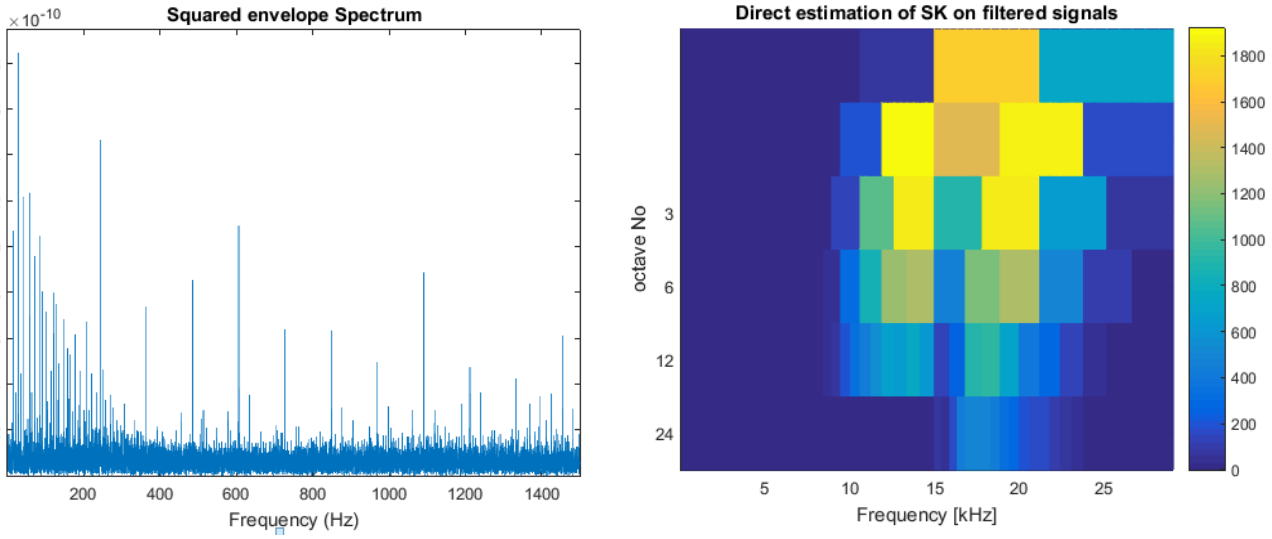

Figure B6 - Wavelet Kurtogram 0% nm for a healthy bearing at 40 bar

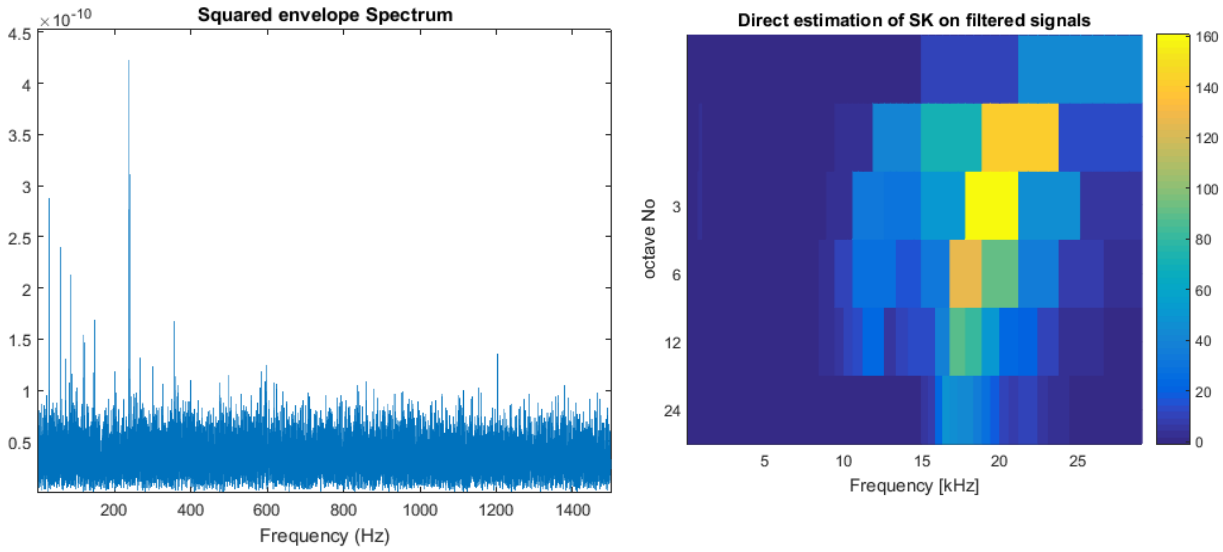

Figure B7 - Wavelet Kurtogram 0.5% of 30 nano for a healthy bearing at 40 bar

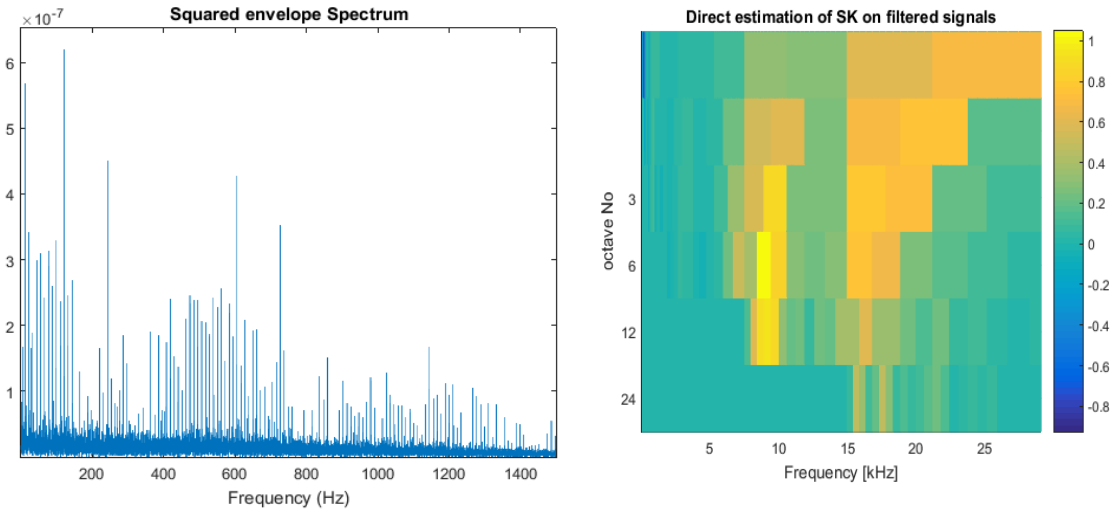

Figure B8 - Wavelet Kurtogram 0.5% of 70 nano for a healthy bearing at 40 bar

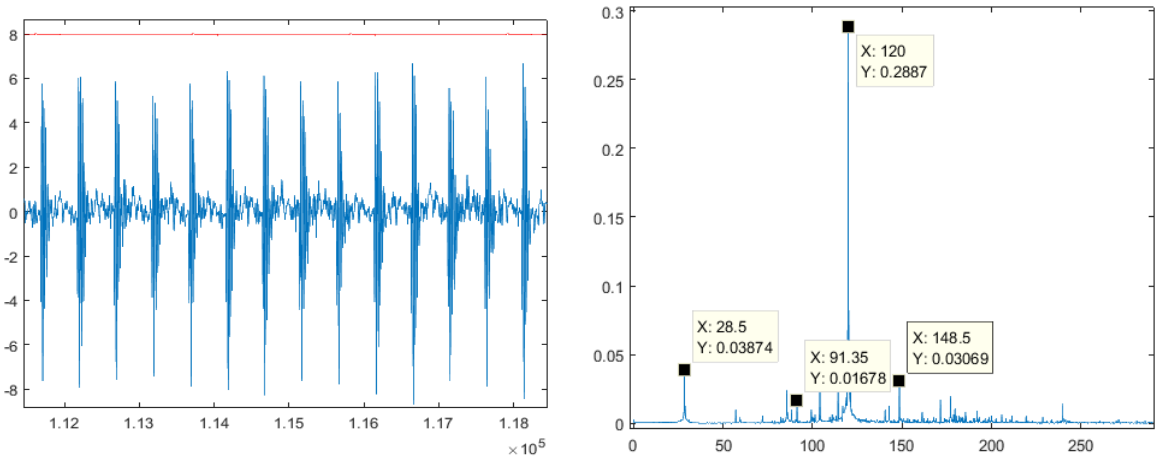

Figure B9 - Time domain and FFT signal for 1 mm outer bearing loaded with 40 bar 0% 30 nano

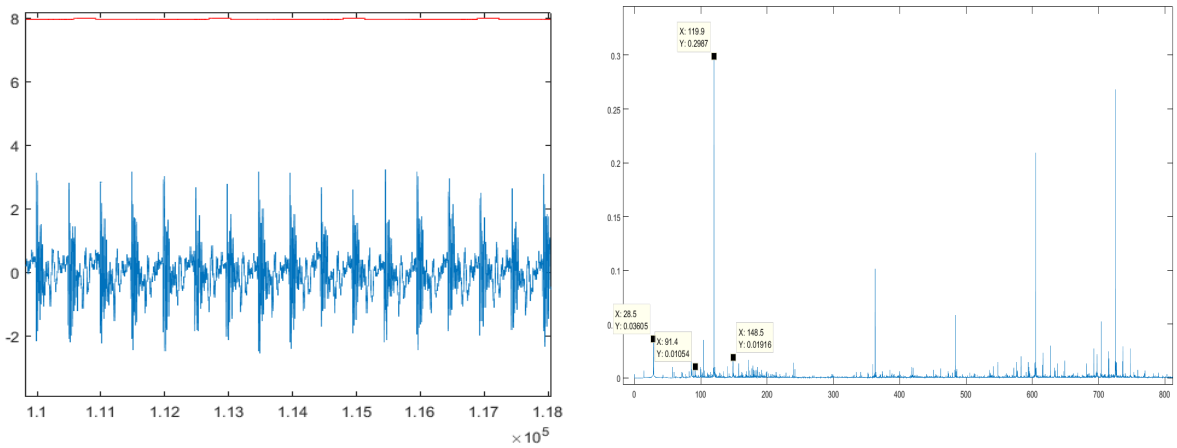

Figure B10 - Time domain and FFT signal for 1 mm outer bearing loaded with 40 bar 0.5% 30 nano

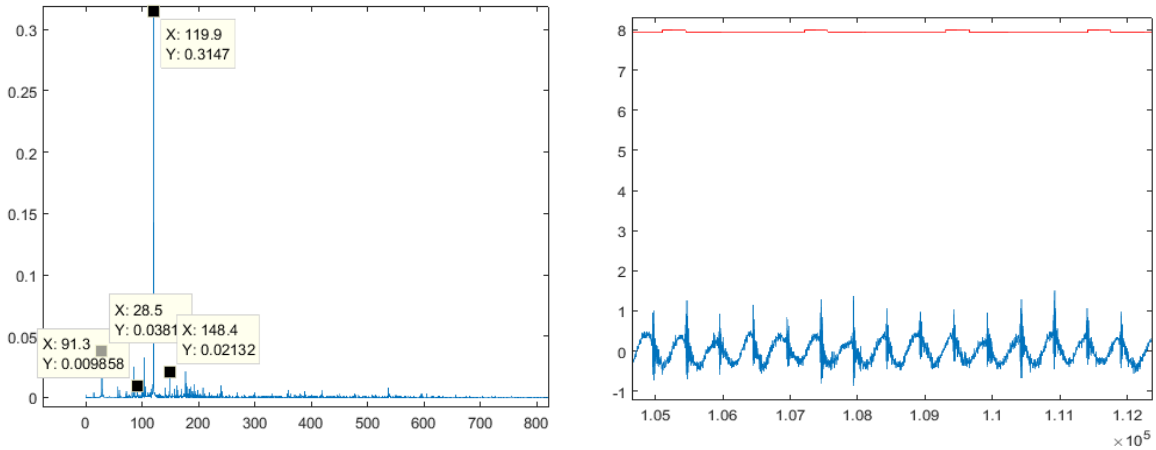

Figure B11 - Time domain and FFT signal for 1 mm outer bearing loaded with 40 bar 0.5% 70 nano

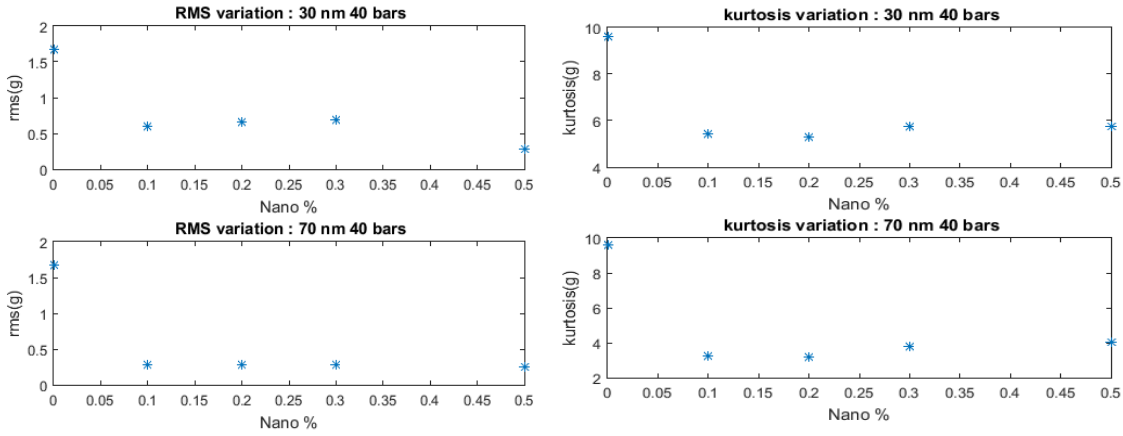

Figure B12 - RMS and Kurtosis values for a 1 mm outer bearing

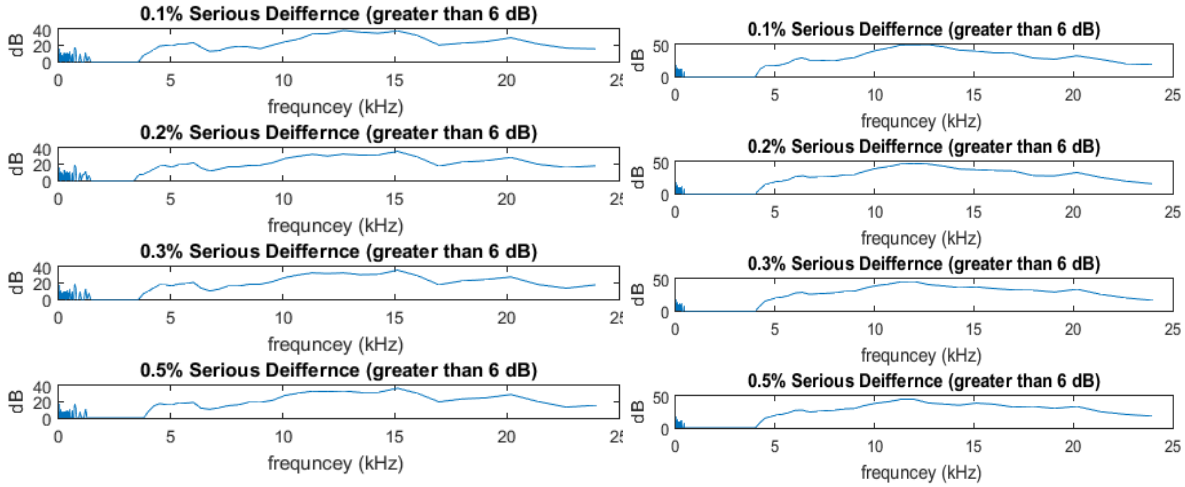

Figure B13 - 1/12 CPB Analysis for a 1 mm outer bearing on the left 30 nm on the right 70 nm at 40 bars

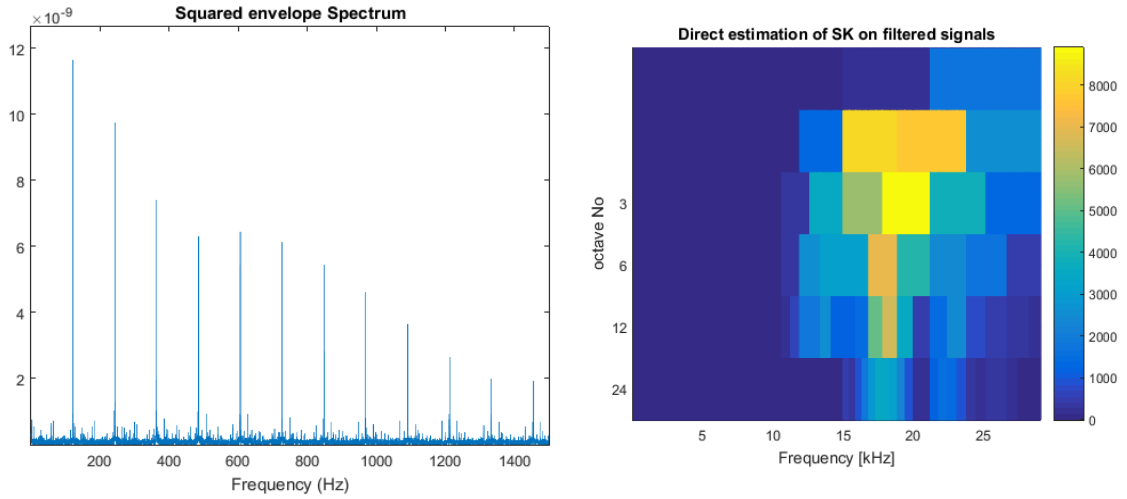

Figure B14 - Wavelet Kurtogram 0% nm for 1 mm outer bearing at 40 bar

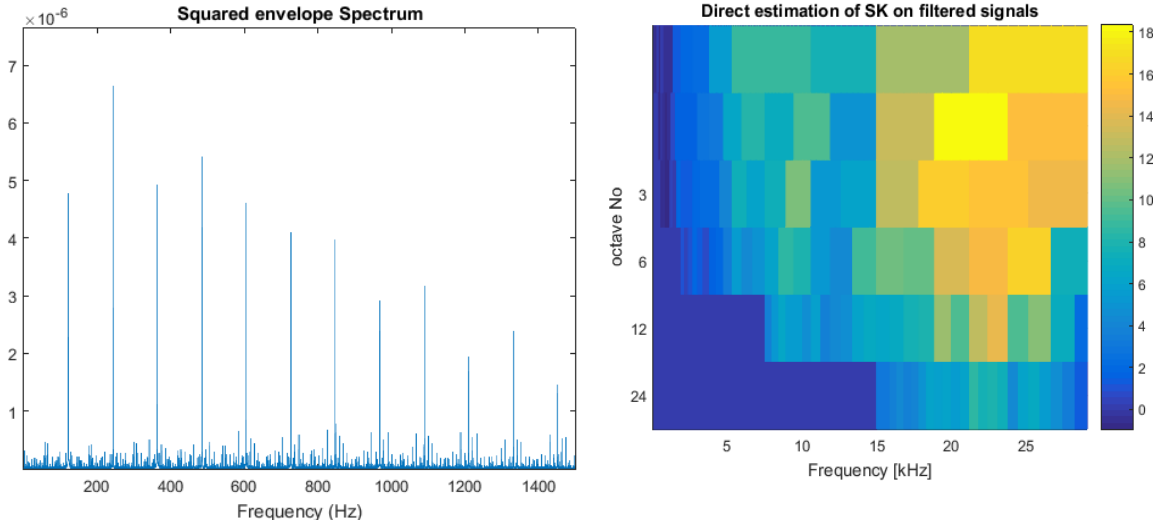

Figure B15 - Wavelet Kurtogram 0.5% of 30 nano for 1 mm outer bearing at 40 bar

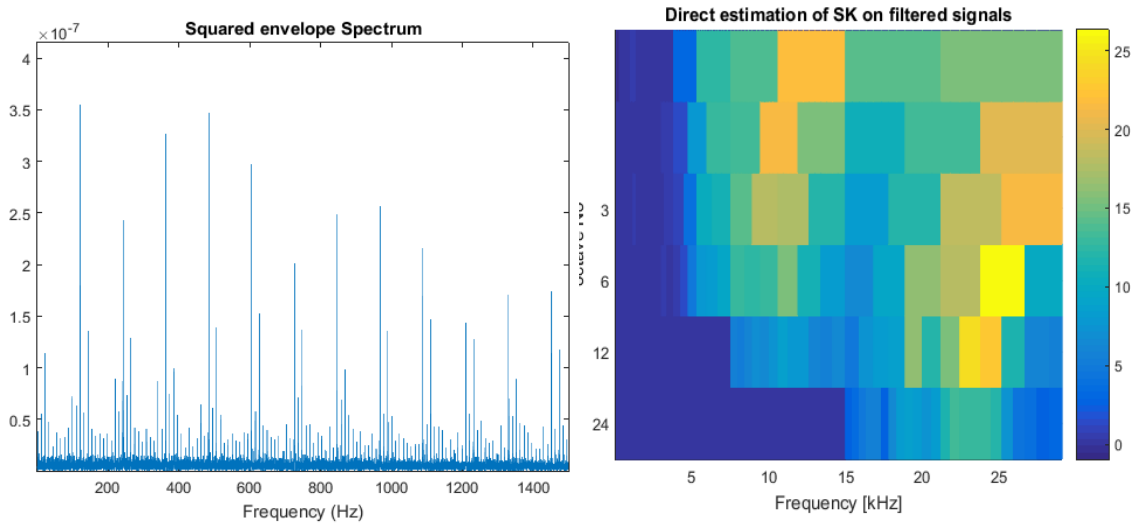

Figure B16 - Wavelet Kurtogram 0.5% of 70 nano for 1 mm outer bearing at 40 bar

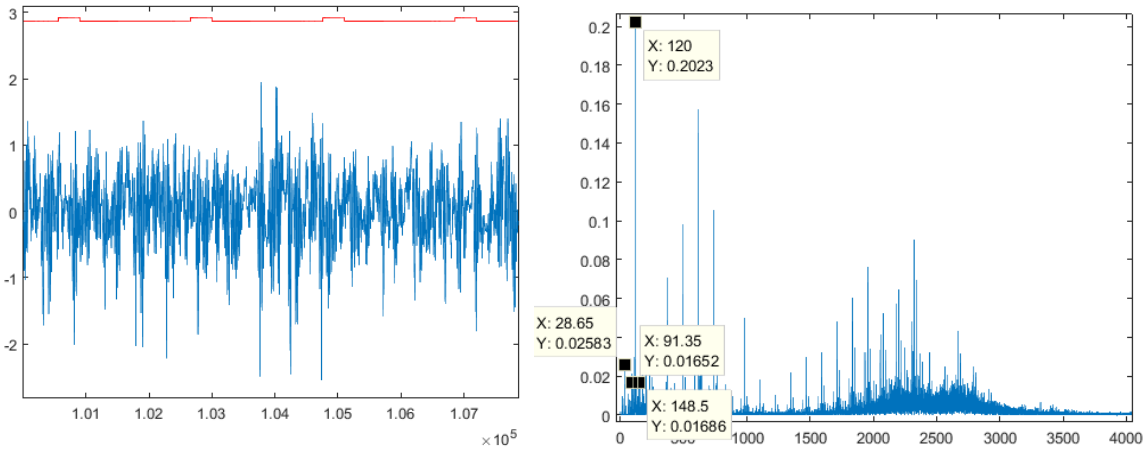

Figure B17 - Time domain and FFT signal for 2 mm outer bearing loaded with 40 bar 0% 30 nano

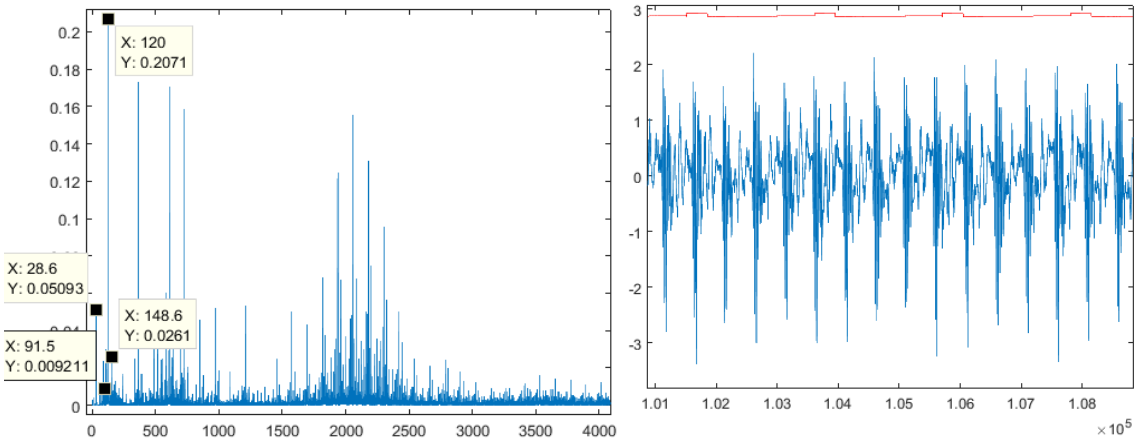

Figure B18 - Time domain and FFT signal for 2 mm outer bearing loaded with 40 bar 0.5% 30 nano

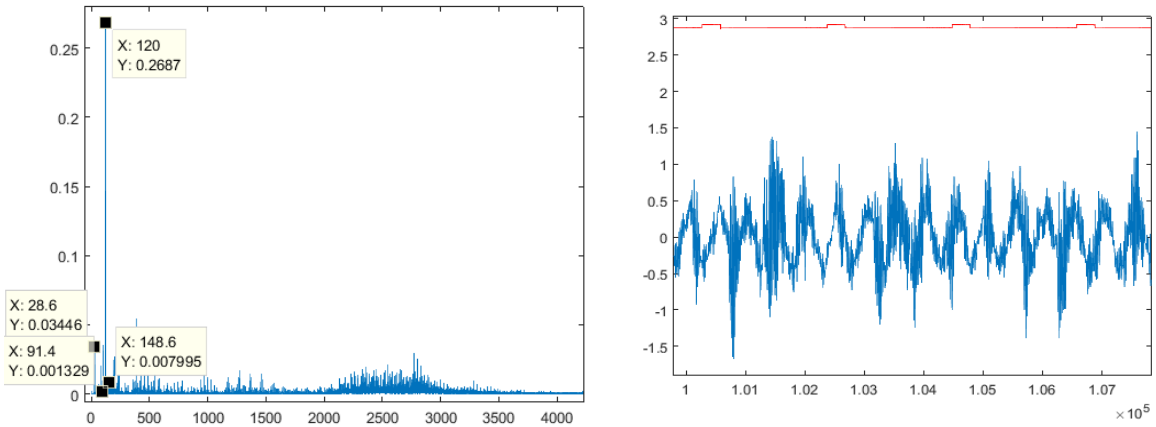

Figure B19 - Time domain and FFT signal for 2 mm outer bearing loaded with 40 bar 0.5% 70 nano

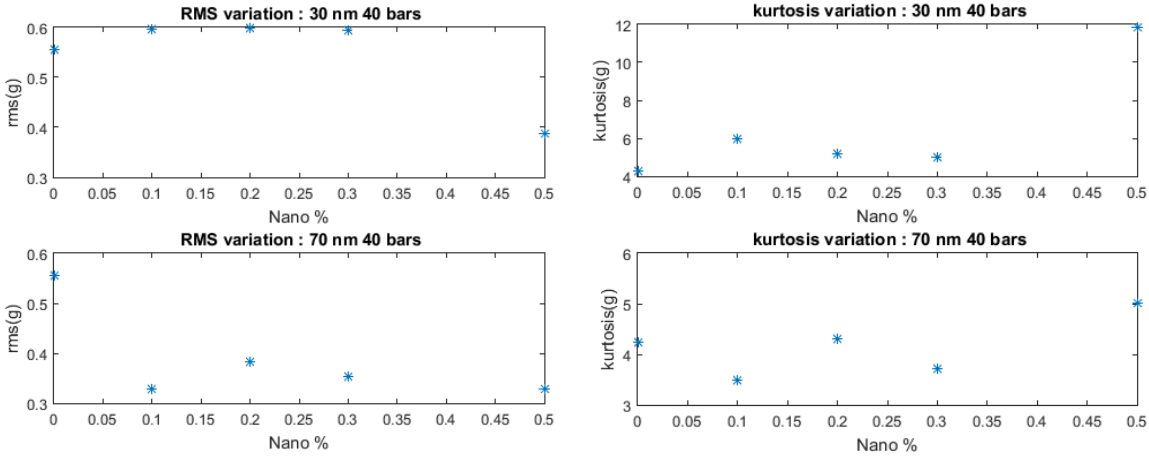

Figure B20 - RMS and Kurtosis values for 2 mm outer bearing

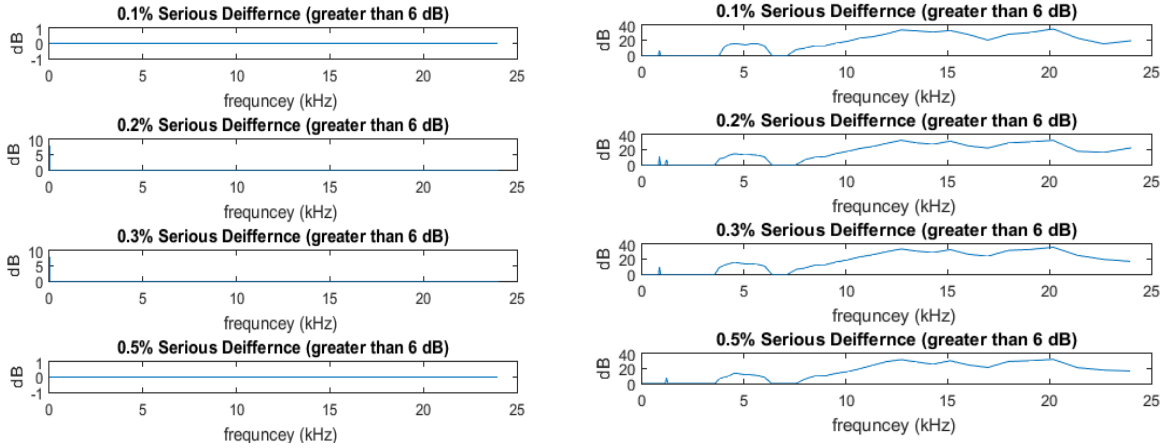

Figure B21 - 1/12 CPB Analysis for a 2 mm outer bearing on the left 30 nm on the right 70 nm at 40 bars

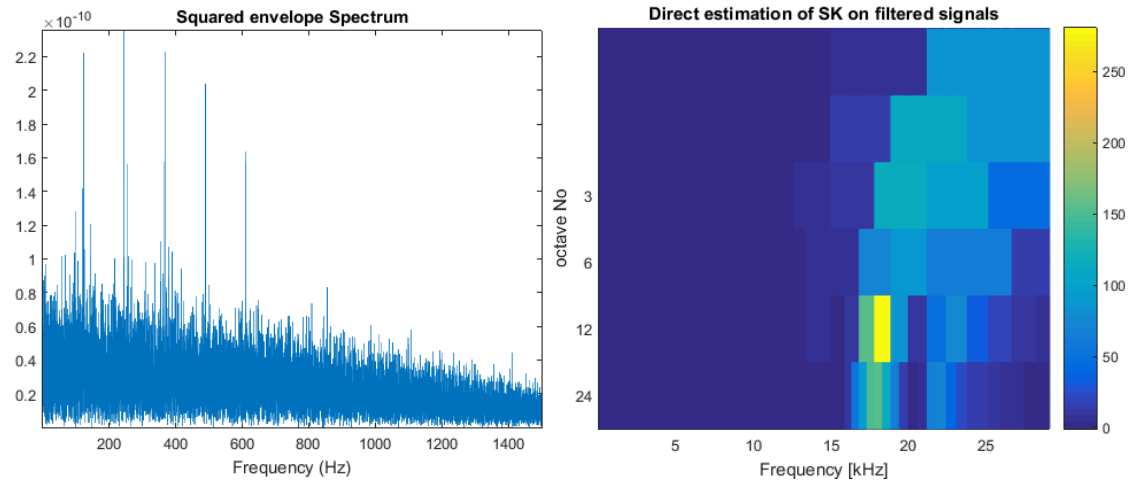

Figure B22 - Wavelet Kurtogram 0% nm for 2 mm outer bearing at 40 bar

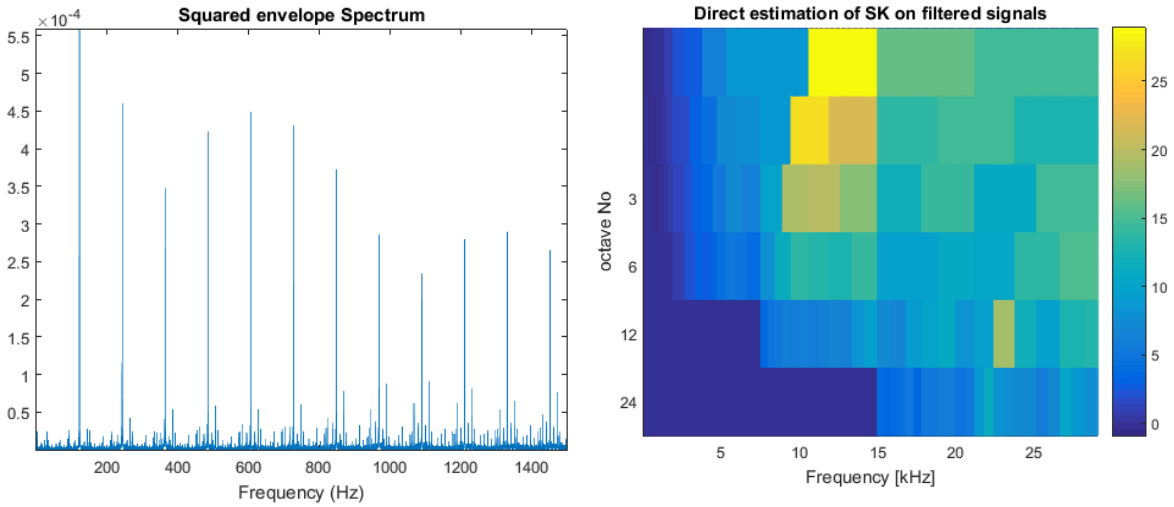

Figure B23 - Wavelet Kurtogram 0.5% of 30 nano for 2 mm outer bearing at 40 bar

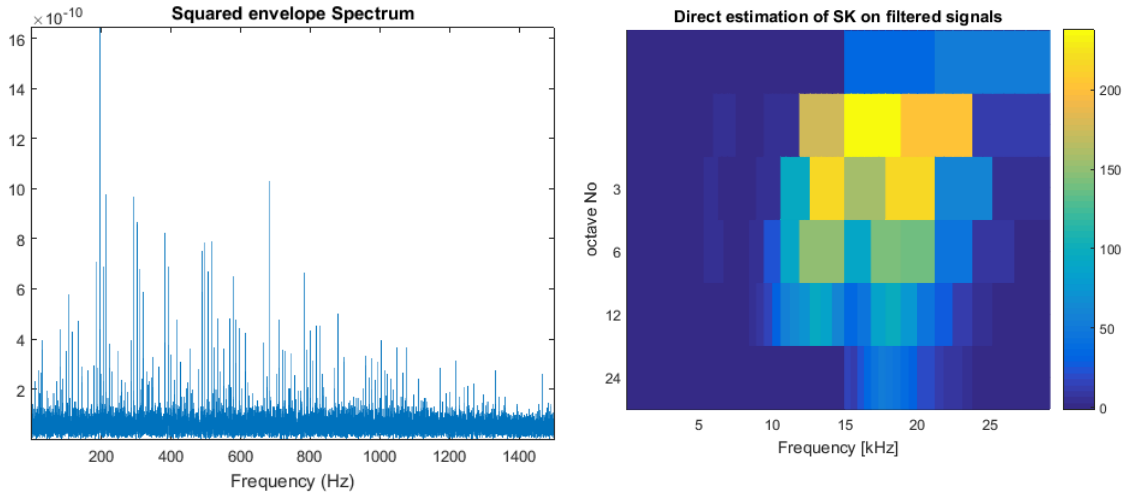

Figure B24 - Wavelet Kurtogram 0.5% of 70 nano for 2 mm outer bearing at 40 bar

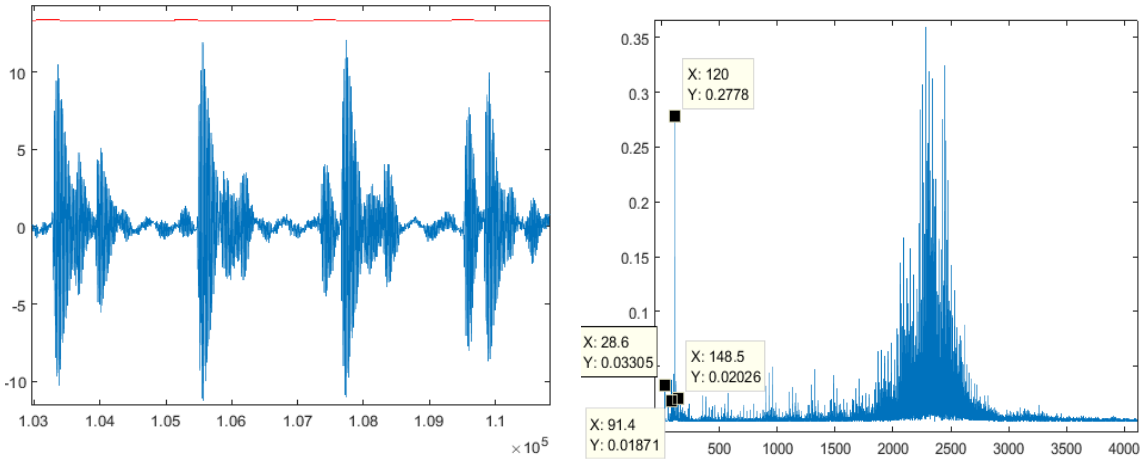

Figure B25 - Time domain and FFT signal for 1 mm inner bearing loaded with 40 bar 0% 30 nano

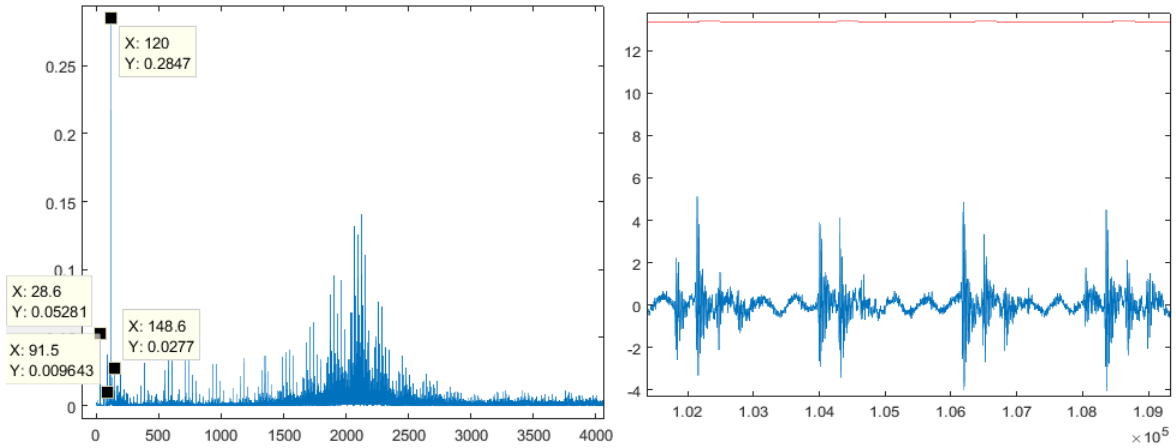

Figure B26 - Time domain and FFT signal for 1 mm inner bearing loaded with 40 bar 0.5% 30 nano

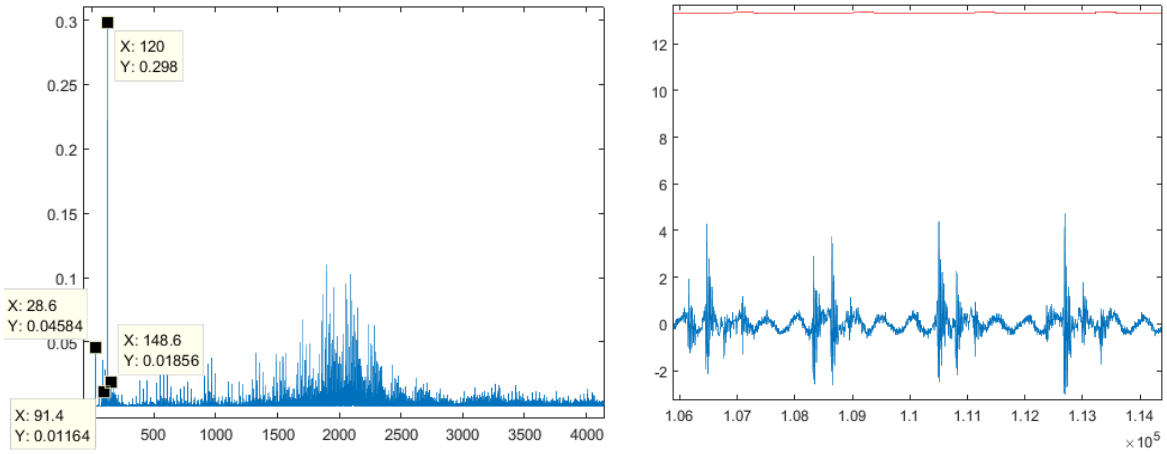

Figure B27 - Time domain and FFT signal for 1 mm inner bearing loaded with 40 bar 0.5% 70 nano

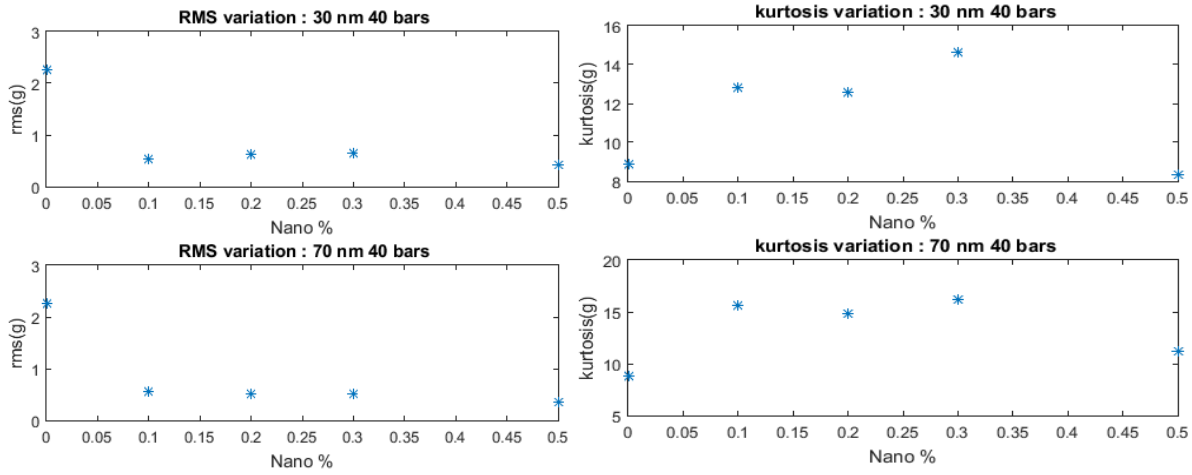

Figure B28 - RMS and Kurtosis values for a 1 mm inner bearing

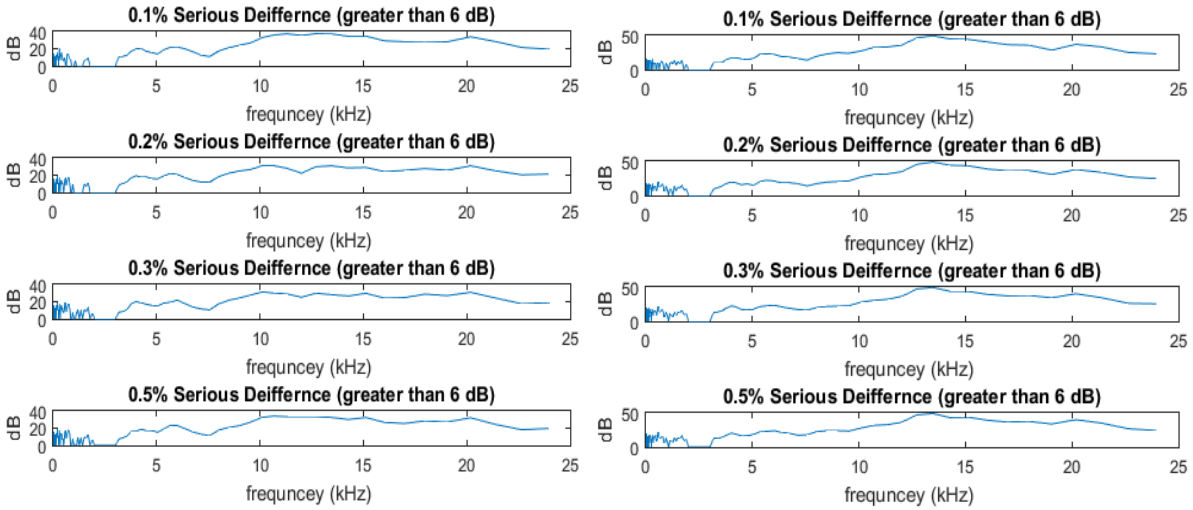

Figure B29 - 1/12 CPB Analysis for a 1 mm inner bearing on the left 30 nm on the right 70 nm at 40 bars

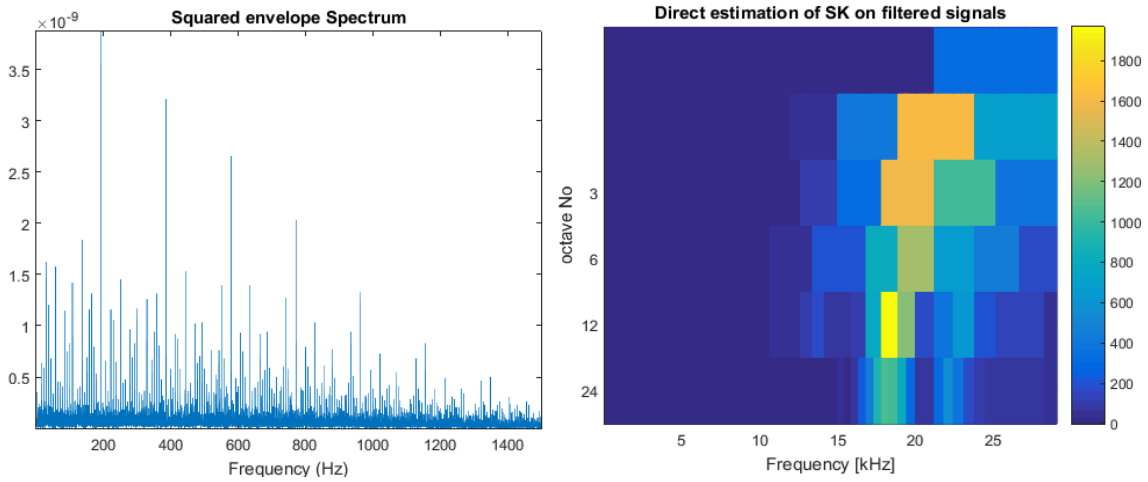

Figure B30 - Wavelet Kurtogram 0% nm for 1 mm inner bearing at 40 bar

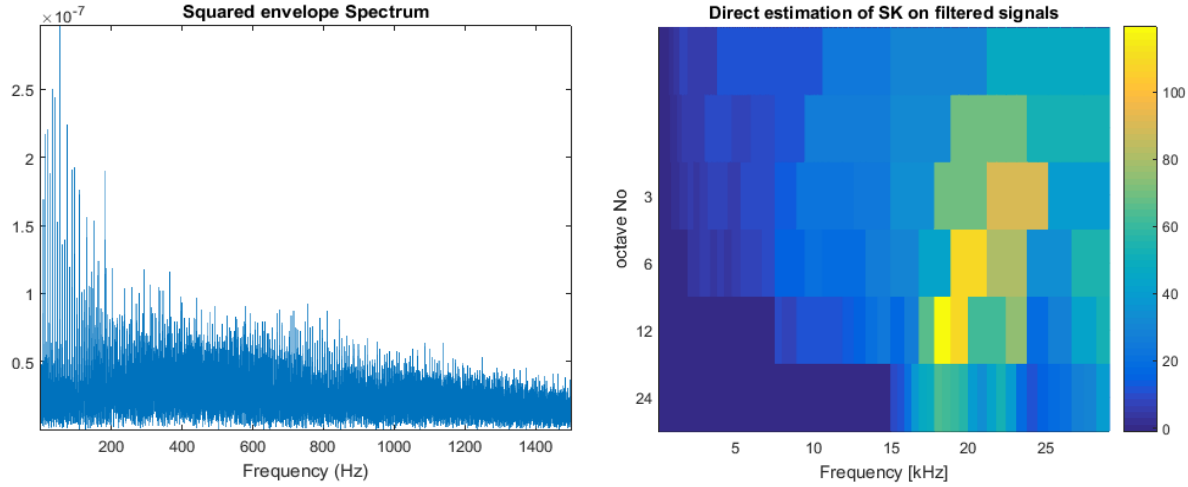

Figure B31 - Wavelet Kurtogram 0.5% of 30 nano for 1 mm inner bearing at 40 bar

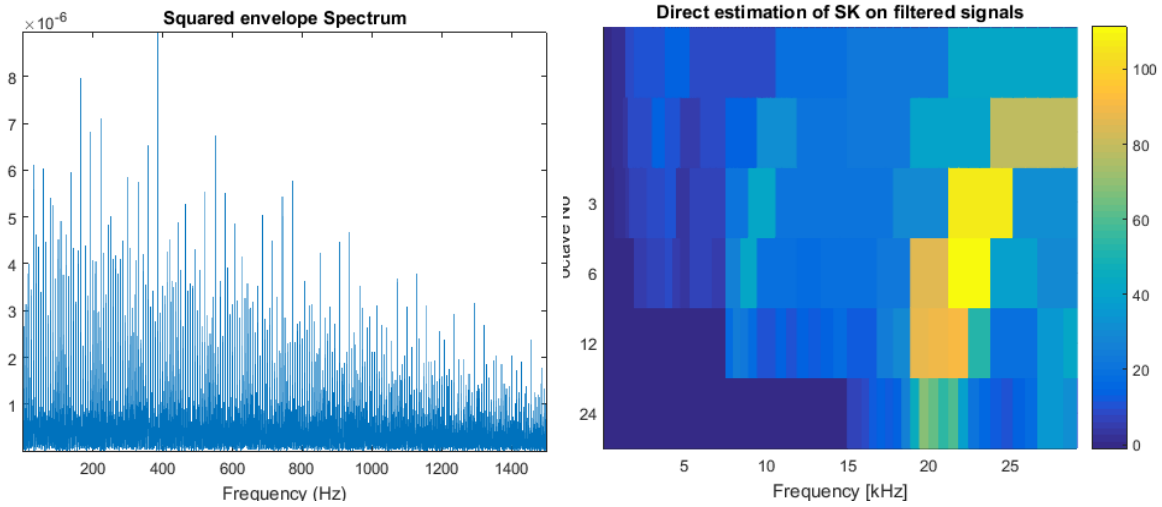

Figure B32 - Wavelet Kurtogram 0.5% of 70 nano for 1 mm inner bearing at 40 bar

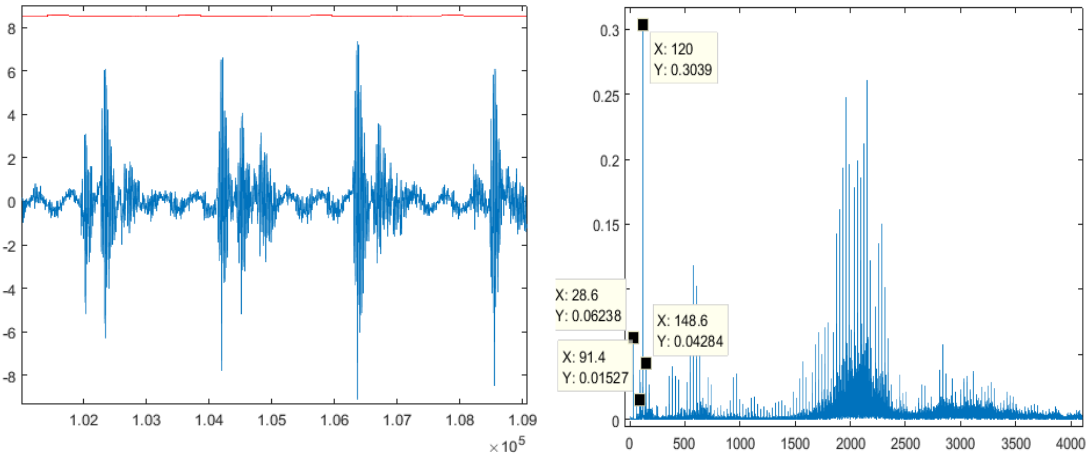

Figure B33 - Time domain and FFT signal for 2 mm inner bearing loaded with 40 bar 0% 30 nano

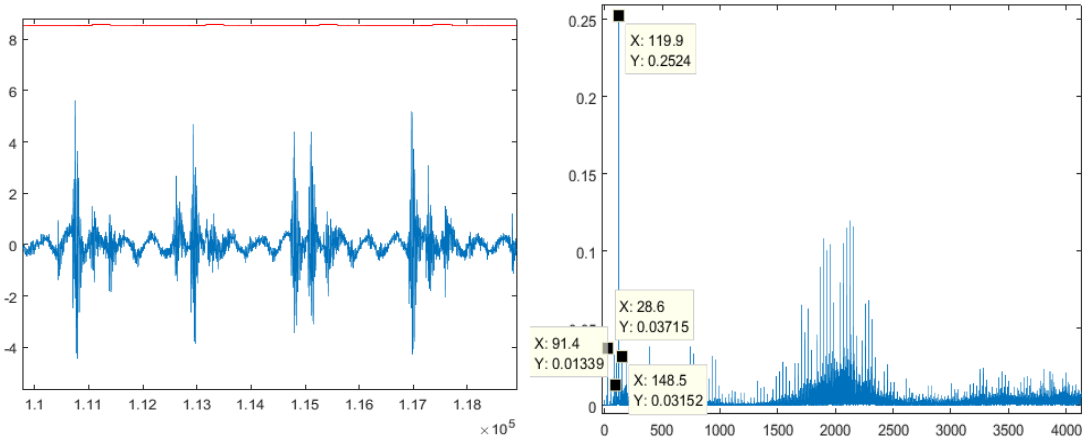

Figure B34 - Time domain and FFT signal for 2 mm inner bearing loaded with 40 bar 0.5% 30 nano

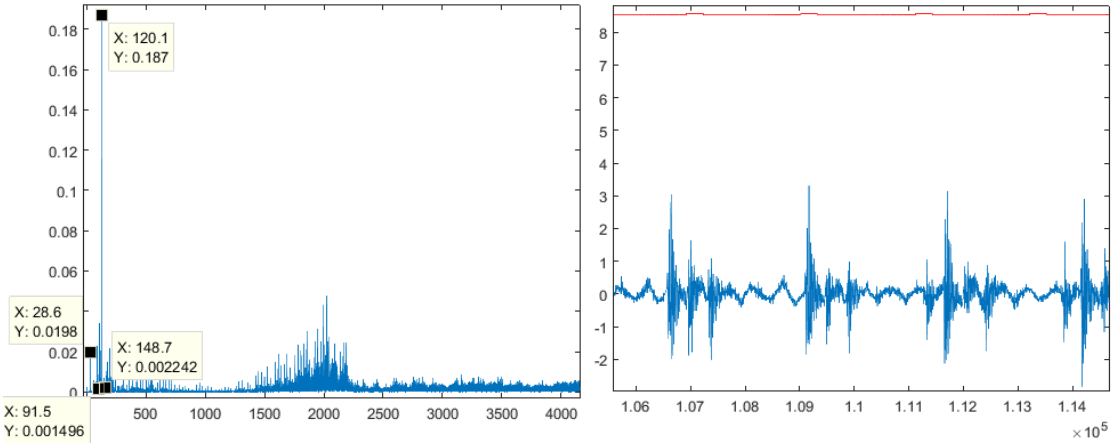

Figure B35 - Time domain and FFT signal for 2 mm inner bearing loaded with 40 bar 0.5% 70 nano

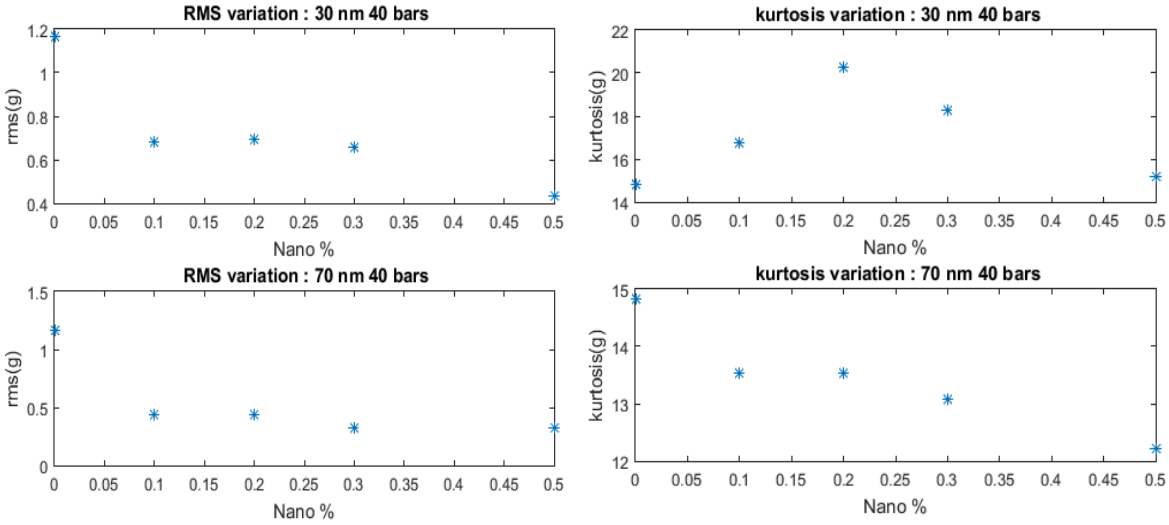

Figure B36 - RMS and Kurtosis values for 2 mm inner bearing

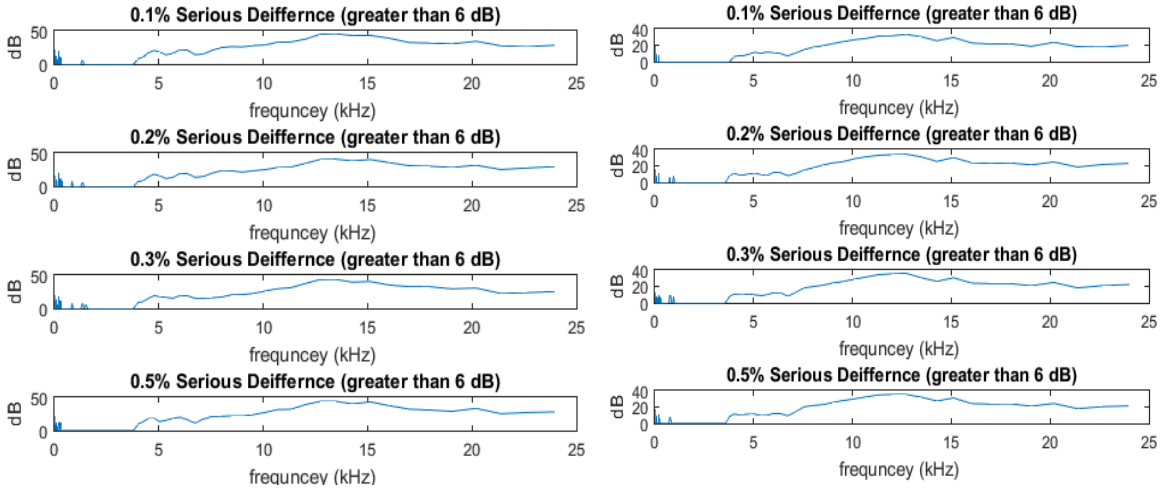

Figure B37 - 1/12 CPB Analysis for a 2 mm inner bearing on the left 30 nm on the right 70 nm at 40 bars

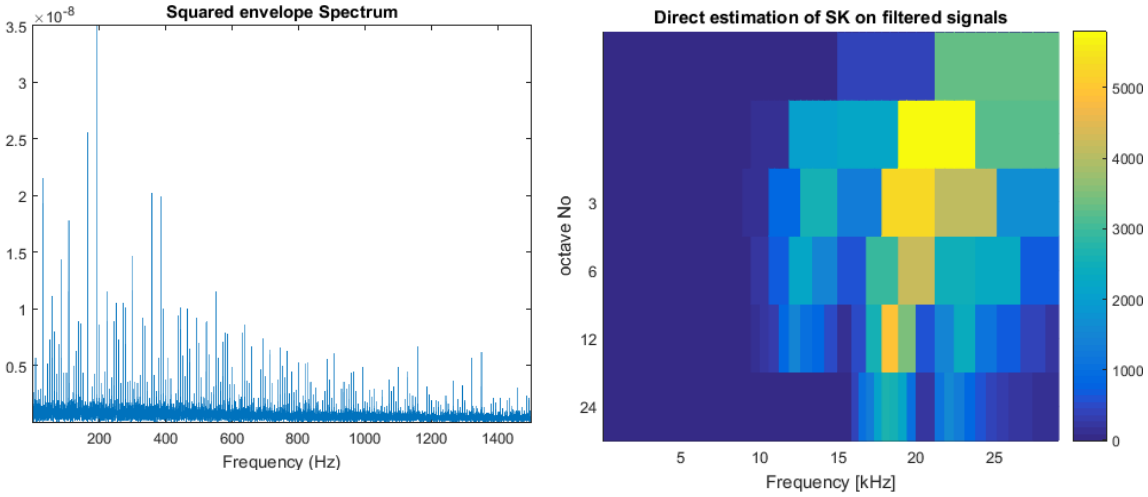

Figure B38 - Wavelet Kurtogram 0% nm for 2 mm inner bearing at 40 bar

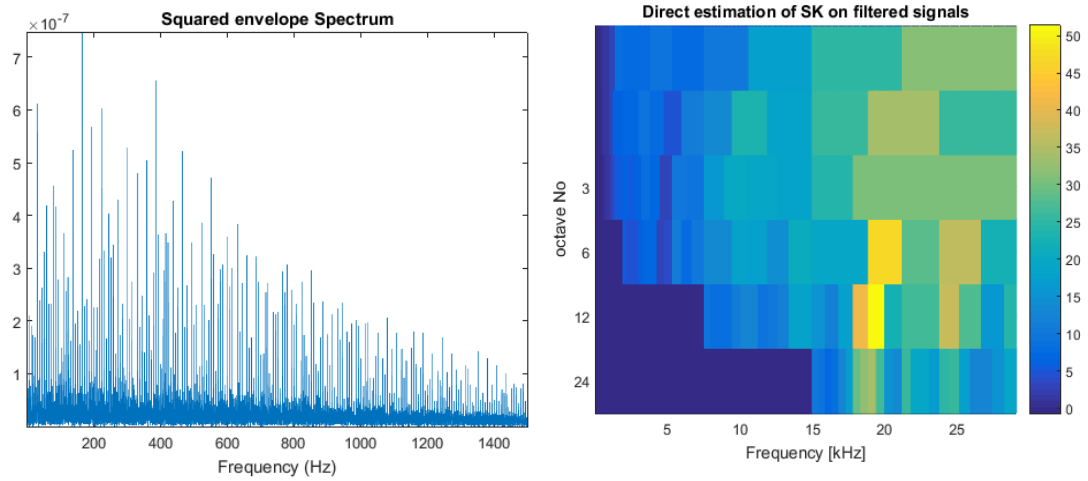

Figure B39 - Wavelet Kurtogram 0.5% of 30 nano for 2 mm inner bearing at 40 bar

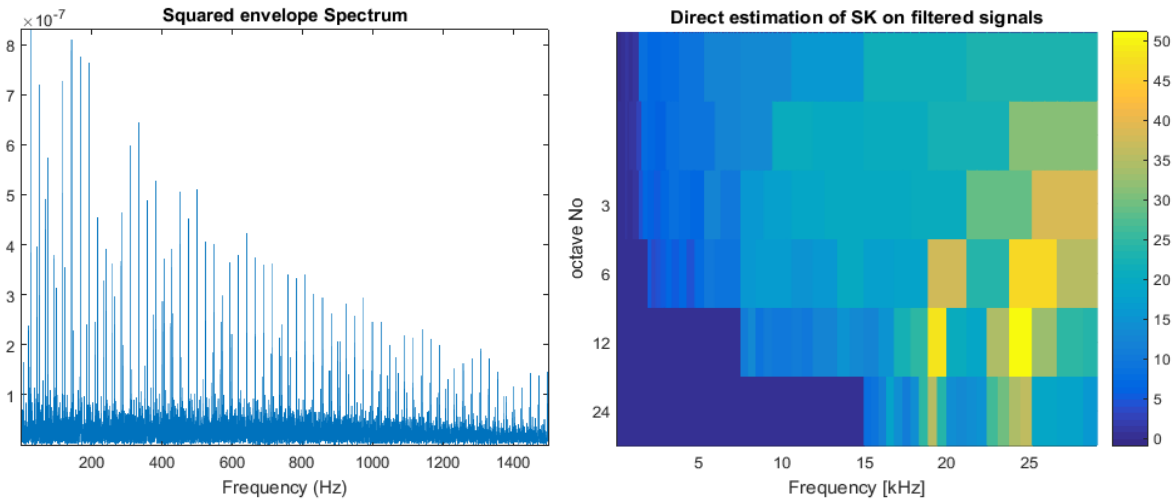

Figure B40 - Wavelet Kurtogram 0.5% of 70 nano for 2 mm inner bearing at 40 bar

Appendix C

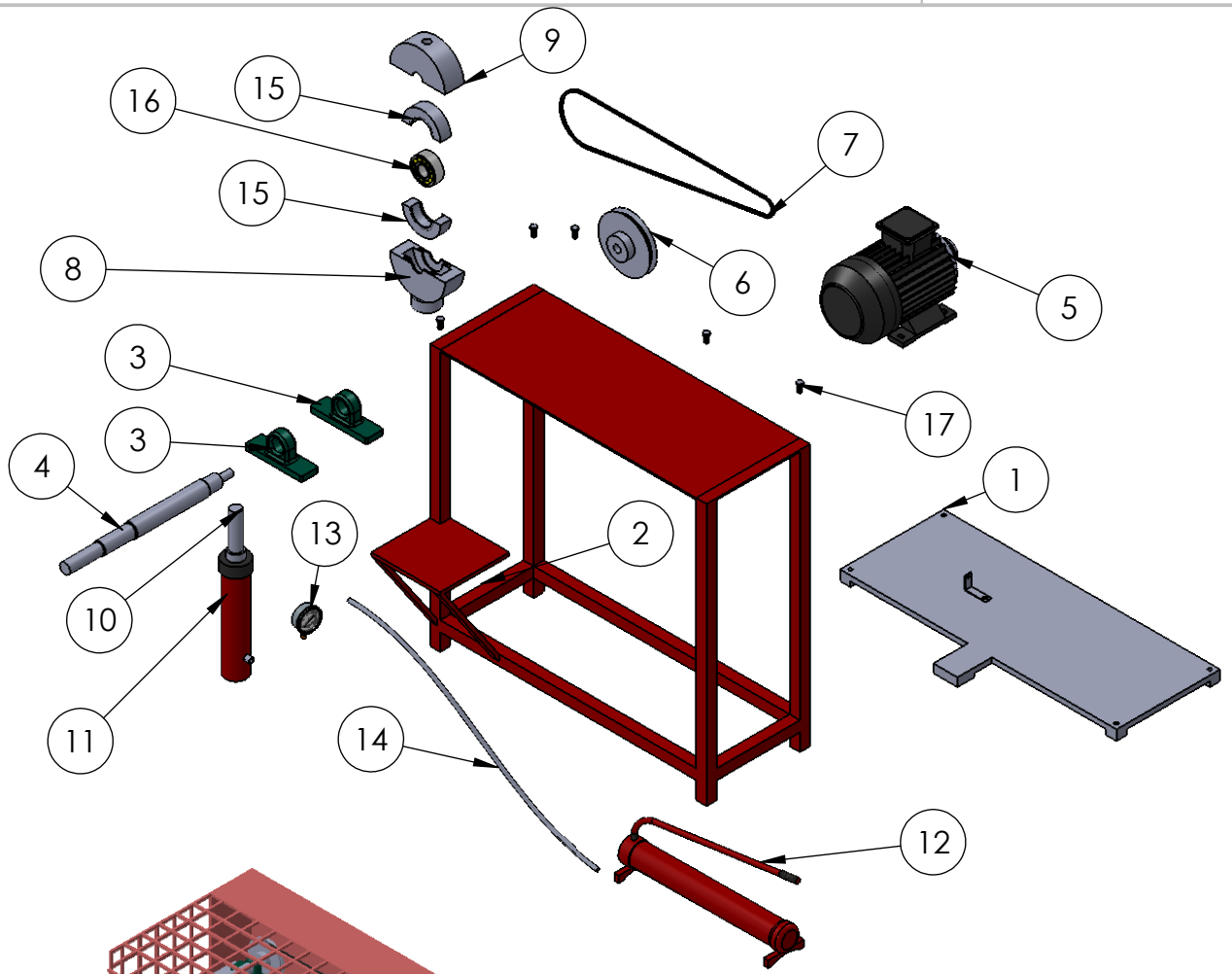

ITEM NO.	PART NUMBER	QTY.
1	base 1	1
2	Base	1
3	Housing	2
4	shaft	1
5	Motor	1
6	shaft pully	1
7	pully	1
8	Tank bottom	1
9	Tank top	1
10	hydraulic bar	1
11	hydraulic jack	1
12	hydraulic pump	1
13	Pressure Gauge	1
14	hose	1
15	Casing	2
16	2306 Self-aligning ball bearings	1
17	bults	5

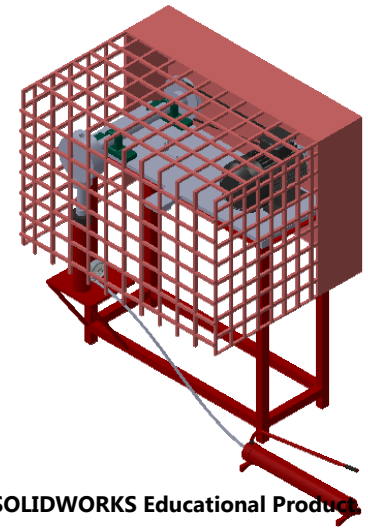

Name	ID
Ahmed Aldakheel	201303886
Mohammed Alhawaj	201303710
Mohammed Alshubaily	201101678
Sultan Hamdi	201300790
Rami Al Gassab	201301568

SIZE A | DWG. NO. Test rig | REV

SCALE: 1:32 | WEIGHT: | SHEET 1 OF 1

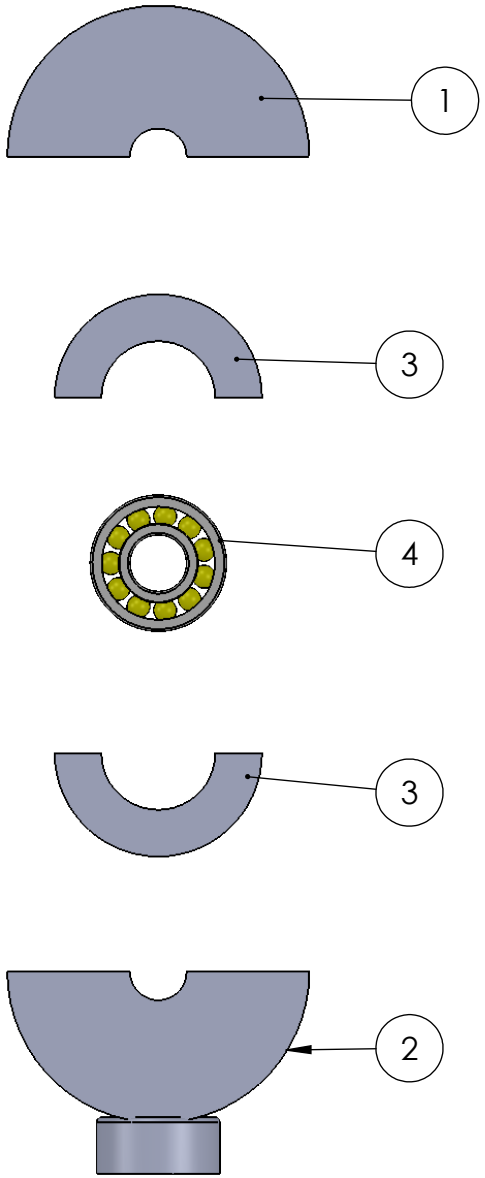

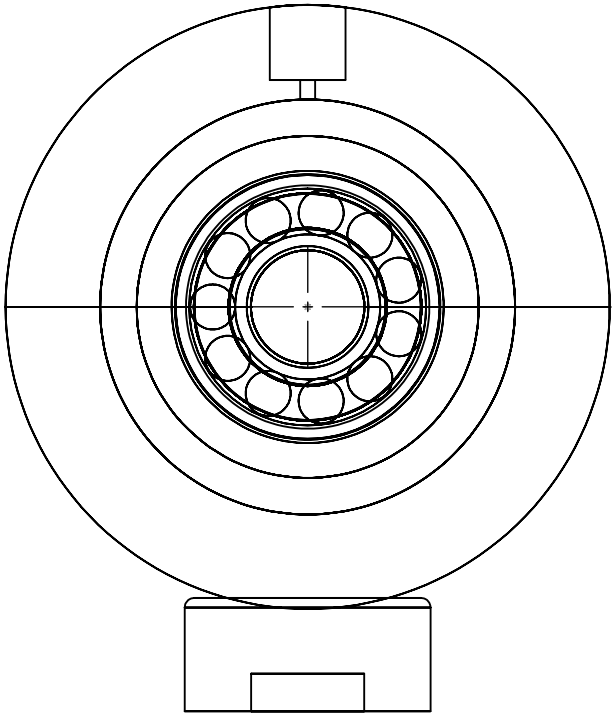

ITEM NO.	PART NUMBER	QTY.
1	2306 Self-aligning ball bearings	1
2	Casing	2
3	Tank bottom	1
4	Tank top	1

Name	ID
Ahmed Aldakheel	201303886
Mohammed Alhawaj	201303710
Mohammed Alshubaily	201101678
Sultan Hamdi	201300790
Rami Al Gassab	201301568

SIZE	DWG. NO.	REV
A	Oil Tank Casing	
SCALE: 1:8	WEIGHT:	SHEET 1 OF 1

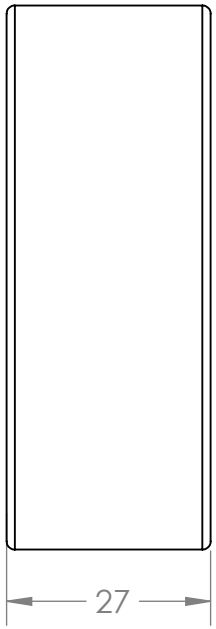

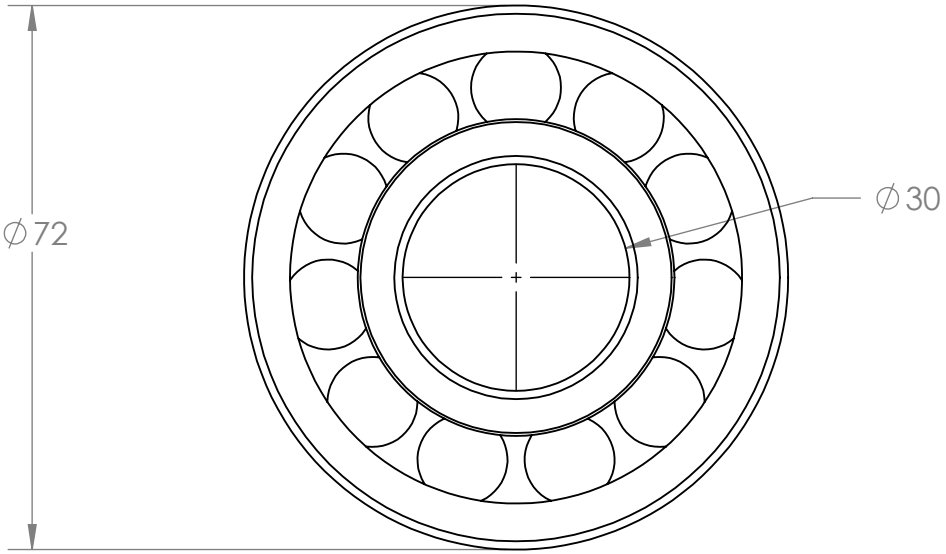

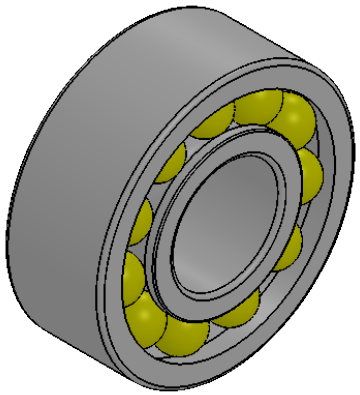

Name	ID
Ahmed Aldakheel	201303886
Mohammed Alhawaj	201303710
Mohammed Alshubaily	201101678
Sultan Hamdi	201300790
Rami Al Gassab	201301568

SIZE	DWG. NO.	REV
A	Self-aligning bearing	
SCALE: 1:2	WEIGHT:	SHEET 1 OF 1

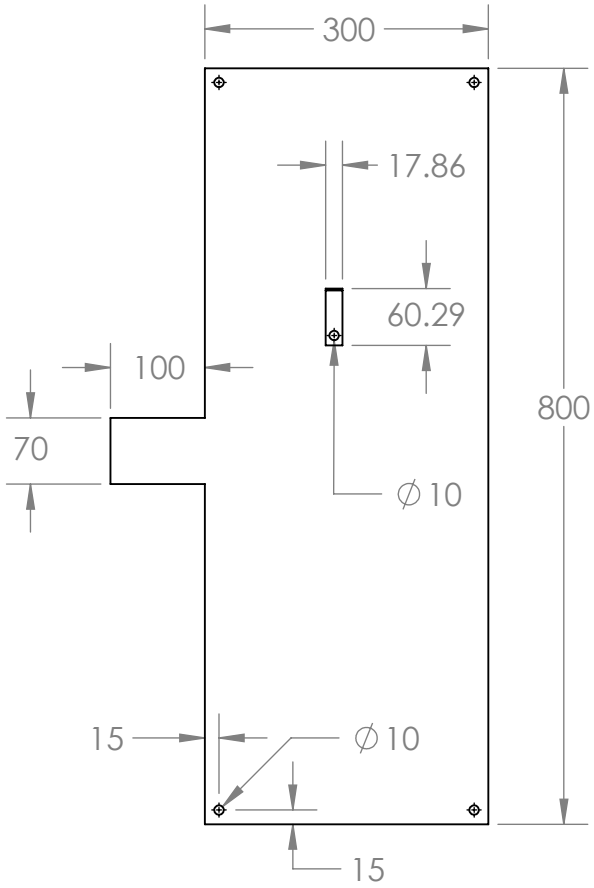

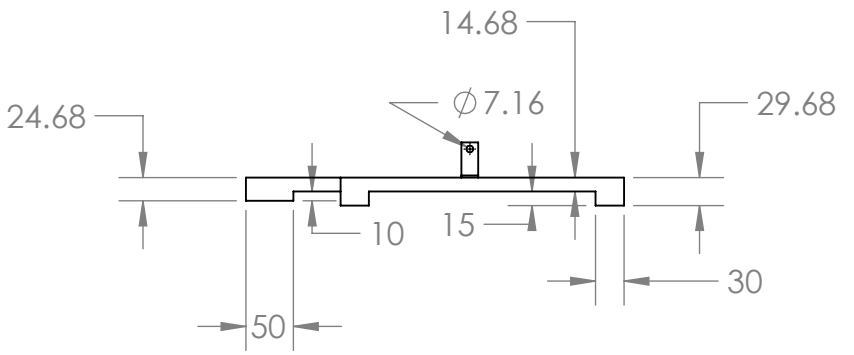

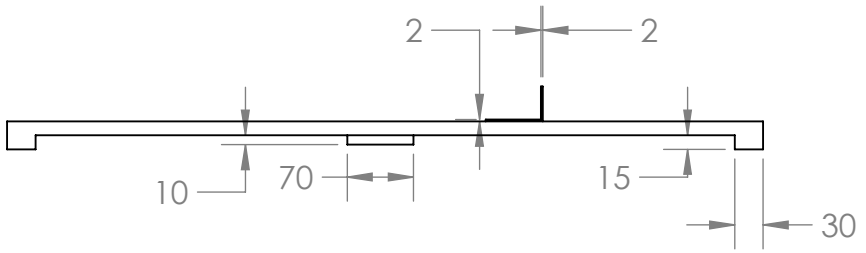

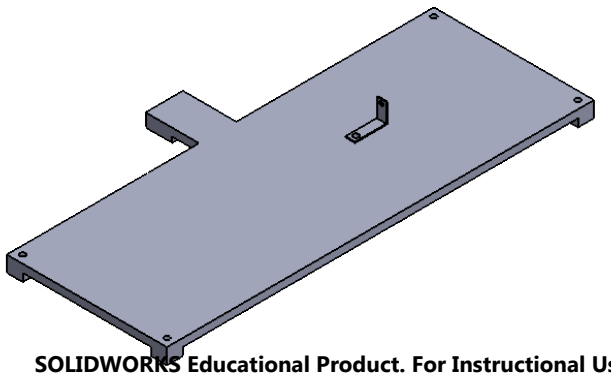

SOLIDWORKS Educational Product. For Instructional Use Only

Name	ID
Ahmed Aldakheel	201303886
Mohammed Alhawaj	201303710
Mohammed Alshubaily	201101678
Sultan Hamdi	201300790
Rami Al Gassab	201301568

SIZE	DWG. NO.	REV
A	Table	
SCALE: 1:8	WEIGHT:	SHEET 1 OF 1

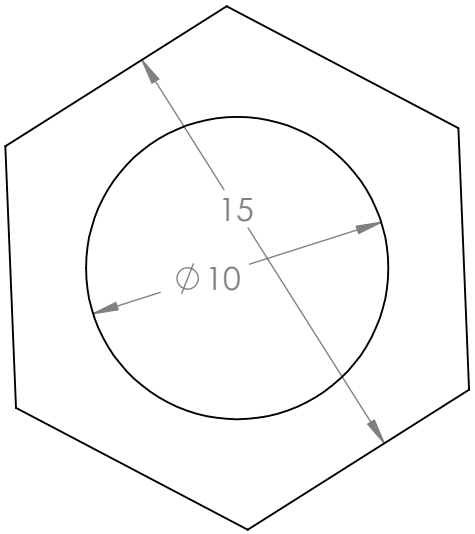

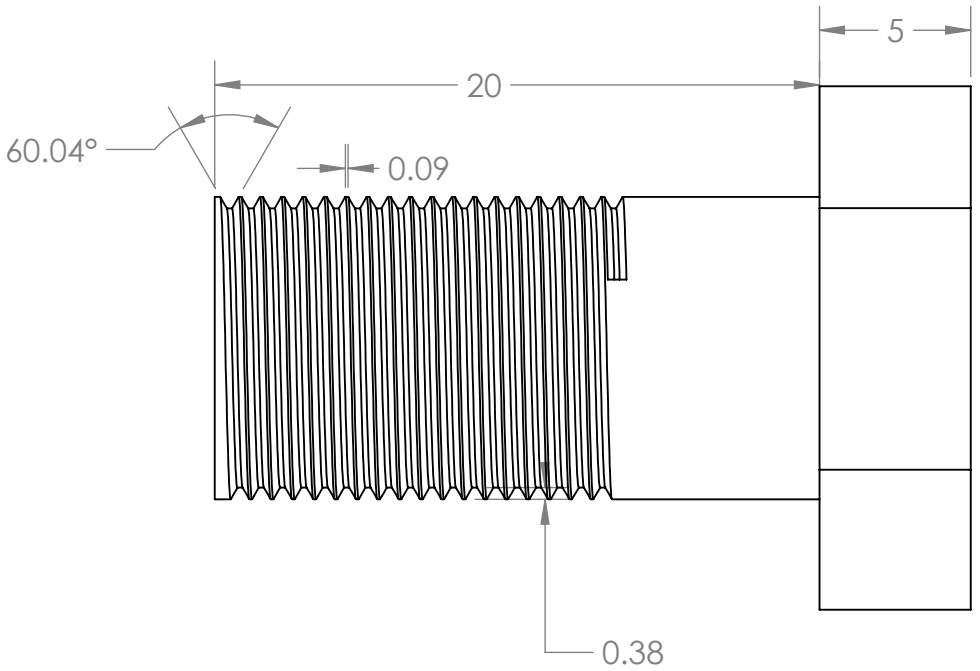

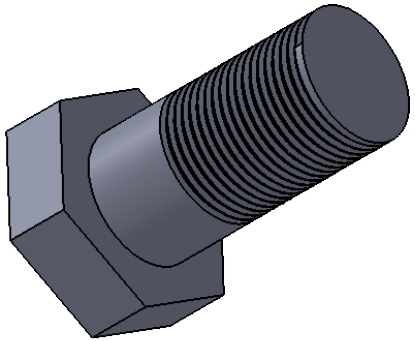

SOLIDWORKS Educational Product. For Instructional Use Only

Name	ID
Ahmed Aldakheel	201303886
Mohammed Alhawaj	201303710
Mohammed Alshubaily	201101678
Sultan Hamdi	201300790
Rami Al Gassab	201301568

SIZE	DWG. NO.	REV
A	bults	
SCALE: 2:1	WEIGHT:	SHEET 1 OF 1

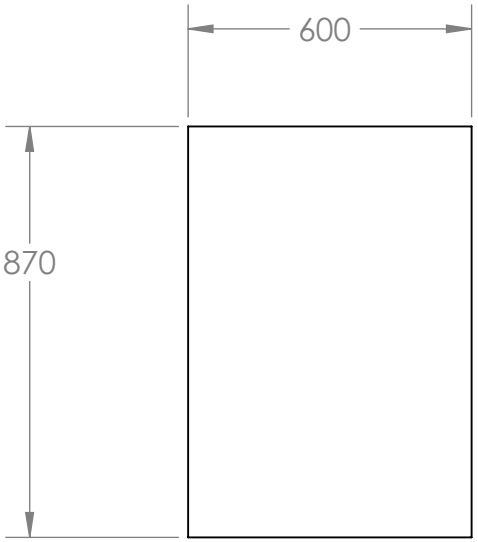

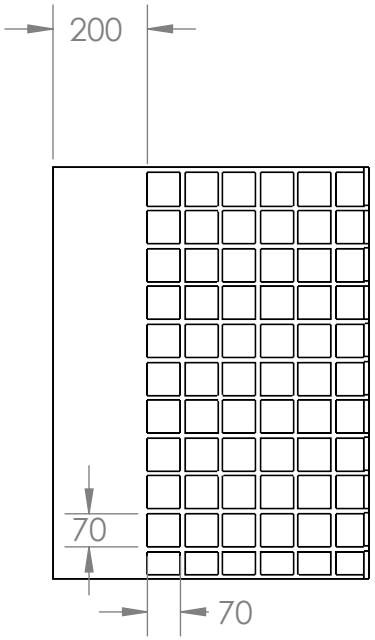

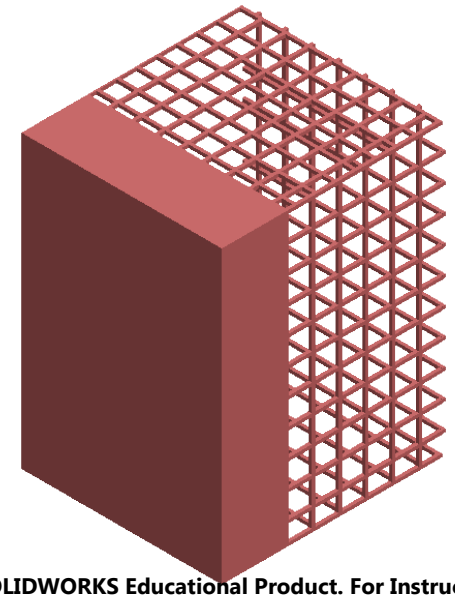

SOLIDWORKS Educational Product. For Instructional Use Only

Name	ID
Ahmed Aldakheel	201303886
Mohammed Alhawaj	201303710
Mohammed Alshubaily	201101678
Sultan Hamdi	201300790
Rami Al Gassab	201301568

SIZE	DWG. NO.	REV
A	Safety Cage	
SCALE: 1:16	WEIGHT:	SHEET 1 OF 1

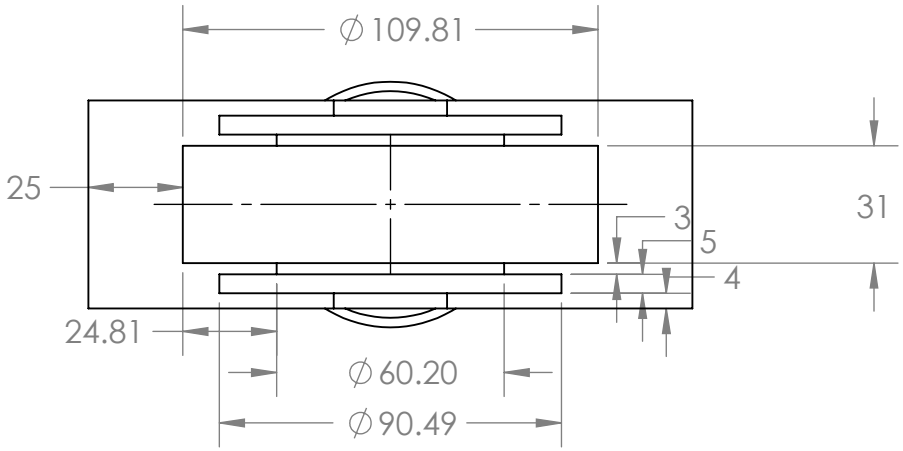

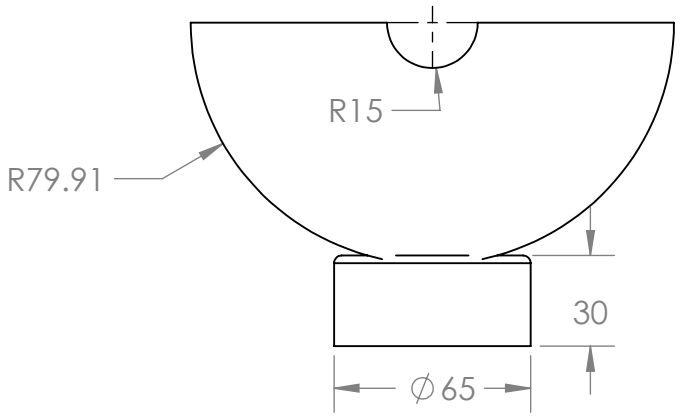

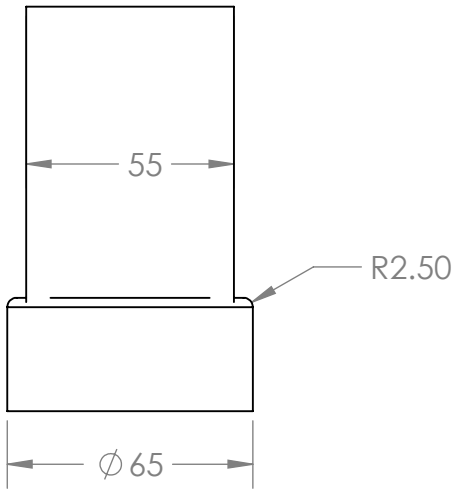

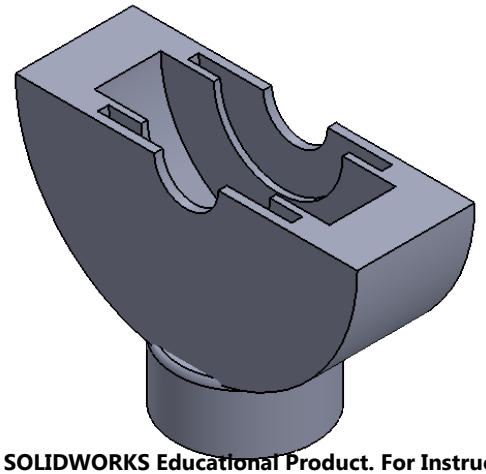

SOLIDWORKS Educational Product. For Instructional Use Only

Name	ID
Ahmed Aldakheel	201303886
Mohammed Alhawaj	201303710
Mohammed Alshubaily	201101678
Sultan Hamdi	201300790
Rami Al Gassab	201301568

SIZE	DWG. NO.	REV
A	Casing bottom	
SCALE: 1:2	WEIGHT:	SHEET 1 OF 1

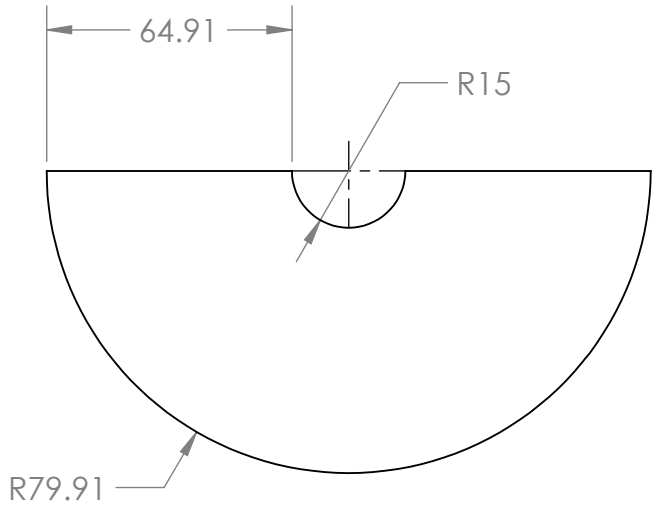

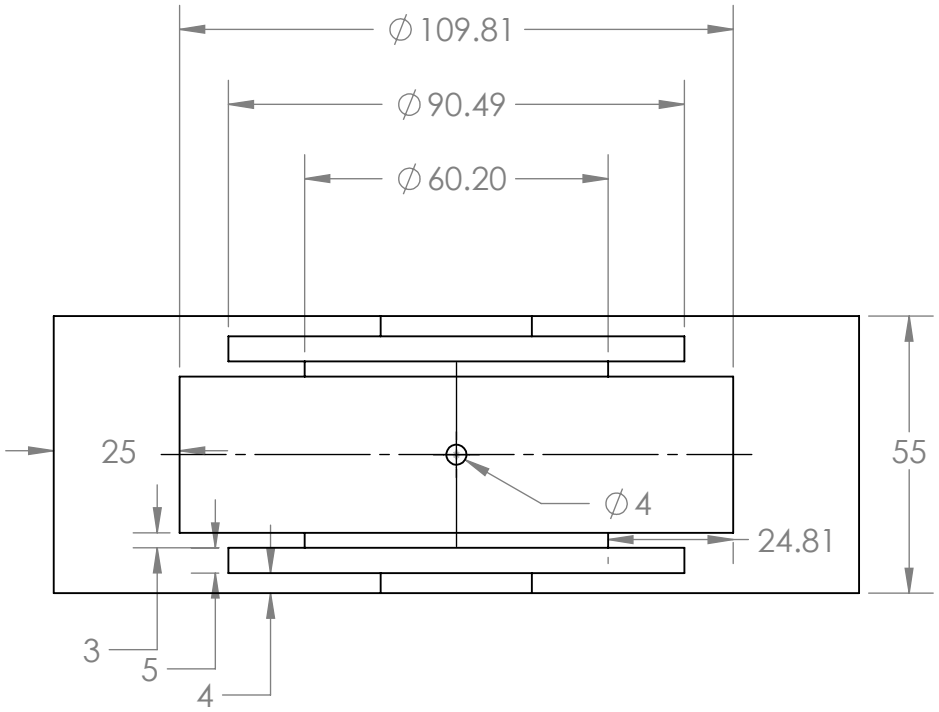

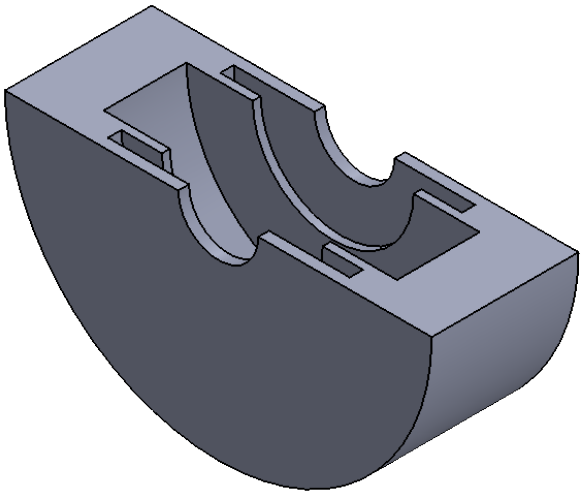

SOLIDWORKS Educational Product. For Instructional Use Only

Name	ID
Ahmed Aldakheel	201303886
Mohammed Alhawaj	201303710
Mohammed Alshubaily	201101678
Sultan Hamdi	201300790
Rami Al Gassab	201301568

SIZE	DWG. NO.	REV
A	casing top	
SCALE: 1:2	WEIGHT:	SHEET 1 OF 1

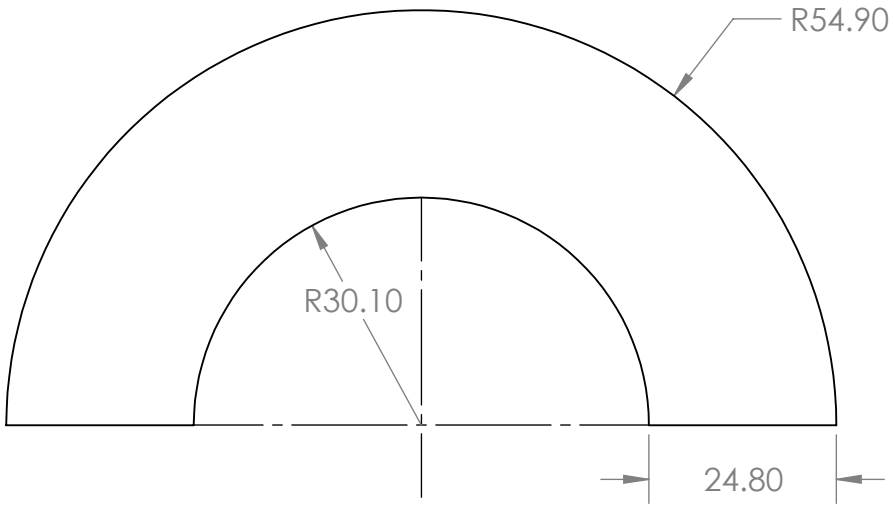

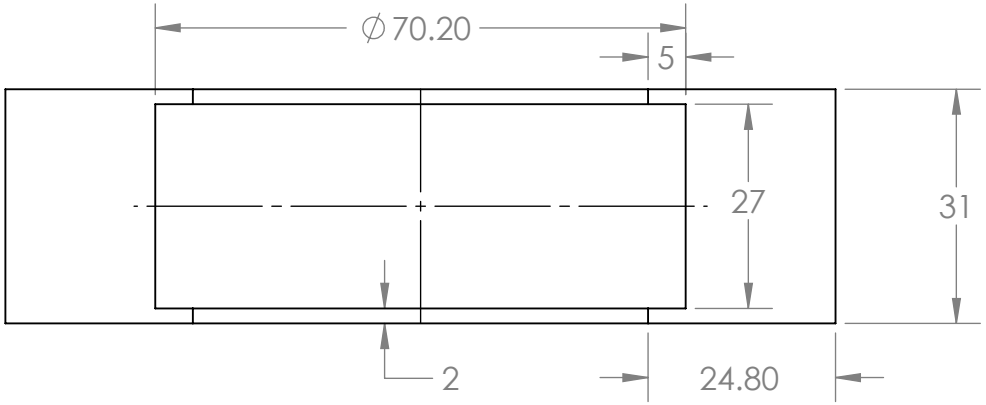

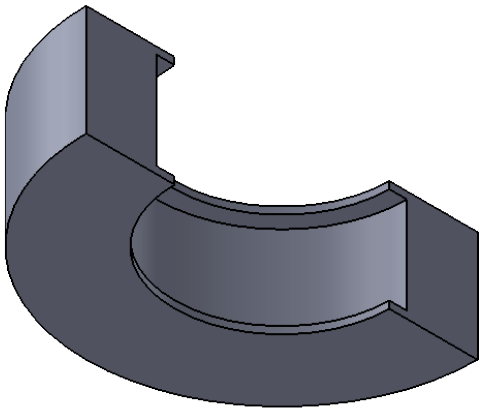

Name	ID
Ahmed Aldakheel	201303886
Mohammed Alhawaj	201303710
Mohammed Alshubaily	201101678
Sultan Hamdi	201300790
Rami Al Gassab	201301568

SIZE A | DWG. NO. Casing | REV

SCALE: 1:2 | SHEET 1 OF 1

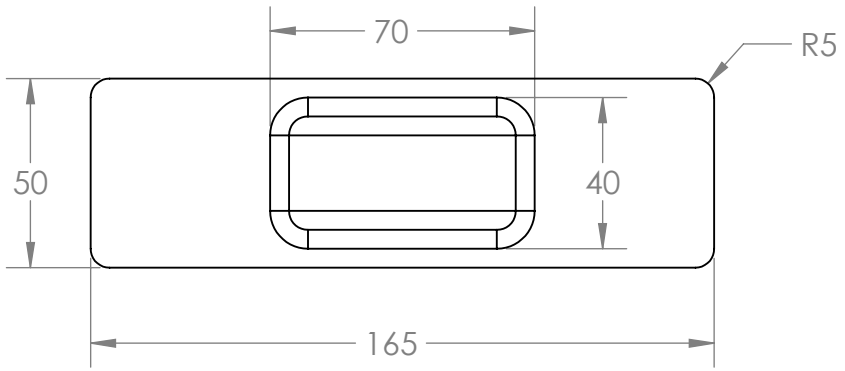

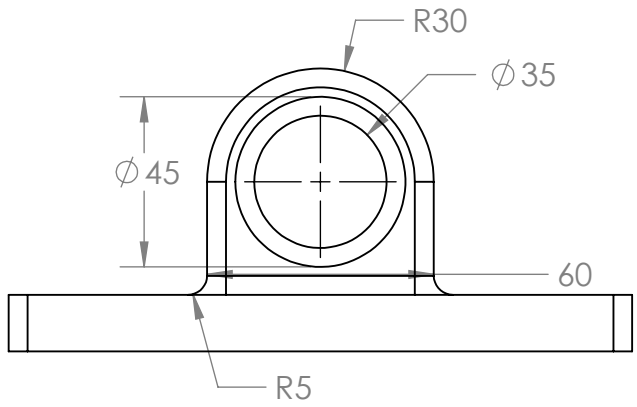

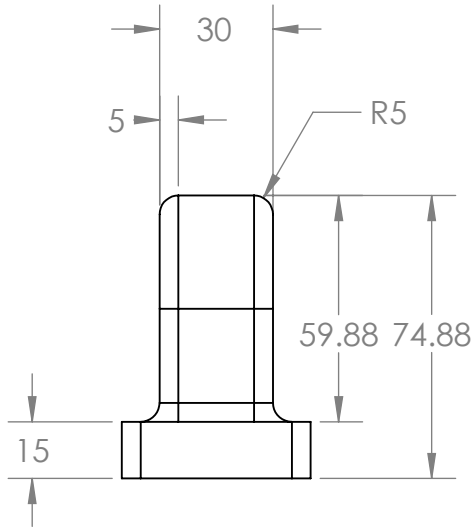

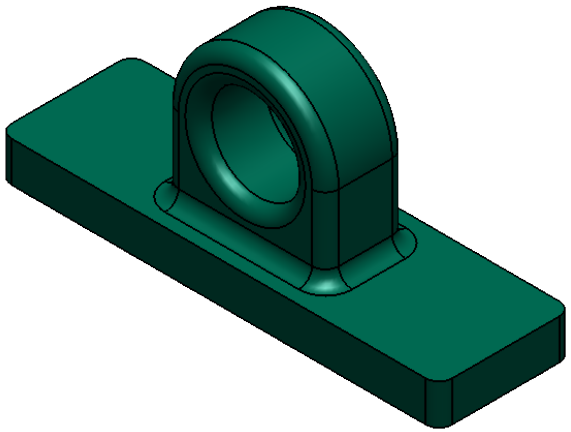

SOLIDWORKS Educational Product. For Instructional Use Only

Name	ID
Ahmed Aldakheel	201303886
Mohammed Alhawaj	201303710
Mohammed Alshubaily	201101678
Sultan Hamdi	201300790
Rami Al Gassab	201301568

SIZE	DWG. NO.	REV
A	Housing	
SCALE: 1:2	WEIGHT:	SHEET 1 OF 1

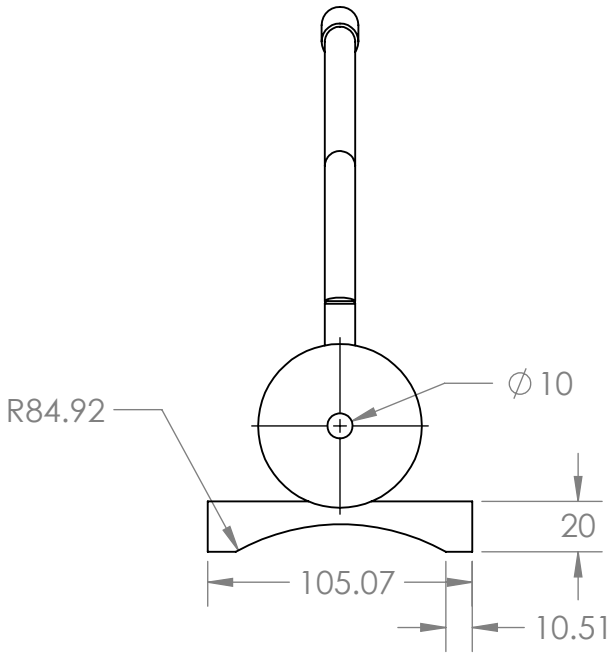

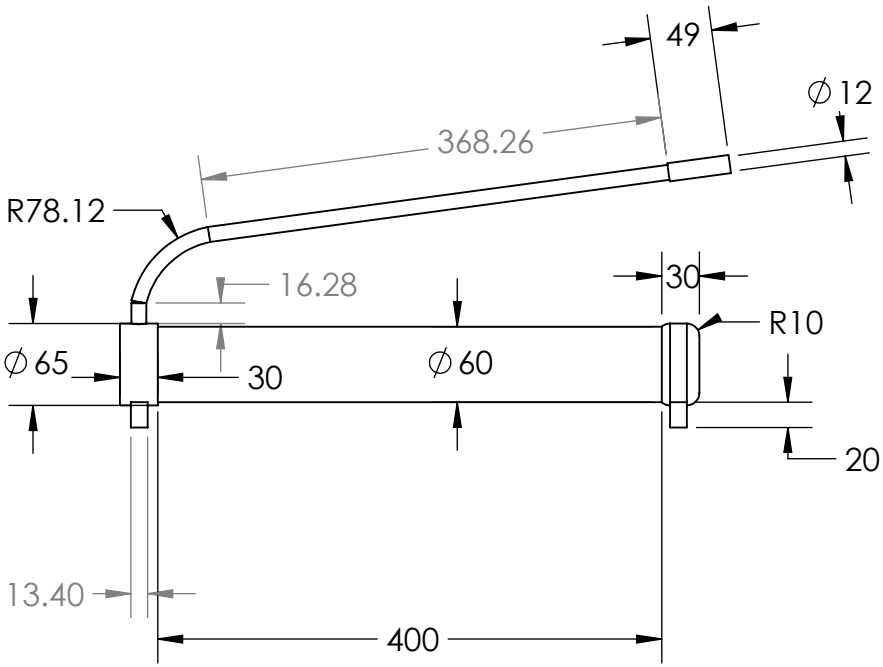

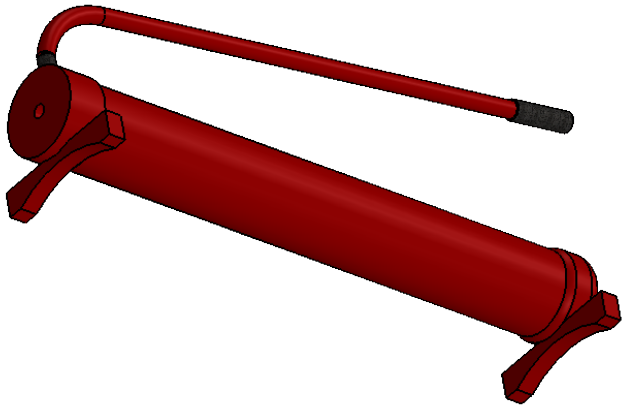

SOLIDWORKS Educational Product. For Instructional Use Only

Name	ID
Ahmed Aldakheel	201303886
Mohammed Alhawaj	201303710
Mohammed Alshubaily	201101678
Sultan Hamdi	201300790
Rami Al Gassab	201301568

SIZE	DWG. NO.	REV
A	hydraulic pump	
SCALE: 1:8	WEIGHT:	SHEET 1 OF 1

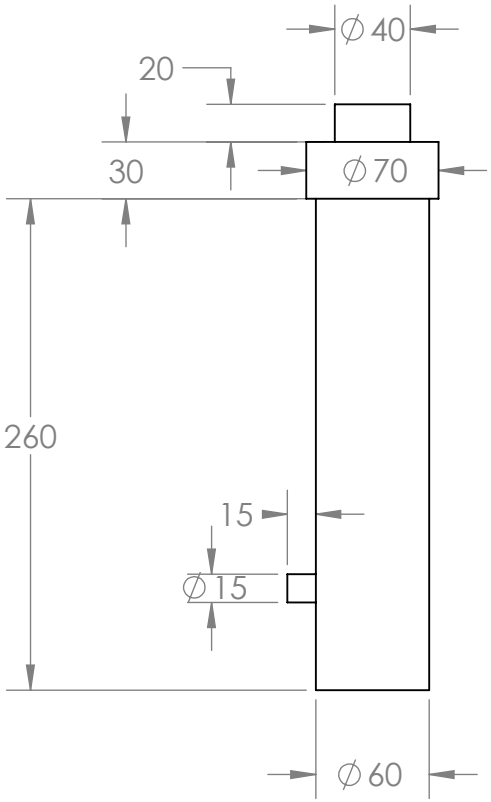

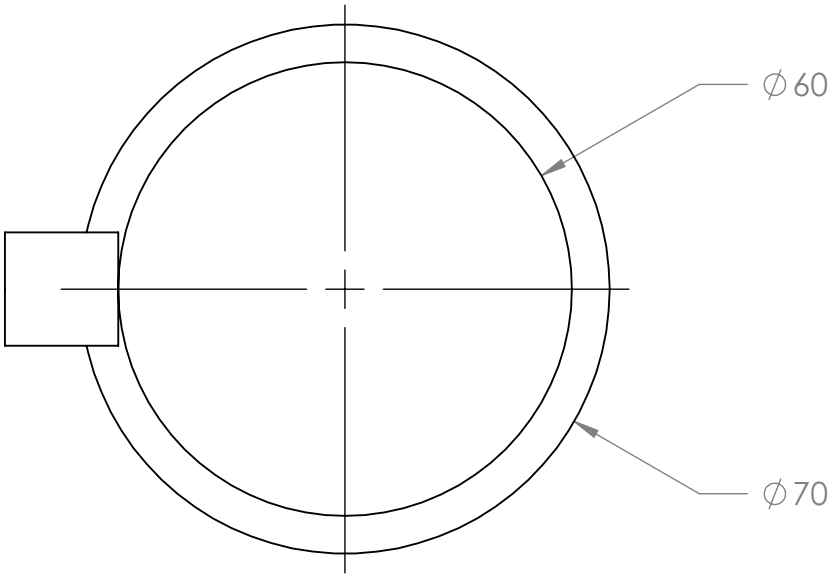

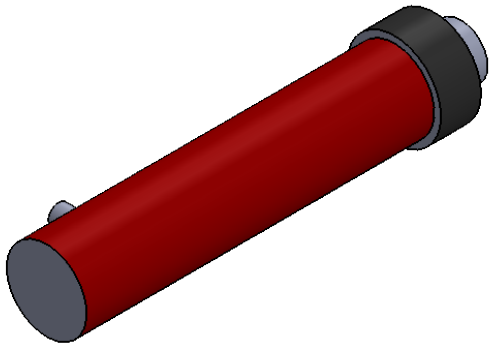

SOLIDWORKS Educational Product. For Instructional Use Only

Name	ID
Ahmed Aldakheel	201303886
Mohammed Alhawaj	201303710
Mohammed Alshubaily	201101678
Sultan Hamdi	201300790
Rami Al Gassab	201301568

SIZE	DWG. NO.	REV
A	hydraulic	
SCALE: 1:4	WEIGHT:	SHEET 1 OF 1

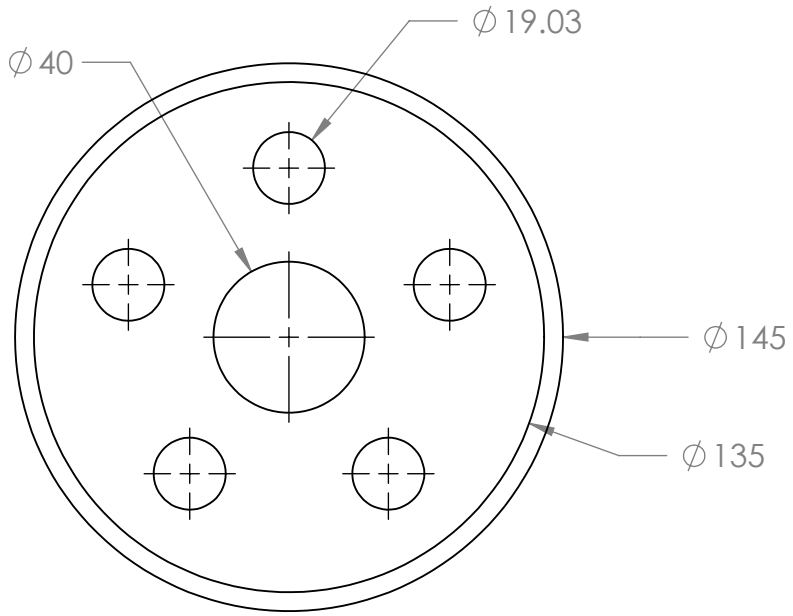

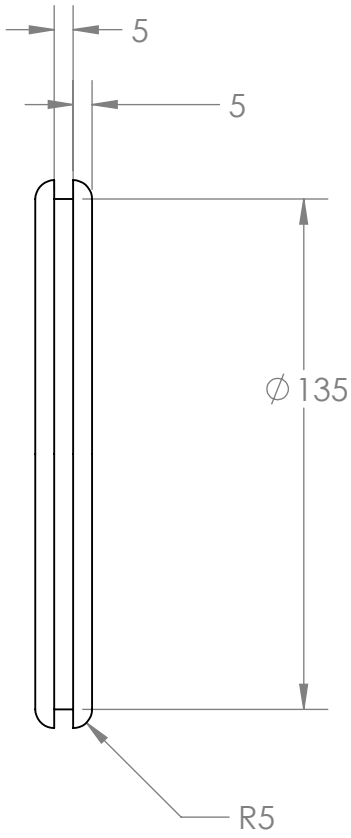

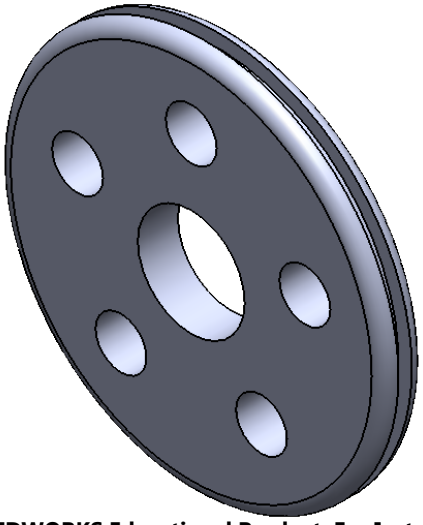

SOLIDWORKS Educational Product. For Instructional Use Only

Name	ID
Ahmed Aldakheel	201303886
Mohammed Alhawaj	201303710
Mohammed Alshubaily	201101678
Sultan Hamdi	201300790
Rami Al Gassab	201301568

SIZE	DWG. NO.	REV
A	Motor large pully	
SCALE: 1:2	WEIGHT:	SHEET 1 OF 1

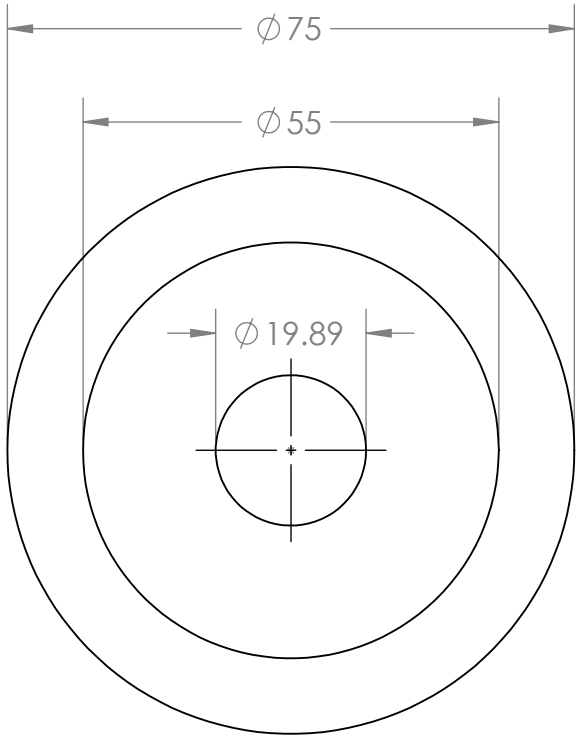

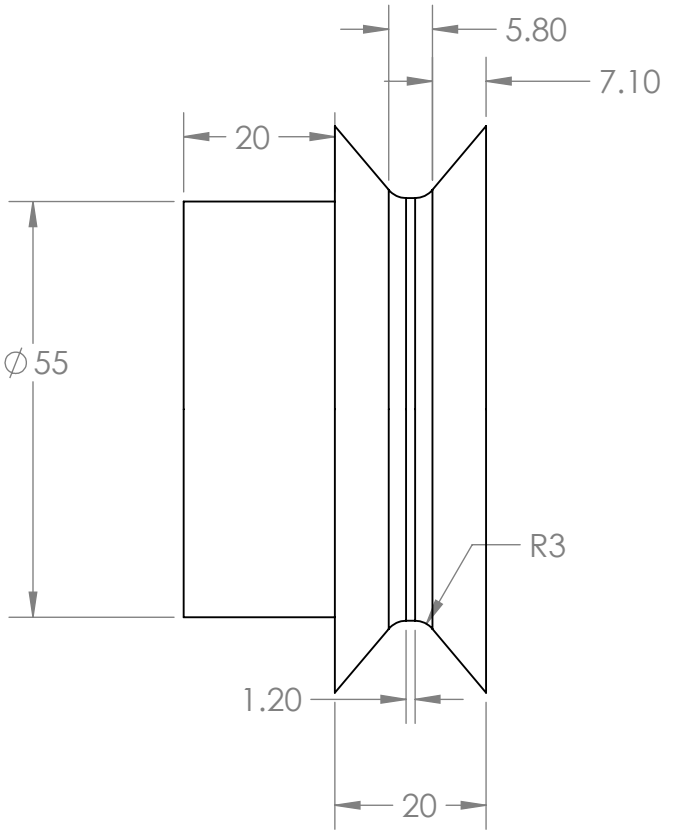

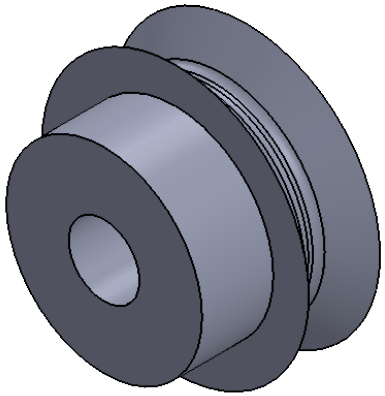

SOLIDWORKS Educational Product. For Instructional Use Only

Name	ID
Ahmed Aldakheel	201303886
Mohammed Alhawaj	201303710
Mohammed Alshubaily	201101678
Sultan Hamdi	201300790
Rami Al Gassab	201301568

SIZE	DWG. NO.	REV
A	Motor small pully	
SCALE: 1:1	WEIGHT:	SHEET 1 OF 1

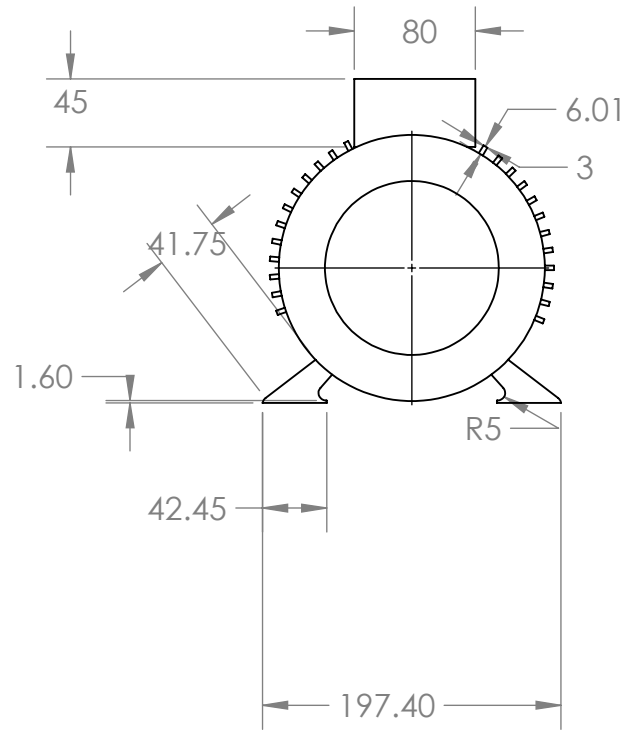

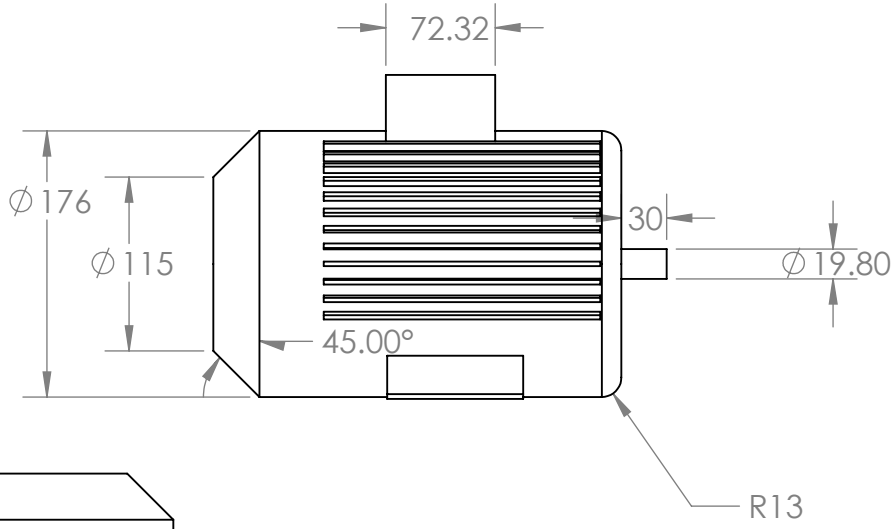

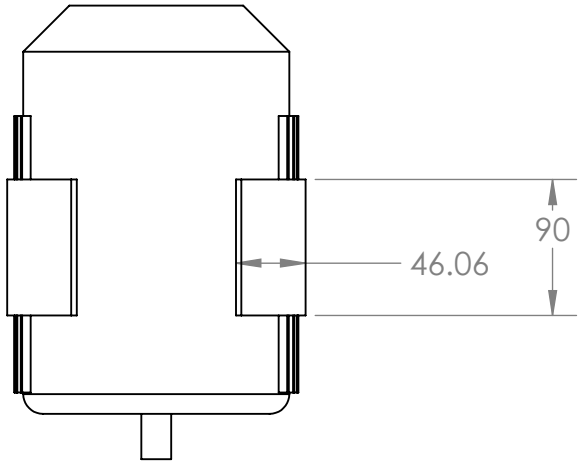

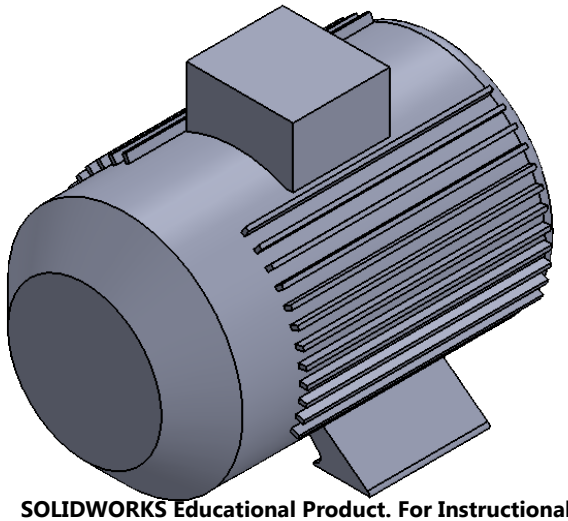

SOLIDWORKS Educational Product. For Instructional Use Only

Name	ID
Ahmed Aldakheel	201303886
Mohammed Alhawaj	201303710
Mohammed Alshubaily	201101678
Sultan Hamdi	201300790
Rami Al Gassab	201301568

SIZE	DWG. NO.	REV
A	motor	
SCALE: 1:8	WEIGHT:	SHEET 1 OF 1

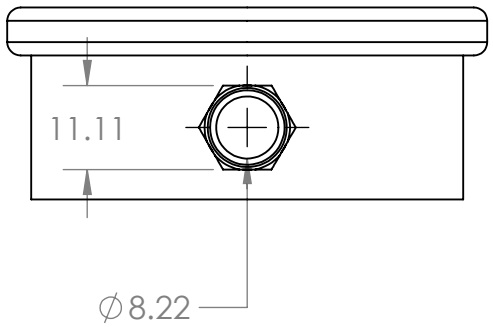

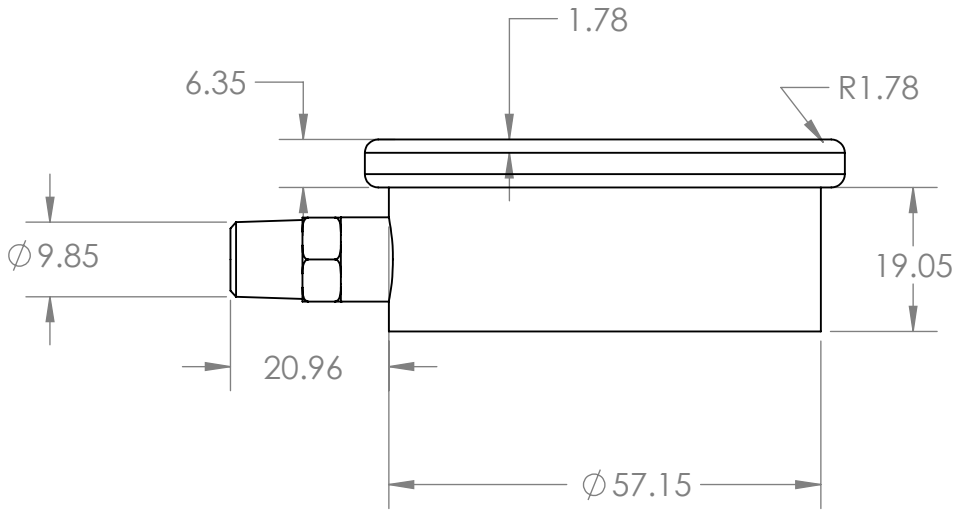

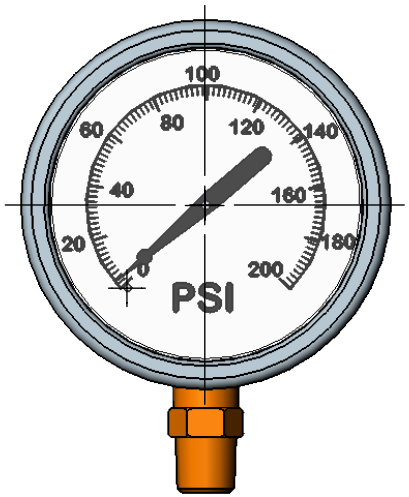

SOLIDWORKS Educational Product. For Instructional Use Only

Name	ID
Ahmed Aldakheel	201303886
Mohammed Alhawaj	201303710
Mohammed Alshubaily	201101678
Sultan Hamdi	201300790
Rami Al Gassab	201301568

SIZE	DWG. NO.	REV
A	Pressure Gauge	
SCALE: 1:1	WEIGHT:	SHEET 1 OF 1

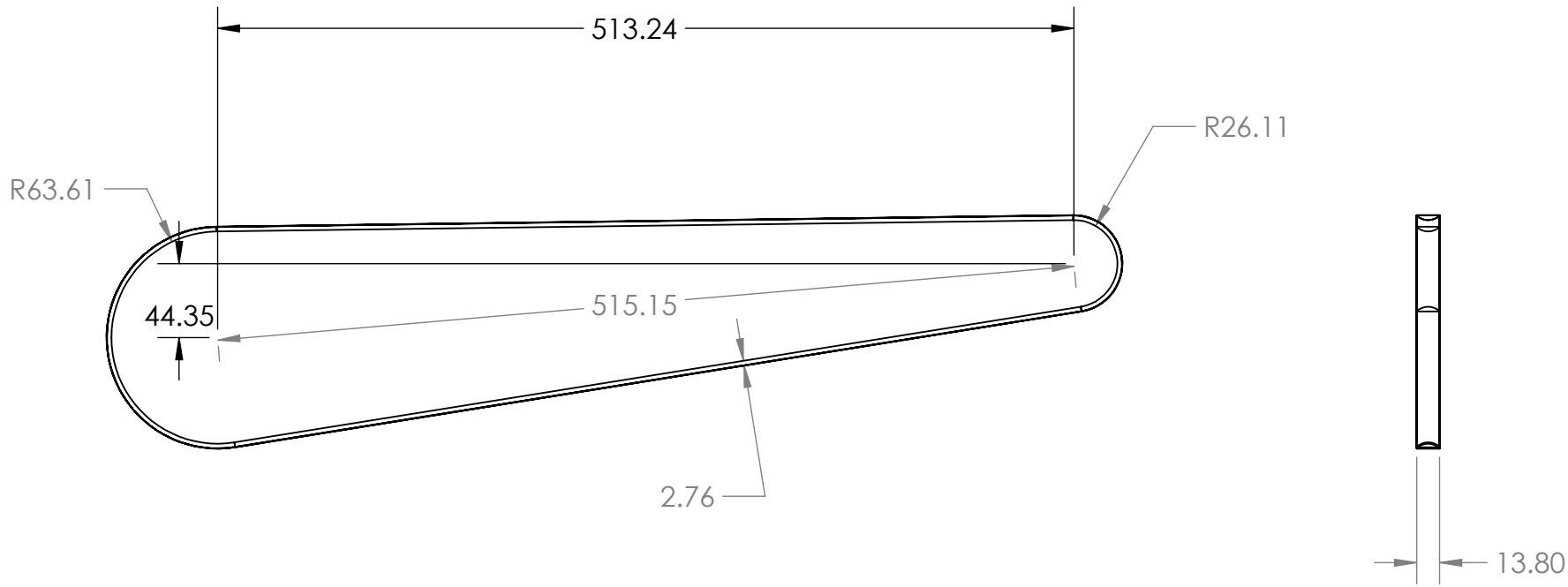

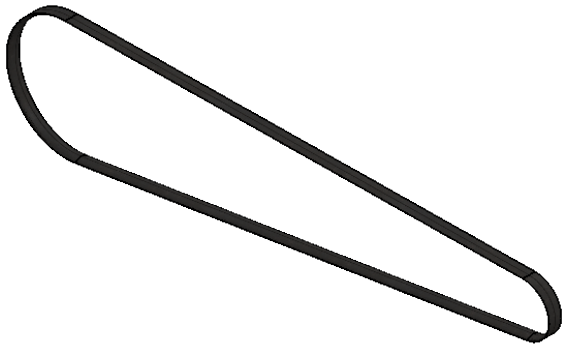

SOLIDWORKS Educational Product. For Instructional Use Only

Name	ID
Ahmed Aldakheel	201303886
Mohammed Alhawaj	201303710
Mohammed Alshubaily	201101678
Sultan Hamdi	201300790
Rami Al Gassab	201301568

SIZE	DWG. NO.	REV
A	pully	
SCALE: 1:8	WEIGHT:	SHEET 1 OF 1

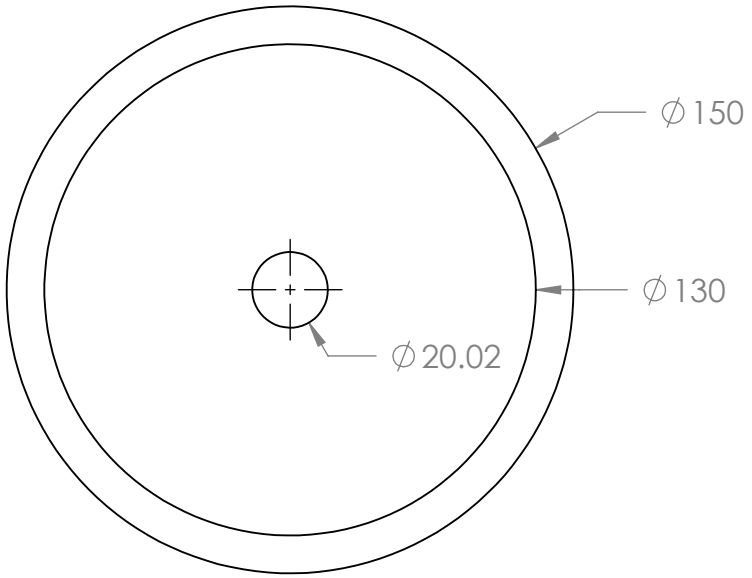

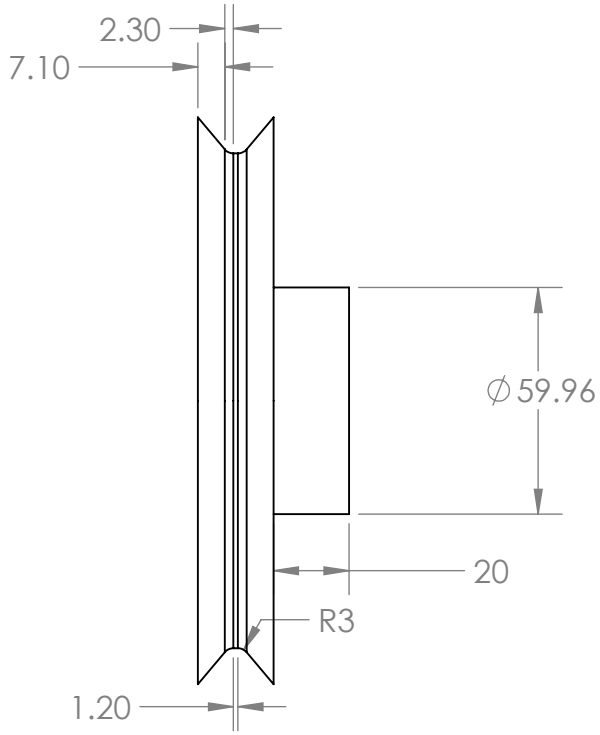

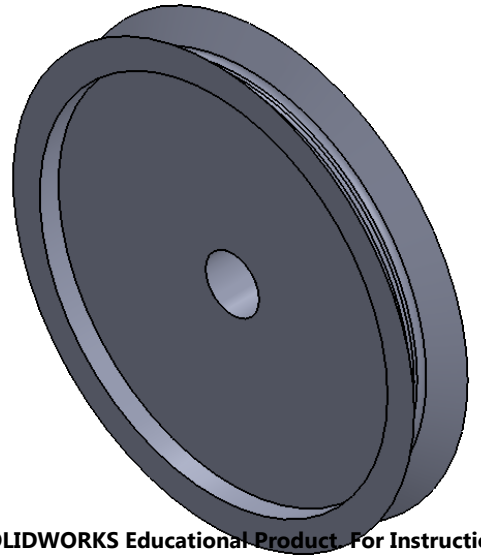

SOLIDWORKS Educational Product. For Instructional Use Only

Name	ID
Ahmed Aldakheel	201303886
Mohammed Alhawaj	201303710
Mohammed Alshubaily	201101678
Sultan Hamdi	201300790
Rami Al Gassab	201301568

SIZE	DWG. NO.	REV
A	shaft pully	
SCALE: 1:2	WEIGHT:	SHEET 1 OF 1

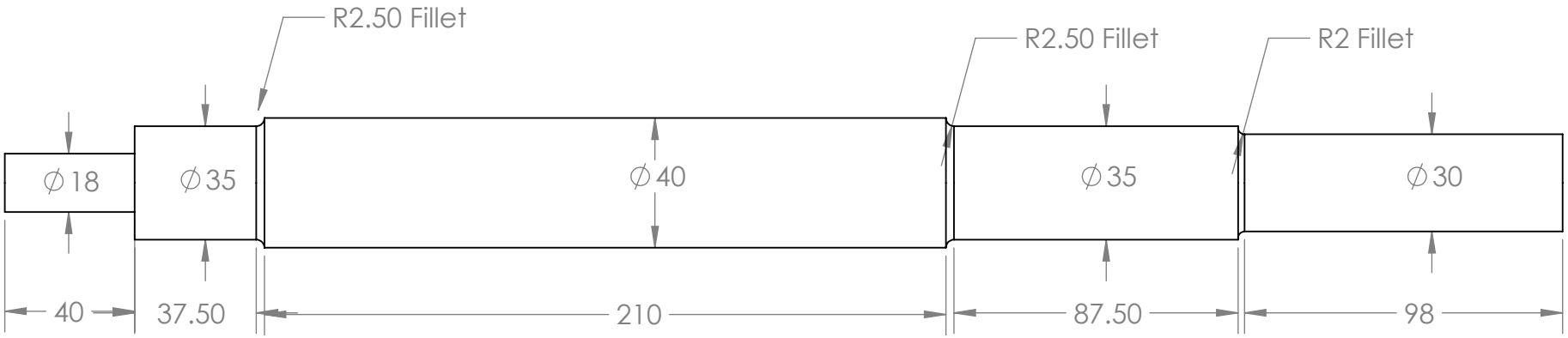

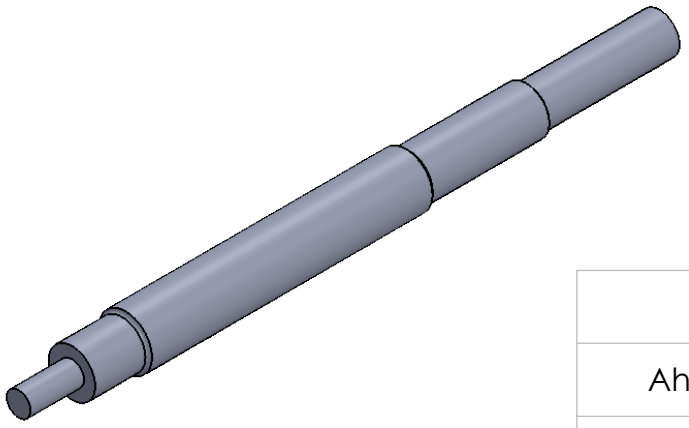

Name	ID
Ahmed Aldakheel	201303886
Mohammed Alhawaj	201303710
Mohammed Alshubaily	201101678
Sultan Hamdi	201300790
Rami Al Gassab	201301568

SIZE	DWG. NO.	REV
A	shaft	
SCALE: 1:8		SHEET 1 OF 1